

50

LEVEL

ARO (13876.1-EX)

18

19

12

AD A 096756

6

AN INVESTIGATION OF INSTANTANEOUS HEAT TRANSFER RATES IN THE EXHAUST PORT OF AN INTERNAL COMBUSTION ENGINE.

9

Final Report

10

Rakesh Sachdev  
S. C. Sorenson

11

January 1981

12 120

14

WILU-ENG-80-4008

DTIC  
SELECTED  
MAR 24 1981

U. S. Army Research Office

15

DAAG29-78-G-01338

DAAG29-76-G-0265

Department of Mechanical and Industrial Engineering  
University of Illinois at Urbana-Champaign  
Urbana, IL 61801

DTIC FILE COPY

Approved for Public Release  
Distribution Unlimited

400833

81 3 24 009

SECURITY CLASSIFICATION OF THIS PAGE (When Data Entered)

REPORT DOCUMENTATION PAGE		READ INSTRUCTIONS BEFORE COMPLETING FORM
1. REPORT NUMBER UILU ENG - 80-4008	2. GOVT ACCESSION NO. AD-A096	3. RECIPIENT'S CATALOG NUMBER 756
4. TITLE (and Subtitle) An investigation of instantaneous heat transfer rates in the exhaust port of an internal combustion engine.	5. TYPE OF REPORT & PERIOD COVERED Final	
	6. PERFORMING ORG. REPORT NUMBER UILU ENG - 80-4008	
7. AUTHOR(s) Rakesh Sachdev S. C. Sorenson	8. CONTRACT OR GRANT NUMBER(s) 76 G 0265; NSC DAA.G 29-78-G-0133	
9. PERFORMING ORGANIZATION NAME AND ADDRESS Department of Mech. & Ind. Engr. University of Illinois at Urbana-Champaign Urbana, IL 61801	10. PROGRAM ELEMENT, PROJECT, TASK AREA & WORK UNIT NUMBERS	
11. CONTROLLING OFFICE NAME AND ADDRESS U. S. Army Research Office Post Office Box 12211 Research Triangle Park, NC 27709	12. REPORT DATE January 1981	
	13. NUMBER OF PAGES	
14. MONITORING AGENCY NAME & ADDRESS (if different from Controlling Office)	15. SECURITY CLASS. (of this report) Unclassified	
	15a. DECLASSIFICATION/DOWNGRADING SCHEDULE NA	
16. DISTRIBUTION STATEMENT (of this Report)  Approved for public release; distribution unlimited.		
17. DISTRIBUTION STATEMENT (of the abstract entered in Block 20, if different from Report)  NA		
18. SUPPLEMENTARY NOTES  The findings in this report are not to be construed as an official Department of the Army position, unless so designated by other authorized documents.		
19. KEY WORDS (Continue on reverse side if necessary and identify by block number)  Heat Transfer, internal combustion engines		
20. ABSTRACT (Continue on reverse side if necessary and identify by block number)  Recently, the growing concern over the exhaust emissions, cooling requirements and design of exhaust system devices has led to the study of the instantaneous heat transfer rates in the straight portion of the engine exhaust port and the port itself. In this study, experimental measurements were made of the instantaneous exhaust gas temperatures and the instantaneous wall surface temperatures at four different positions in the exhaust port for a range of engine operating conditions. The calculated instantaneous heat transfer rates and the instantaneous		

DTIC  
ELECTRA  
S  
MAR 24 1981

SECURITY CLASSIFICATION OF THIS PAGE(When Data Entered)

heat transfer coefficients were found to be significantly dependant on the geometrical position in the exhaust port, the engine speed and the engine load and depicted a consistent trend in the results.

Unclassified

SECURITY CLASSIFICATION OF THIS PAGE(When Data Entered)

## TABLE OF CONTENTS

	Page
1. INTRODUCTION.....	1
2. LITERATURE SURVEY.....	3
3. DESCRIPTION OF EXPERIMENTAL APPARATUS.....	7
3.1 DESCRIPTION OF TEST SECTION.....	7
3.2 WALL TEMPERATURE MEASUREMENTS. ....	7
3.3 GAS TEMPERATURE MEASUREMENT.....	11
3.4 EXHAUST GAS MASS FLOW RATE MEASUREMENTS.....	14
3.5 CRANK ANGLE PULSE GENERATOR.....	16
4. DESCRIPTION OF THE DATA ACQUISITION SYSTEM.....	20
4.1 F.M. TAPE RECORDER AND ITS CAPABILITIES.....	20
4.2 INTERFACING THE TAPE RECORDER WITH THE TRANSDUCERS.....	20
4.3 DIGITIZATION OF THE ANALOG SIGNALS ON A MINI-COMPUTER.....	23
4.4 DATA PROCESSING AND ANALYSIS.....	23
5. EXPERIMENTAL PROCEDURE.....	25
6. DETERMINATION OF THE INSTANTANEOUS HEAT FLUX.....	29
6.1 FINITE DIFFERENCE APPROACH.....	29
6.2 COMPARISON WITH FOURIER-SERIES EXPANSION METHOD.....	32
6.3 STABILITY OF THE FORWARD-DIFFERENCE TECHNIQUE AND THE SELECTION OF THE GRID IN SPACE AND TIME.....	33
7. EXPERIMENTAL RESULTS.....	37
7.1 TYPICAL SET OF DATA.....	37
7.2 WALL TEMPERATURE RISE DUE TO MOVEMENT OF VOLUME OF GAS IN TEST SECTION FROM PREVIOUS EXHAUST STROKE.....	40
7.3 EFFECT OF TEST-SECTION GEOMETRY.....	46
7.4 EFFECT OF ENGINE SPEED AND ENGINE LOAD.....	51
8. CONCLUSIONS.....	67
REFERENCES.....	69
APPENDICES:	
A. OPTICAL TECHNIQUE FOR THE DETERMINATION OF GAS TEMPERATURE.....	71
B. VOLTAGE CALIBRATION OF F.M. TAPE RECORDER.....	73

Accession For	
NTIS GRA&I	<input checked="" type="checkbox"/>
DTIC TAB	<input type="checkbox"/>
Unannounced	<input type="checkbox"/>
Justification	
By _____	
Distribution/	
Availability Codes	
Dist	Avail and/or Special
A	

- C. TEMPERATURE DISTRIBUTION IN A FLAT PLATE WITH ONE SURFACE TEMPERATURE A PERIODIC FUNCTION OF TIME.....77
- D. FLOW RATE OF AN IDEAL GAS THROUGH AN ORIFICE.....81
- E. SIMULATION OF WALL TEMPERATURE RISE IN TEST SECTION DUE TO SUDDEN FLOW OF GAS AT CONSTANT TEMPERATURE.....84
- F. GRAPHS OF MEASURED AND CALCULATED DATA.....86
- G. COMPUTER PROGRAMS.....103

## 1. INTRODUCTION

The design and development of Internal Combustion Engines is demanding more and more scientific and accurate techniques as the standards of performance, economy, and pollution control are raised. Computer technology has now made it possible to acquire and simulate large amounts of engine data and use this for the design of new engines. The success of such a design based on a mathematical model, however, would definitely depend on the accuracy of the assumptions made in the model. Hence, along with other information, a knowledge of local instantaneous heat transfer rates from the combustion gases to the engine surfaces would be a major factor in the design, especially where problems of severe thermal stresses have to be avoided. Most of the work done so far in this area has been the study of the convective and radiative heat transfer rates in the combustion chamber itself. However, recently, the concern over the exhaust emissions and cooling requirements has led to the study of the instantaneous heat transfer rates in the straight portion of the exhaust port and the port itself.

In conventional piston type I.C. Engines; the high pressure gas filling the cylinder rapidly rushes past the exhaust valve as it just begins to open, driving the pressures and the temperatures in the exhaust to reach their maximum value. With a further opening of the exhaust valve the pressure and temperature of the exhaust gases begin to drop. A detailed knowledge of these extremely rapid changes in the temperatures and pressures of the exhaust gases is very important from the stand point of exhaust system device applications such as turbochargers, catalytic converters and thermal reactors. For example, accurate turbine-inlet temperatures are required to interpret the performance characteristics of turbochargers when matched with internal combustion engines. The oxidation of hydrocarbon species in the exhaust is

also very strongly influenced by the temperature time history of the exhaust gas. Also, by reducing the amount of heat transferred in the exhaust port, the power needed to drive cooling fans and pumps could be decreased. Moreover, the determination of peak heat fluxes that future engines would be subjected to, would be a deciding factor in the design of exhaust valves and is also one of the primary reasons of this non-steady heat transfer research.

## 2. LITERATURE SURVEY

A great deal of experimental and theoretical work has been done by various people to study and predict the convective heat transfer in internal combustion engines both in the combustion chamber and in the exhaust. So far a reasonably accurate correlation does not exist for pulsating flows and estimates are usually drawn from steady-state correlations.

The instantaneous heat fluxes at the surface of a wall is usually expressed by Newton's law of cooling with the use of surface heat transfer coefficients

$$Q/A(\theta) = h(\theta) (T_g(\theta) - T_w(\theta)) \quad (1)$$

where

$\theta$  = crank angle (analogous to time)

$Q/A$  = heat flux

$h$  = heat transfer coefficient

$T_g$  = Mass averaged gas temperature

$T_w$  = Wall surface temperature

Nusselt (1), by incorporating a term to account for forced convection due to piston motion, used the results from a spherical bomb experiment to the situation in an engine and formulated an expression for the surface heat transfer coefficient

$$h(t) = 0.0278(1 + 0.38v_p) [p(t)^2 T_g(t)]^{1/3} + 1.275 \times 10^{-10} \frac{(T_g(t)^4 - T_w(t)^4)}{(T_g(t) - T_w(t))} \quad (2)$$

where  $p(t)$  = instantaneous cylinder gas pressure in psia

$T_g(t)$  = instantaneous cylinder gas temperature in  $^{\circ}R$

$v_p$  = mean piston speed in ft./sec.

$T_w$  = instantaneous surface wall temperature in  $^{\circ}R$

The first term on the right hand side of the above equation represents the convective heat transfer while the second term gives the radiative portion.

Although Eichelberg's (2) correlation is a modification of Nusselt's, it deserves special mention because of its wide usage. He did extensive research with the use of subsurface thermocouples to study the instantaneous surface heat flux and proposed the correlation

$$h(t) = 0.0565 v_p^{1/3} (p(t) T_g(t))^{1/2} \quad (3)$$

Anand (3) formulated the relation for the instantaneous surface heat flux as

$$q(t) = a \frac{k(t)}{D} (Re)^b (T_g(t) - T_w(t)) + c(T_g(t)^4 - T_w(t)^4) \quad (4)$$

where  $k(t)$  = gas conductivity

$D$  = bore diameter

and  $a$ ,  $b$ ,  $c$  are constants.

More recently, Woschni (4) suggested a method to evaluate the heat transfer coefficient for internal combustion engines from the laws of similarity governing convective heat transfer and derived an equation containing two convective terms, one accounting for the piston motion and the other for the convection due to combustion. T. LeFeuvre, P. S. Myers and D. A. Uyehara (5) used surface thermocouples to measure instantaneous temperatures and calculated the instantaneous heat fluxes at several positions on the cylinder head and sleeve of a direction injection diesel engine for both motored and fired operation. They used a boundary layer model and arrived at an expression for the heat flux for the motored engine.

$$q(t) = a \frac{k(t)}{r} Re(t)^{0.8} Pr(t)^{0.33} (T_g(t) - T_w(t)) \quad (5)$$

Generally the simplest type of relation used to correlate the experimental data by the use of the principles of dimensional analysis and physical similarity for flow in tubes is of the form (6)

$$Nu_D = c Re_D^m Pr^n \quad (6)$$

where  $Nu_D$  = Nusselt number based on the tube diameter  $D$

$Re_D$  = Reynolds number based on the tube diameter  $D$

$Pr$  = Prandtl number

and  $c$ ,  $m$  and  $n$  are constants determined from the experimental data. The papers of Annand (3); Woschni (4); LeFeuvre, et. al. (5); and some others provide between them extensive reviews of the existing literature on engine heat transfer, the comparative assessments of the various correlations proposed over the years, and the presentation of newer correlations. However all the above correlations apply to steady flow situations. There is still very little experimental data and information available for correlating the heat transfer coefficient in pulsating flows. In the exhaust the pressures, temperatures and velocities change with time and thus the use of time averaged data to compute the maximum heat transfer rates would be inaccurate.

It is pointed out in studies on single-phase flow (7,8) that periodic flow rate variations affect heat transfer and the mechanism of heat and momentum transfer. V. V. Mamayev, et al (9) found that the higher the frequency of mechanical pulsations, the lower the velocity of single phase flow at which turbulence occurs. For example, El'perin et al (7) proved by visual observations of pulsed flow in a circular pipe that when the frequency is increased from 0 to 20 Hz, the critical Reynolds number,  $Re_{cr}$  changed from 2310 to 1500. Work done on heat transfer in pulsed turbulent flows at high frequencies (10) showed that the heat rate increased by 40%, while Parnas found the augmentation to be 20%. In other work, it was shown that in pulsed flows the heat transfer coefficient increased by 50% as the frequency increased from 0.5 to 2 Hz.

West and Taylor determined that at equivalent time averaged Reynolds numbers between 30000 and 85000, the heat transfer coefficient in pulsating flow of water through a pipe increased as much as 70% over the steady flow situation (11). However in some other independent investigation at lower Reynolds numbers, no such increase in the heat transfer coefficient was observed (12,13). In situations of fully developed turbulent flow of a fluid in a tube, Barnett and Vachon found significant increases in heat transfer at low frequencies of pulsation while a decrease in the heat transfer coefficient was observed for frequencies greater than 10 Hz (14). Results obtained by Havemann and Narayan (15) who studied the flow of heated air in a tube for Reynolds numbers varying from 5000 to 3500 and frequencies from 5 to 33 Hz, showed a change in the heat transfer coefficient as much as 30%. The change was found to be negative below a certain critical frequency and positive above it. A number of other people like Chaletban (16), Koshkin et al. (17), Hwu (18), Goluba (19), Bayley (20) found varied effects on the heat transfer in pulsating flows. However, it can be inferred that the heat transfer coefficient is dependent upon the Reynolds number and the frequency of pulsation, and that pulsations generally tend to increase the heat transfer.

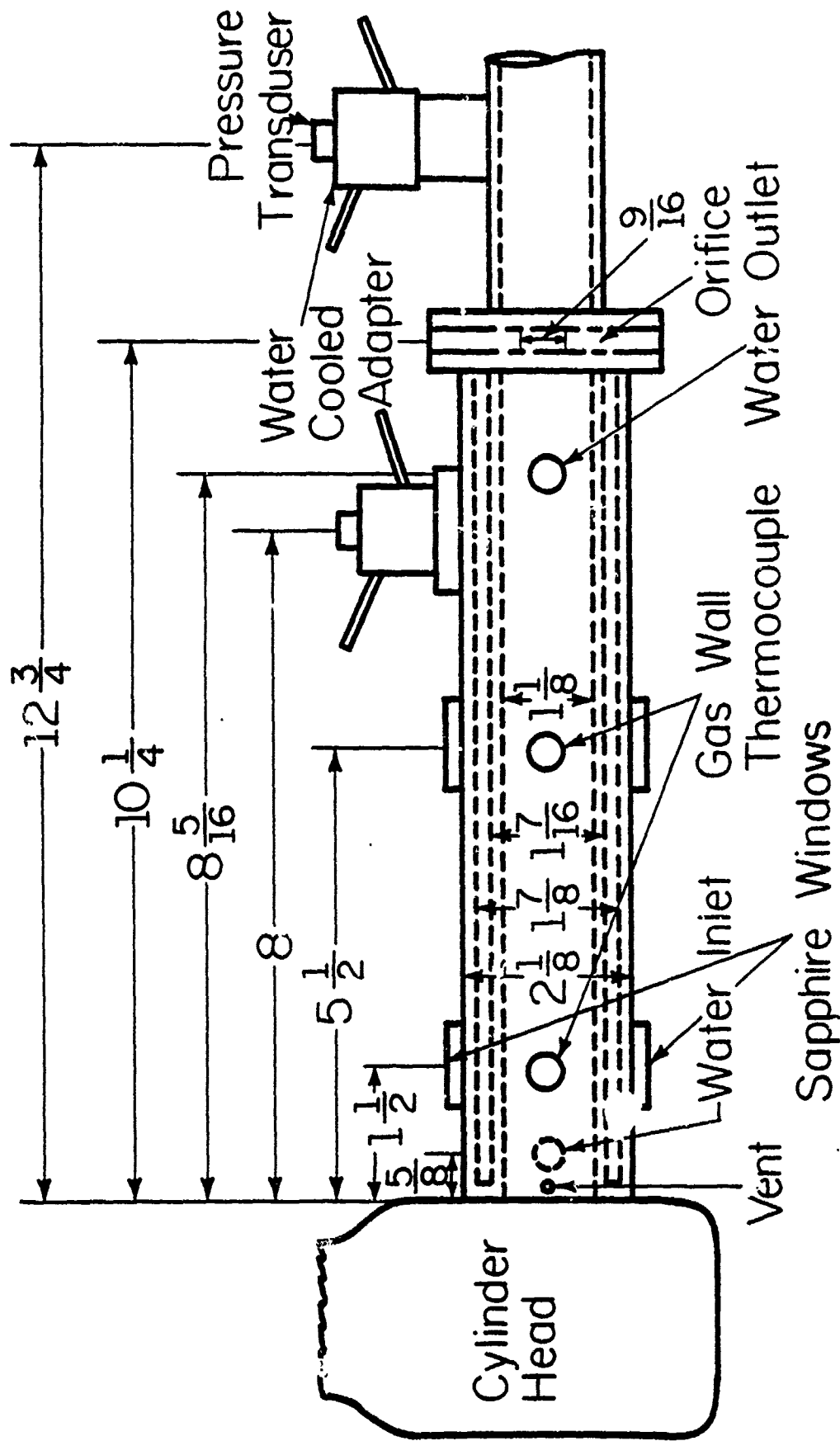
### 3. DESCRIPTION OF EXPERIMENTAL APPARATUS

#### 3.1 DESCRIPTION OF TEST SECTION

To enable the study of heat transfer at the exhaust with convenience, a four-stroke, two-cylinder 325 Honda motorcycle engine having a bore and stroke of 2.52 in. and 2.00 in., respectively, was used. A test section consisting of two concentric stainless steel cylinders (see Fig. 3.1) was then machined and affixed at the exhaust end of one of the air cooled cylinder heads which had earlier been modified to enable the mating of the two components. Cooling water was provided in the annular region of the test section near the exhaust valve and was allowed to flow out downstream of the section with the aid of 0.5 in. copper tubing. Thus the flow of water was in the same direction as that of the exhaust gases. A vent was also provided at the top of the test section to remove any trapped air in the cooling jacket. Measurements of wall surface temperatures, both at the exhaust gas side and the water side along with the exhaust gas temperatures could be made at two different axial locations in the test section--one approximately 4 in. and the other about 8 in. from the exhaust valve seat. An orifice along with pressure transducers on either side of it were incorporated in the test section to determine the instantaneous exhaust gas mass flow rate (see Fig. 3.2).

#### 3.2 WALL TEMPERATURE MEASUREMENTS

The temperatures of the wall surface next to the exhaust gas as well next to the water were measured at each axial location. The temperatures were measured at diagonally opposite positions at each location (see Fig. 3.3). The gas side surface wall temperature measurements were made with Bendersky type chromel alumel thermocouples (21) (Medtherm Model TCS-099T-K-2.00-CR-GGS6-132-0). These thermocouples were screw-in type and were mounted flush with the exhaust gas side wall. Moreover, these thermocouples have been noted to have



All dimensions in inches

Figure 3.1 Test section (top view)

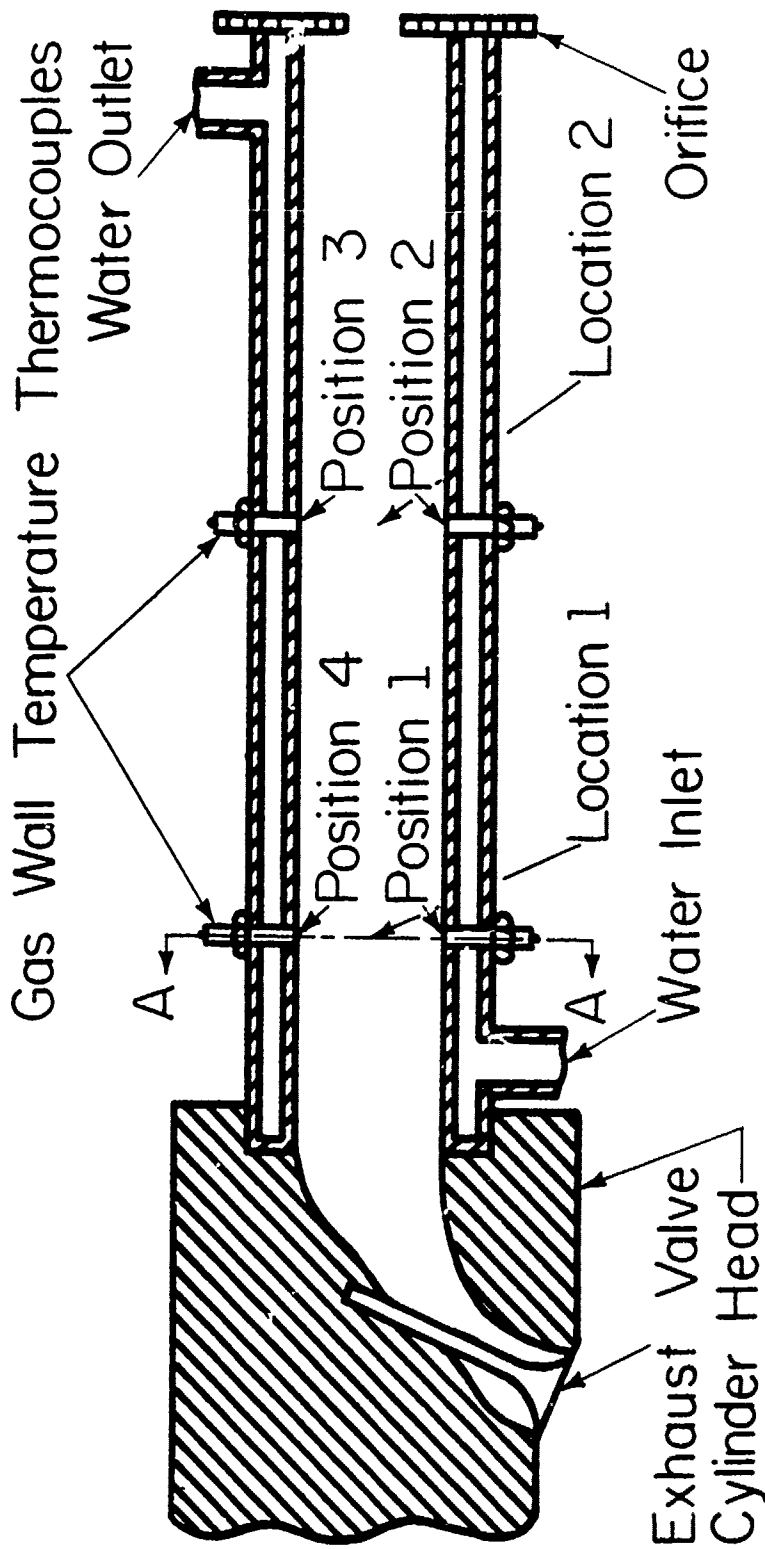


Figure 3.2 Test section (sectional side view)

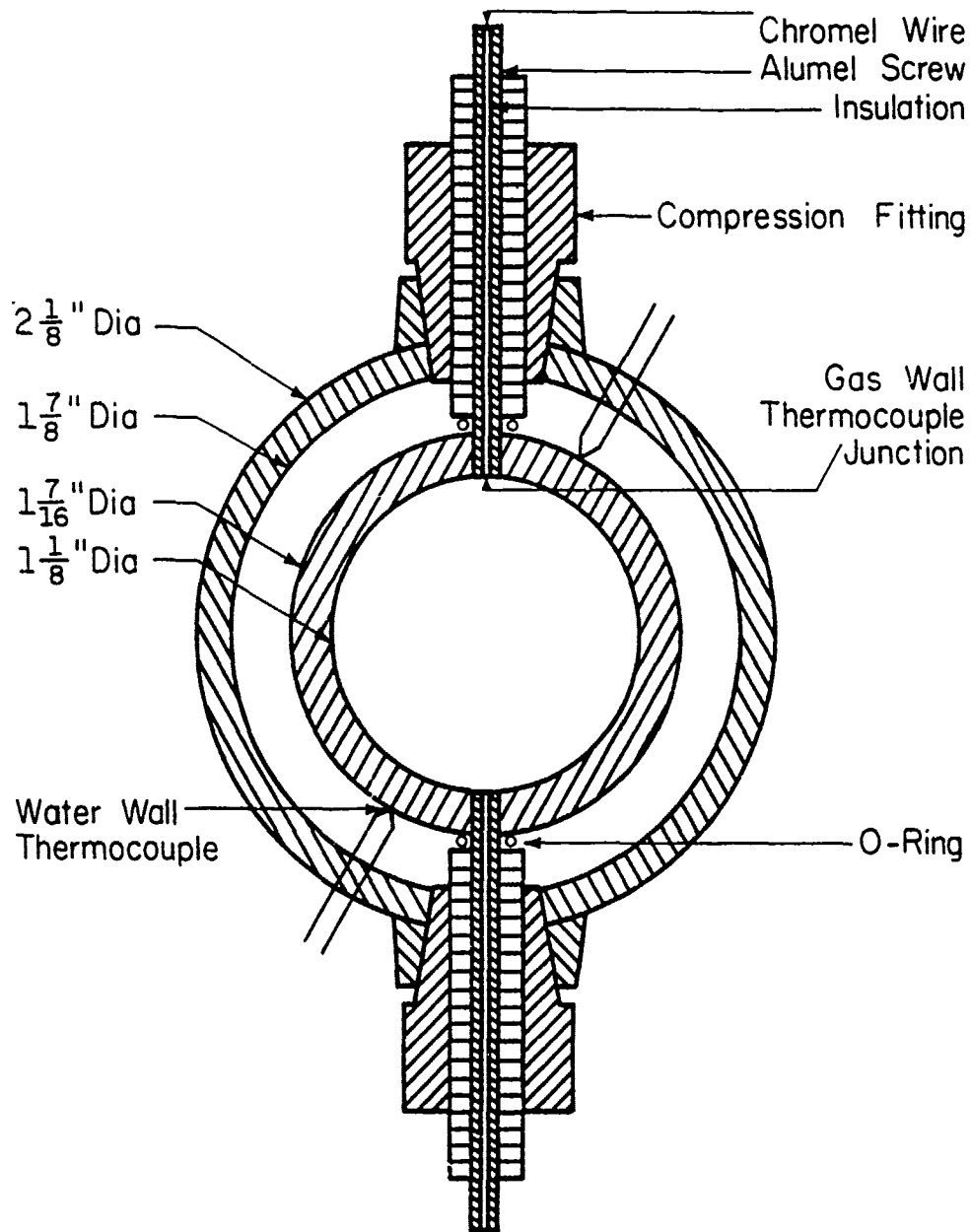


Figure 3.3 Gas side and water side wall thermocouples  
(section A-A of Figure 3.2)

a time constant of less than a millisecond which in light of the fact that the object of the study was determining the transient heat transfer rates, made their selection quite a satisfactory one. An ice bath was used as the reference junction. The thermocouple signal was then amplified by a high gain direct current amplifier (BLH Model 5300). In order to obtain a noise free and clean signal without the help of low pass filters which would otherwise filter off many valuable harmonics of the signal, it was found essential to shield all the thermocouple wires, the engine ignition system, and ground all the equipment at one point to avoid the formation of any ground loops. Since measurements could be made only at one thermocouple at a time, the thermocouple leads were connected to a selector switch before the signal entered the high gain amplifier in order to facilitate the selection of any thermocouple desired. The water side surface wall temperature measurements were made by electron beam welding chromel alumel thermocouples to the surface of the wall next to the water. The thermocouple signal measurements for the water wall side were made with the use of a Leeds and Northrup Model 8686 potentiometer. Another selector switch was incorporated to facilitate the selection of the water-wall thermocouple desired for measurement.

### 3.3 GAS TEMPERATURE MEASUREMENT

The determination of gas temperatures by the use of thermocouples, resistance thermometers, metallic or ceramic probes offered considerable experimental difficulties and were not considered feasible since the gas temperatures were excessively high. In this study, an optical method was used to determine the exhaust gas temperature by measuring the thermal radiation of the gas with an infrared photovoltaic indium antimonide detector (Texas Instruments Model ISV 378 with an IRM-026 preamplifier) (see Appendix A). The optical system consisted of a set of four spherical concave front surface

mirrors (see Fig. 3.4). Two sapphire windows were provided in the test section at each of the two locations in order to enable transmit the thermal radiation of the gases onto the mirrors which in turn would reflect the image onto the detector. The windows were fabricated from sapphire because it turns out that at the wavelength of interest they absorb relatively little radiation (less than 15 percent). The sensing medium was carbon dioxide at a wavelength of 4.4 microns (peak of the CO<sub>2</sub> infrared band). In order to maximize the response of the detector, an optical filter with a bandpass of 0.18 microns was placed in the path of the reflected radiation. A two-bladed mechanical chopper coupled by a flexible driveshaft to the engine was placed directly in front of the detector. This provided the necessary fluctuations for the input radiation to the detector while the engine was running. The calibration of the detector was done with the aid of a known temperature blackbody source (Barnes Infrared Radiation Reference Source Model 11-210). An electrically operated chopper was placed directly in front of the blackbody source to provide the recurring zero signal level necessary to obtain an accurate calibration. This chopped calibration eliminated any errors that might have arisen from a direct current drift of the detection system. A variable diameter iris was also included in the optical path to provide for optical attenuation of the image intensity (22). The maximum opening of the iris was fixed so that no possible light path through the system could fall on the edge of any of the optical elements. This provided uniform illumination of the image by radiation with both the engine viewing optics and the calibration optics and made possible the viewing of the same solid angle by the detector for either optics. The centerline of the optical system was aligned with the help of an He-Ne laser beam and the mirrors were positioned in a manner so as to produce the images of the center of the test section and the blackbody source at the detector.

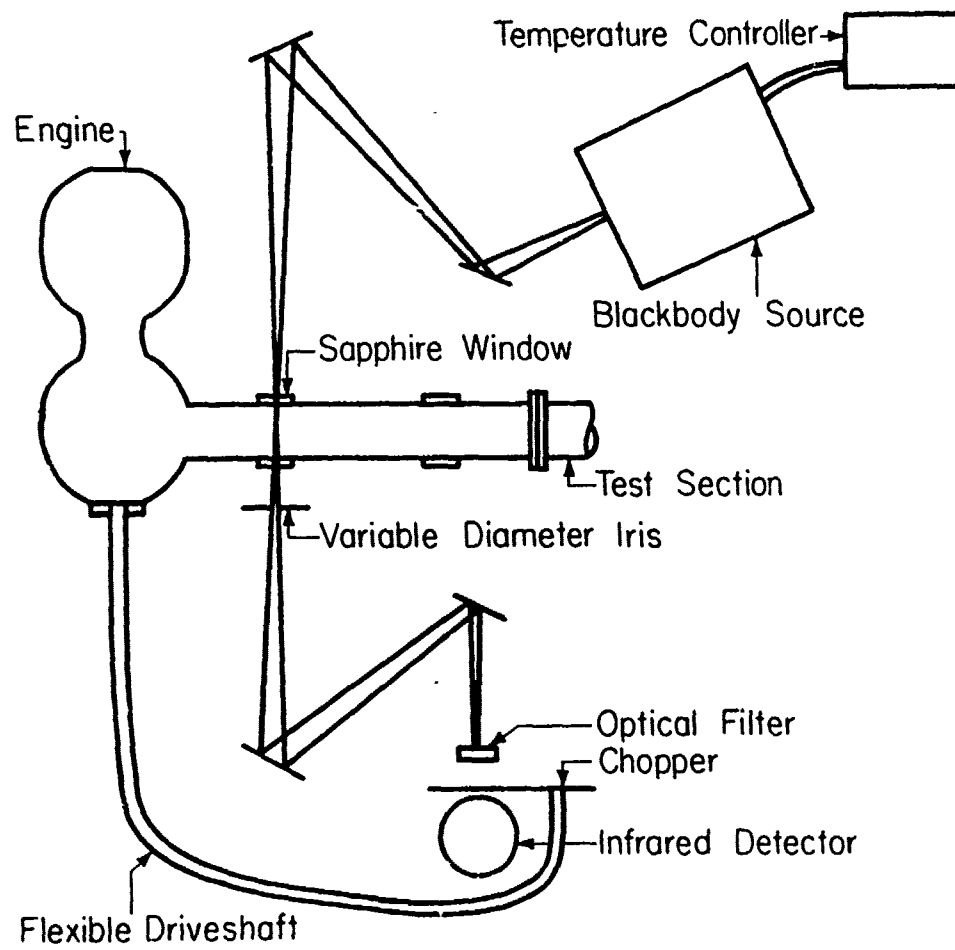


Figure 3.4 Exhaust gas temperature measurement system  
(top view)

Since surface deposits form on the windows while the engine is running, it was necessary to calibrate the window and surface deposit transmission (see Fig. 3.5). However, it was noted that the accumulation of the deposits was not very prominent for a single engine run. The entire gas temperature measurement system was mounted on a moveable table to enable measurements at either location of the test section.

#### 3.4 EXHAUST GAS MASS FLOW RATE MEASUREMENTS

The instantaneous exhaust gas mass flow rates were computed by measuring the pressures on either side of a thick plate orifice placed downstream in the test section. The absolute pressures were measured with the use of quartz pressure transducers (Kistler Model 206) which had very high signal to noise ratio and produced a high level and a low impedance signal. The transducers had to be mounted in water cooled adapters to prevent a decrease in the sensitivity at high temperatures. Assuming the flow to be compressible and isentropic, the mass flow rate can be expressed as (see Appendix D)

$$\dot{M} = C_v A_R \left\{ \frac{2\gamma g P_1^2}{(\gamma-1)RT_1} \right\}^{1/2} \left\{ \frac{(P_2/P_1)^2 - (P_2/P_1)^{\gamma+1/\gamma}}{1 - \beta^4 (P_2 - P_1)^{2/\gamma}} \right\}^{1/2} \quad (3.1)$$

where,

$C_v$  = Flow Coefficient

$A_R$  = Restriction Area

$P_1$  = Upstream Pressure

$P_2$  = Downstream Pressure

$T_1$  = Upstream Temperature

$R$  = Exhaust gas constant

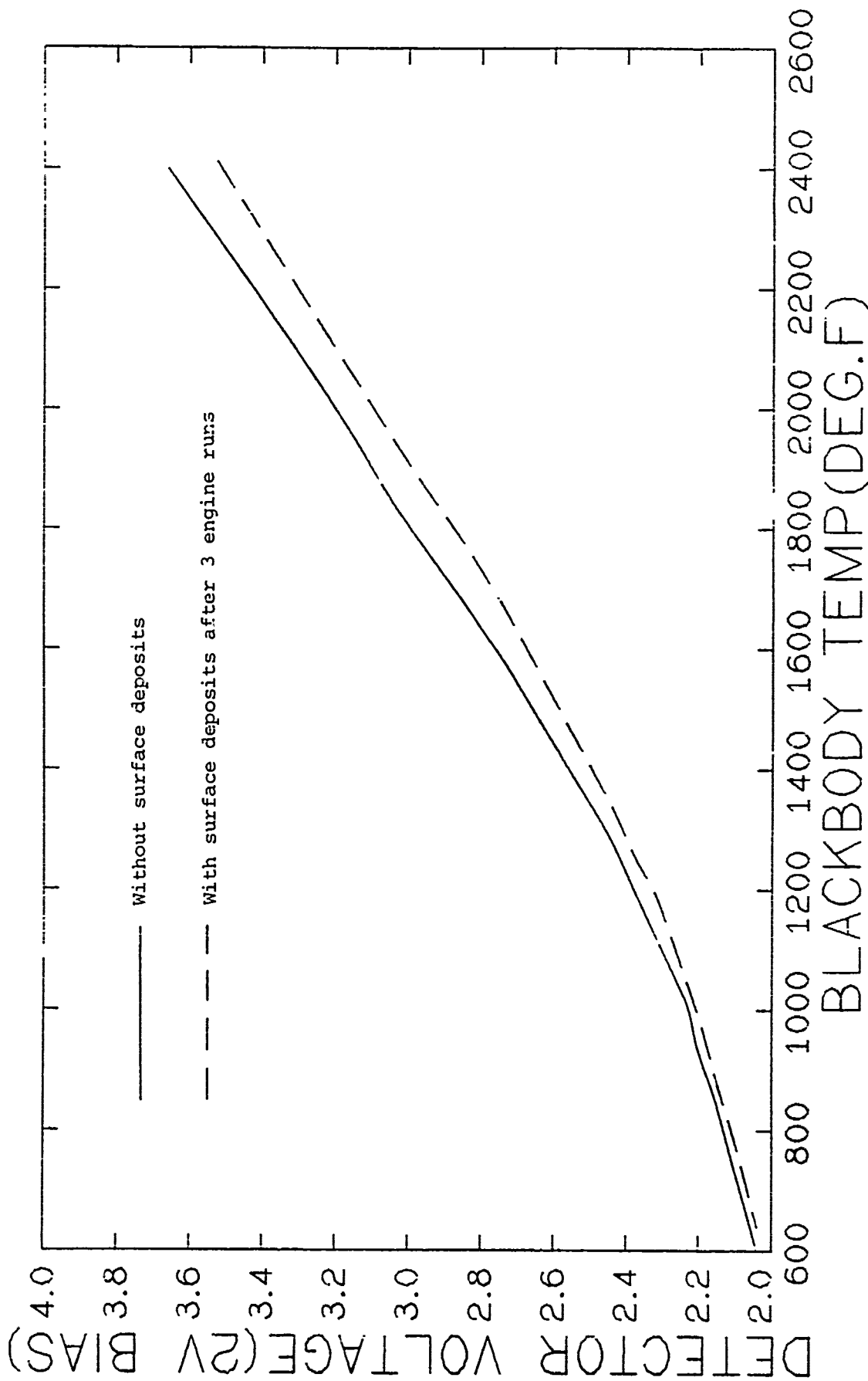


Figure 3.5 Calibration curve for the infra-red detector with and without surface deposits on the windows.

$\beta$  = Diameter Ratio

$\gamma$  = Specific Heat Ratio

The instantaneous values of the pressures and the exhaust gas temperature were used in the above equation to evaluate the instantaneous mass flow rates. To provide a check for the mass flow rate computations and also to determine the air fuel ratio, the air consumption was also measured with the use of a Meriam 50 MC2-2S flowmeter coupled to an inclined tube water manometer. The fuel consumption was measured with a 24 ml burett.

### 3.5 CRANK ANGLE PULSE GENERATOR

As a time reference for all other signals, crank angle pulses were generated every 3 degrees of the crank rotation. A flywheel disc was fabricated with circular holes drilled at every 3 degrees of its outer periphery and another hole was provided at a smaller radius to enable generation of the top-dead center pulse (see Fig. 3.6). The disc was directly coupled to the crankshaft. A rubber pad was provided between the coupling to absorb the vibrations while the engine was running and to absorb the shock when the engine was stopped. Two plastic NPN Silicon Photo transistors (MOT MRD 450) were activated by a direct current light source chopped by the outer periphery of holes and the inner hole. The arrangement and circuitry is shown in Fig. 3.7. The circuit incorporated a monostable multivibrator with Schmitt-Trigger inputs. This allowed stable triggering from inputs with transition rates as slow as 1 volt per second, providing the circuit with an excellent noise immunity. Once fired, the output pulses were independent of further transition of the inputs, i.e., independent of the angular rotation of the flywheel and were a function only of the timing components. The output pulse was designed typically to have a width of 45 microseconds and remain unimpaired up to at least 6 kHz.

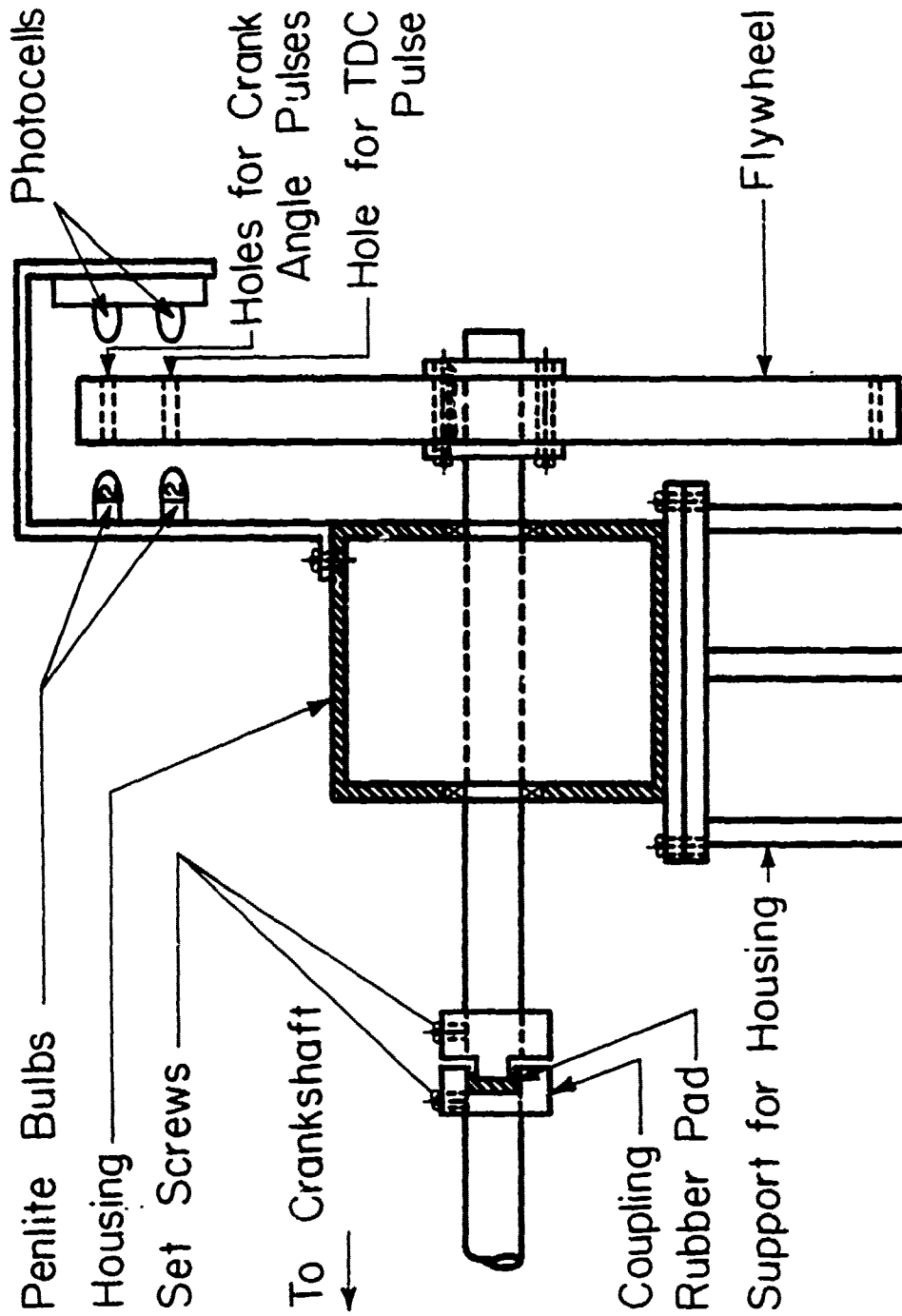


Figure 3.6 Schematic of the flywheel assembly

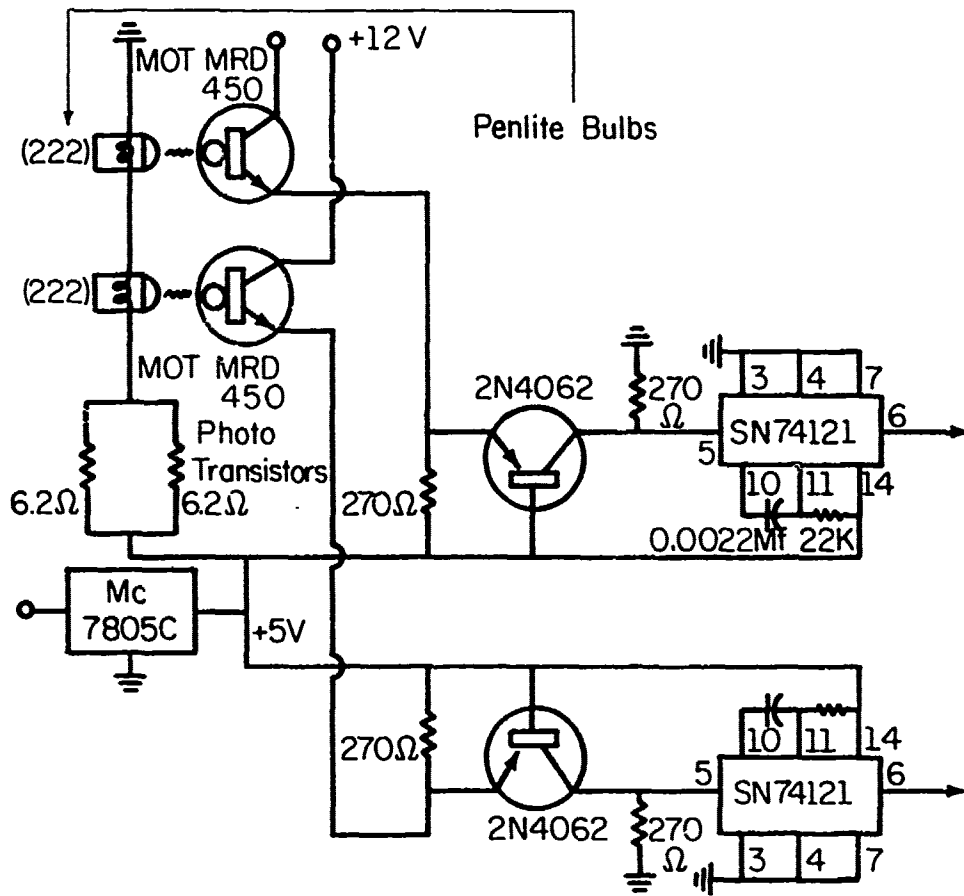


Figure 3.7 Electronics for crankangle and T.D.C. pulse generation

The choice of the fuel used in this investigation was determined by the fact that only a minimum amount of combustion deposits on the sapphire windows could be tolerated for the infrared detector to perceive the maximum amount of exhaust gas radiation. Isoctane, which meets the ASM reference fuel standards, was found to be the most suitable. The engine could be loaded by means of a Genral Electric Model 1-G-337 eddy current dynamometer which was coupled to the engine with a chain and sprocket drive. A strobe light was used to measure the engine rpm. The factory installed constant velocity carburetors were replaced by a variable venturi type (Honda part No. 161 C2 312 034).

#### 4. DESCRIPTION OF THE DATA ACQUISITION SYSTEM

##### 4.1 FM TAPE RECORDER AND ITS CAPABILITIES

In order to obtain a reliable and accurate representation of the engine data, a high speed, multiple channel data acquisition system was essential (see Fig. 4.1). A seven channel, multispeed FM tape recorder (Sangamo Sabre VII) was used to record the analog data. At its highest tape speed (60 in./sec), this tape recorder was capable of a frequency response from dc to 40,000 Hz. At this same tape speed, the signal to noise ratio was better than 50 decibels. The tape recorder was capable of accepting a maximum voltage of anywhere between 0.2 V to 10.0 V. To make full use of the recorders' signal to noise capability, the input signal had to be amplified, or attenuated, depending on the input level so as to reproduce voltages varying between  $\pm 1$  V. This capability was built into the record electronics of the tape recorder.

##### 4.2 INTERFACING THE TAPE RECORDER WITH THE TRANSDUCERS

Since the total level of signal from the gas wall thermocouple, after amplification by the high gain amplifier, was very much larger than that produced by the temperature swing during the engine cycle, it was found essential to bias of the dc level so as to be only left with the fluctuating temperature signal. This signal had to then be amplified further (X30) to bring it up in the feasible range for recording. (see Fig. 4.2). This signal along with the amplified output signals from the infrared detector, the two pressure transducers and the crank angle and top dead center pulse generator electronics were fed to the FM tape recorder. The recording was made at the highest possible tape speed and visual observation of the data was made possible during recording on a four-channel oscilloscope. Approximately 250 consecutive cycles of engine data were recorded per engine run.

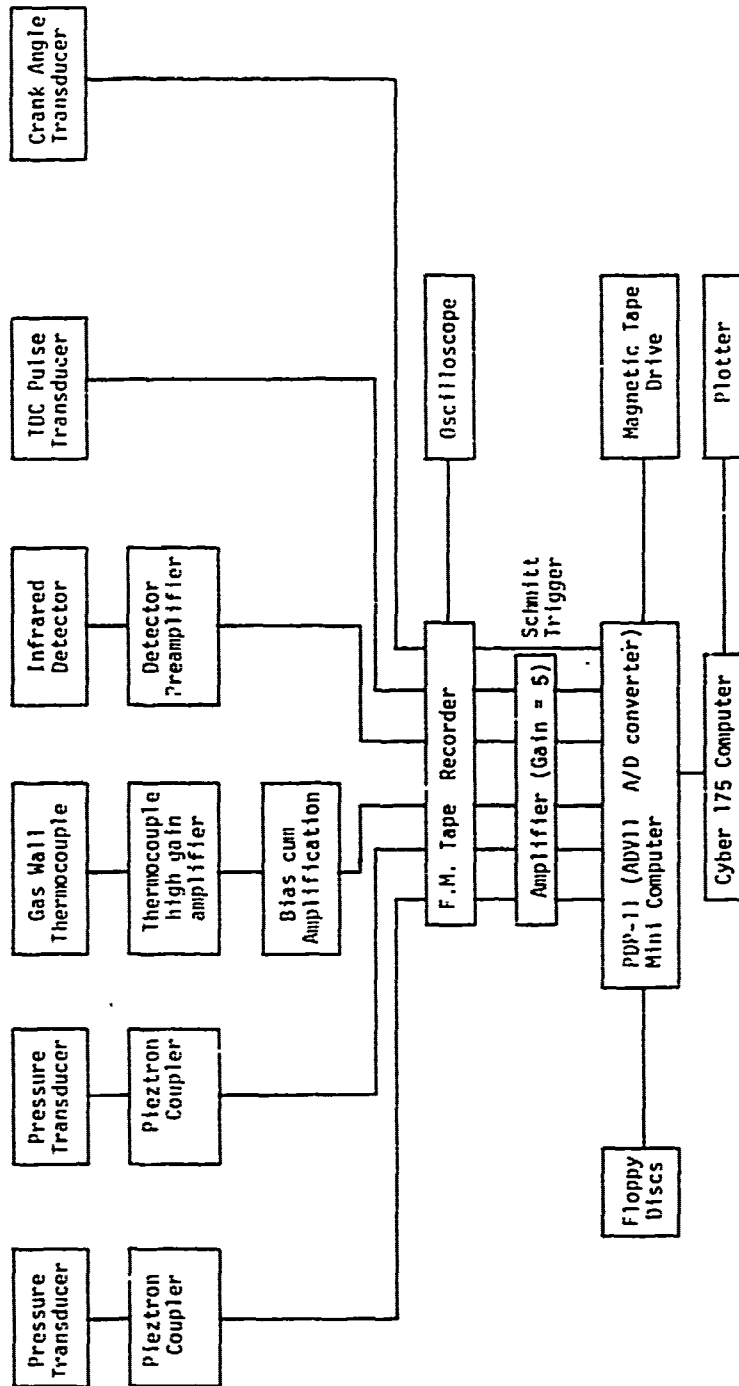


Figure 4.1 Data acquisition system

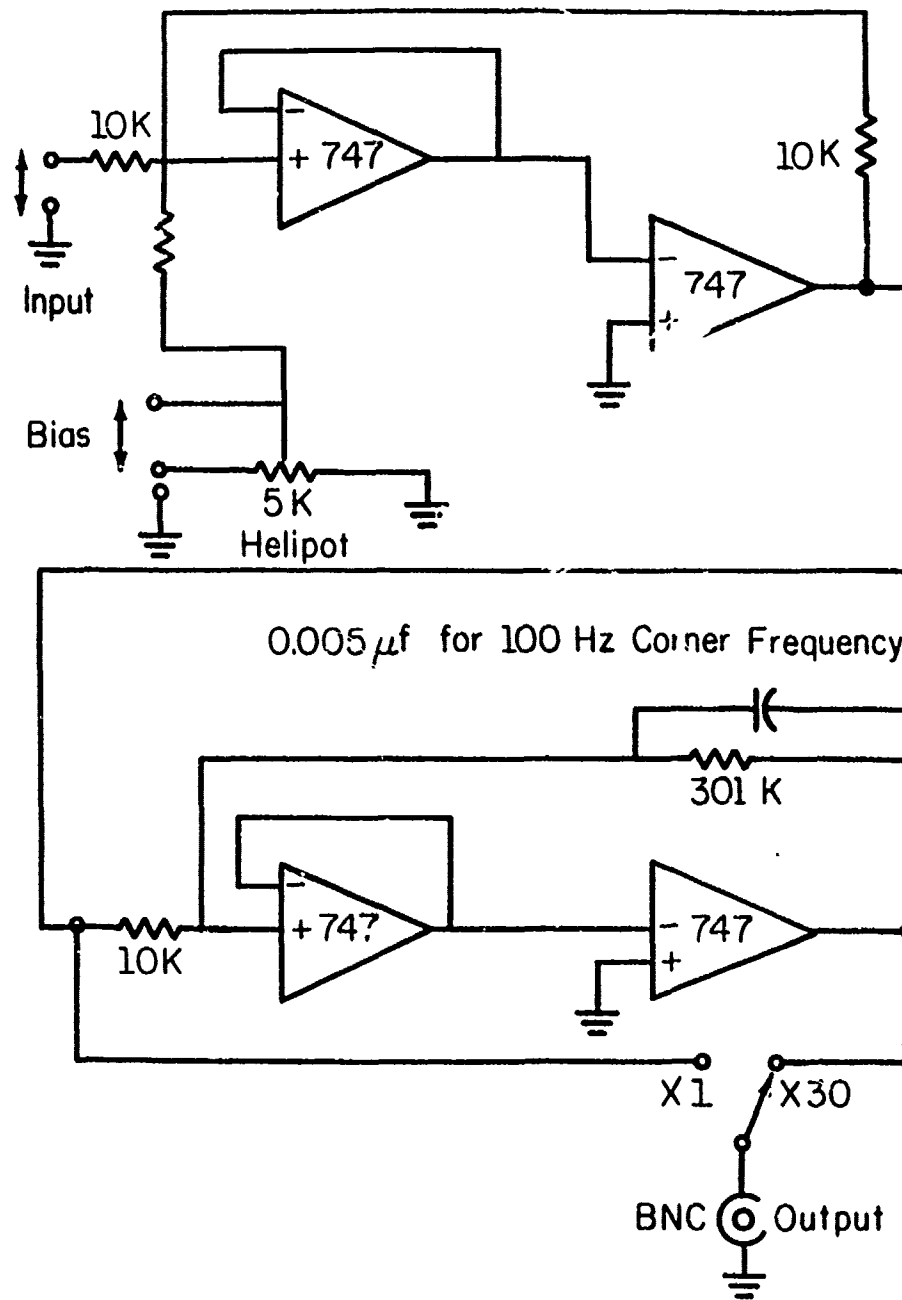


Figure 4.2 Biasing and amplification electronics of gas side wall temperature swing.

#### 4.3 DIGITIZING OF THE ANALOG SIGNALS ON A MINI-COMPUTER

After the recordings, the taped analog signals were then digitized on a PDP-11 mini-computer by an Analog-to-Digital Converter (ADV11-A). This is a 12-bit successive-approximation A/D converter with built-in multiplexer and sample-and-hold, and could accommodate 16 single-ended or eight quasi-differential inputs. The analog to digital conversions were initiated by the crank angle pulses and a real-time sampling (RTS) routine was used for the execution. Since the ADV11-A was designed to accept input voltages in the range of  $\pm 5.12$  V, all the output signals from the tape recorder, which were in the range of  $\pm 1$ V, were amplified (X5) before connecting them to the ADV11-A in order for it to operate near maximum sensitivity. Also for the sampling frequency to remain within the capability of the A/D converter, the FM tape recorder was played back at 1/16 (3.75 in. per second) the recorded tape speed, while digitizing. The digitized data was written onto magnetic floppy disks on the PDP-11 minicomputer and then transferred and stored on a magnetic tape which had a considerably larger storage space than the floppy discs. This enabled the floppy discs to be reused.

#### 4.4 DATA PROCESSING AND ANALYSIS

The digitized data was then transferred from the magnetic tape and floppy discs to a CDC Cyber 175 computer by directly loading the magnetic tape on the Cyber system and also by means of a dataphone. The capabilities of the CDC Cyber 175 far exceeded that of the minicomputer and was the reason why all the digitized data was decided to be analyzed on the Cyber system. A Fortran program was first used to scan the digitized data for the engine cycles, compile them, delete the defective cycles, and then process them into their actual values. A transient heat transfer analysis was then done on each cycle individually. Finally, a specified number of engine cycles were ensemble

averaged to give one averaged cycle of all the distributions of interest. The advantages of averaging a number of cycles, first of all, was eliminating cycle-to-cycle variation of the data and secondly attenuating the random noise, introduced by the various electronic components, by a factor  $1/N^{1/2}$  where N is the number of cycles averaged.(23) Another program was used to compute the instantaneous exhaust gas mass flow rates. Plottings were then finally done using plotting routines. A complete listing of all the programs can be found in the Appendix G.

## 5. EXPERIMENTAL PROCEDURE

Since the recording of the engine data for a single run took a very short time within which quite a lot of measurements had to be made, it was found necessary to have two people carry out the experiment most efficiently. From the start to the end the experimental procedure can be summarized in the following steps:

1. Check the level of the fuel in the fuel tank and insure that it is at least half full.
2. Check the level of the engine oil.
3. Switch on the power to the F. M. Tape Recorder, Thermocouple amplifier, pieztron couplers, Biasing amplifier, Infra-red detector preamplifier, oscilloscope and let the equipment warm up for at least 10 minutes.
4. Remove the sapphire windows from the test section and clean all the combustion deposits that may have formed on the surface from previous runs.
5. Turn on the hot water supply to the test section and insure that the temperature at the inlet steadies out at a minimum of  $110^{\circ}$  by controlling the variac for the water heater. This would prevent any water vapour from condensing on the windows during the engine run.
6. Remove any moisture present in the infrared detector by blowing in it with dry compressed air.
7. Cool the detector by filling it with liquid nitrogen and wait till all the condensed vapour on its surface has evaporated.
8. Standardize the millivolt potentiometer.
9. Place the reference junction, common to both the water wall and gas wall thermocouples, in a crushed ice bath.

10. Turn on the cooling water and switch on the generator set power to the dynamometer.
11. Check and insure that all the set screws on the perforated flywheel shaft and coupling are tight sufficiently.
12. Move the optical table to the desired location of measurement.
13. Set the selector switch in position for gas wall thermocouple measurements.
14. Set the secondary selector switches to the particular gas wall thermocouple intended for measurement.
15. Set the detector preamplifier bias at 2.0 volts output allowing the detector to operate near maximum sensitivity.
16. Energize the crank angle electronics and the penlite bulbs with a 12 V battery.
17. Note the initial reading of the inclined water monometer.
18. Unlock the dynamometer and open the fuel valves.
19. Connect the engine ignition system to a 12 V battery and after putting on the ignition switch, kick start the engine in a neutral gear.
20. Start the engine cooling fan.
21. Shift the transmission into second gear.
22. Adjust the dynamometer setting and throttle to the desired engine speed and load. Wait for a few minutes for the engine to stabilize.
23. With the help of visual observation on the oscilloscope adjust the thermocouple bias so as to eliminate most of the dc signal and obtain the temperature swing around a mean of 0 volts. Note this biased voltage and also the level of the thermocouple signal before the high gain amplification as a check.

24. Start recording all the signals on the FM tape recorder and make the recording for at least 45 seconds to insure the taping of at least 250 cycles of data.
25. Set the selector switch in position for water wall thermocouple measurements and set the secondary selector switches to the desired water wall thermocouple. With the aid of the millivolt potentiometer, note down the output reading.
26. Note the reading on the inclined water manometer.
27. Measure the fuel rate by timing the flow of the fuel through the burette using a stop watch.
28. Set the selector switch back to the position for gas wall thermocouple measurements and then set the secondary selector switches to the diametrically opposite gas wall thermocouple for the same previous location in the test section. Repeat steps 23 and 24.
29. Gently reduce the load and the engine speed simultaneously till idle condition.
30. Engage the clutch and shift the transmission into neutral. Open the ignition switch to stop the engine.
31. Lock the dynamometer and shut the fuel valves.
32. Let the cooling water and the cooling fan be turned on for at least 10 minutes after completion of the test preventing any damage to the test section or the engine.
33. Playback all the recorded data on the oscilloscope and check all the channels of data.
34. Record a voice commentary at the end of each run on the tape recorder in order to keep track of the data on the tape for later digitization work on the minicomputer.

35. When enough data has been recorded, transport the tape recorder to the computer room and interface it with the PDP-11 minicomputer. Digitize and process all the analog data.
36. Transfer the processed data to the Cyber 175 computer by means of a data phone. Finally carry out all the heat transfer calculations and plottings.

## 6. DETERMINATION OF THE INSTANTANEOUS HEAT FLUX

### 6.1 FINITE-DIFFERENCE APPROACH

In order to determine the heat flux through the walls of the test section at a particular location and at any point of time, or equivalently at any crank rotation during the engine cycle, it was necessary to obtain the temperature distribution in the wall. Since the engine cycles are comprised of periods during which the exhaust valve is closed and open, the mass flow rate of the exhaust gases and the exhaust gas temperature are functions of the crank position. Consequently the gas wall temperature is a function of time and location in the test section. This is then a boundary value problem with two known boundary conditions, i.e. known temperatures at either end of the wall thickness at a particular location in the test section (see Fig. 6.1). The cooling water forces the temperature of the wall on the water side to be fixed. The temperature of the wall next to the gas, i.e. the gas wall temperature is a known function of time. A one-dimensional forward difference technique can be developed to obtain the temperature distribution in the wall. Assuming constant thermal properties for the wall, the governing differential equation can be written as

$$\frac{\partial T}{\partial t} = \alpha \frac{\partial^2 T}{\partial x^2} \quad \dots(6.1)$$

where  $\alpha$  = thermal diffusivity. The wall can be divided into grids with equal grid length and the temperature of the nodal points can be determined at equal time intervals.

$$T(x, t) = T_i^j$$

The subscript  $i$  denotes the  $x$  position and  $j$  denotes the time increment

$$T(x + \Delta x, t) = T_{i+1}^j$$

$$T(x, t + \Delta t) = T_i^{j+1}$$

The second partial derivative can be approximated by

$$\frac{\partial^2 T}{\partial x^2} = \frac{1}{(\Delta x)^2} (T_{i+1}^j + T_{i-1}^j - 2T_i^j)$$

The time derivative can be approximated by

$$\frac{\partial T}{\partial t} = \frac{1}{\Delta t} (T_i^{j+1} - T_i^j)$$

Incorporating these approximations in Eqn. (6.1)

$$T_i^{j+1} = \frac{\alpha \Delta t}{(\Delta x)^2} (T_{i+1}^j + T_{i-1}^j) + (1 - \frac{2\alpha \Delta t}{(\Delta x)^2}) T_i^j \quad \dots(6.2)$$

Thus if the temperatures of the various nodes are known at any particular time, the temperatures after a time increment  $\Delta t$  can be calculated by writing an equation like Eq. (6.2) for each node and obtaining the values of  $T_i^{j+1}$ . To determine the heat flux  $Q^j$  convected into the wall at any time increment  $j$ , a transient energy balance can be made on the node ( $m$ ) on the surface by setting the sum of the energy conducted and convected into the node equal to the increase in the internal energy of the node (see Fig. 6.2)

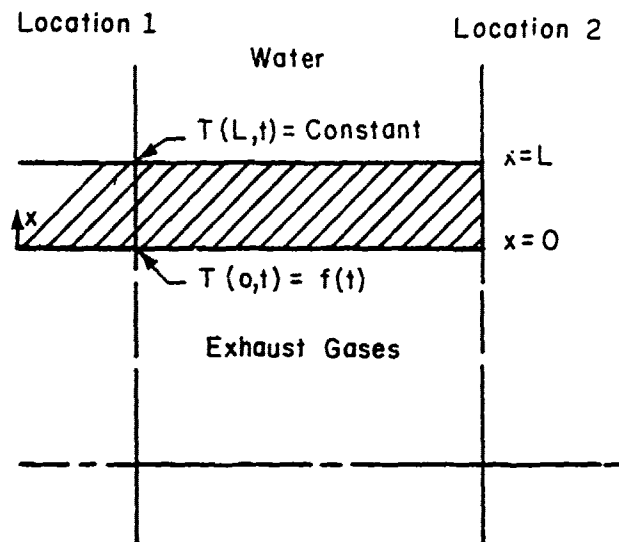


Figure 6.1 Boundary conditions imposed on the test section wall during the engine cycle

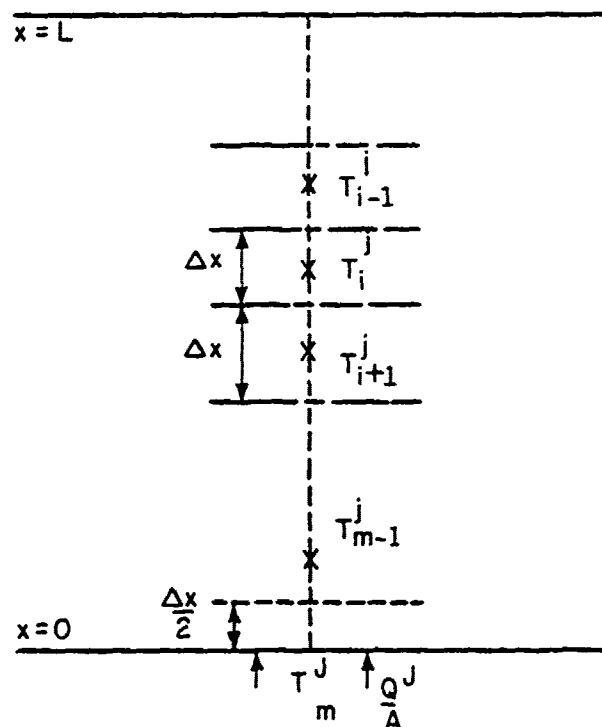


Figure 6.2 Imaginary grid construction in the test section wall.

$$kA \frac{(T_{m+1}^j - T_m^j)}{\Delta x} + Q^j = \rho CA \frac{\Delta x}{2} \frac{(T_m^{j+1} - T_m^j)}{\Delta t}$$

where  $k$  = thermal conductivity of the test section material. Rearranging, the heat flux  $\frac{Q^j}{A}$  is

$$\frac{Q^j}{A} = \frac{k}{\Delta x} [(T_m^j - T_{m-1}^j) + \frac{(\Delta x)^2}{2 \alpha \Delta t} (T_m^{j+1} - T_m^j)]$$

This transient heat flux was then used to determine a transient convective heat transfer coefficient,  $h^j$

$$\frac{Q^j}{A} = h^j (T_g^j - T_m^j)$$

where  $T_g^j$  is the exhaust gas temperature at a time increment  $j$ .

The temperature distribution in the wall, the heat flux and the convective heat transfer coefficient were computed at every three degrees of the crank rotation, i.e. at 240 points in time during the engine cycle. A listing of the computer program is in Appendix G.

## 6.2 COMPARISON WITH FOURIER-SERIES EXPANSION METHOD

The solution to the above problem can also be obtained in a fourier series expansion. However, in order to obtain the temperature distribution in the wall it is necessary to express the gas wall temperature as a known function of time. To facilitate any easy comparison of the finite difference

approximation with the fourier series expansion method the gas wall temperature was expressed as cosine function (see Fig. 6.3) and the water wall temperature was assumed constant. The solution to the above problem expressed in a fourier series expansion can be found in Appendix C. The computer programs are listed in Appendix G. Since the temperature of the gas wall was being measured at every 3 degrees of crank rotation, this required the series to be summed 240 times for every engine cycle. The computer time involved in using the fourier expansion method for the above problem was found to be of the same order as the time required for the finite difference approximation method. The solutions, however, determined by using both the methods agreed extremely well. This can be seen in Fig. 6.4 where the instantaneous heat flux computed separately by each method is plotted. Moreover, in this study, each cycle had to be analysed individually which would require the determination of a new set of constants for the Fourier series for each cycle due to cycle to cycle variation. This would then cause a substantial increase in the computer time involved. The use of the finite difference approach was thus justified.

### 6.3 STABILITY OF THE FORWARD-DIFFERENCE TECHNIQUE AND THE SELECTION OF THE GRID IN SPACE AND TIME

It can be seen that for the finite difference approach, the larger the values of  $\Delta x$  and  $\Delta t$ , the more rapidly will the solution proceed. On the other hand, the smaller the value of these increments in the independent variables, the more accuracy will be obtained. However, the finite-difference equations limit these values. In order that the second law of Thermodynamics be not violated, a stability condition generated requires

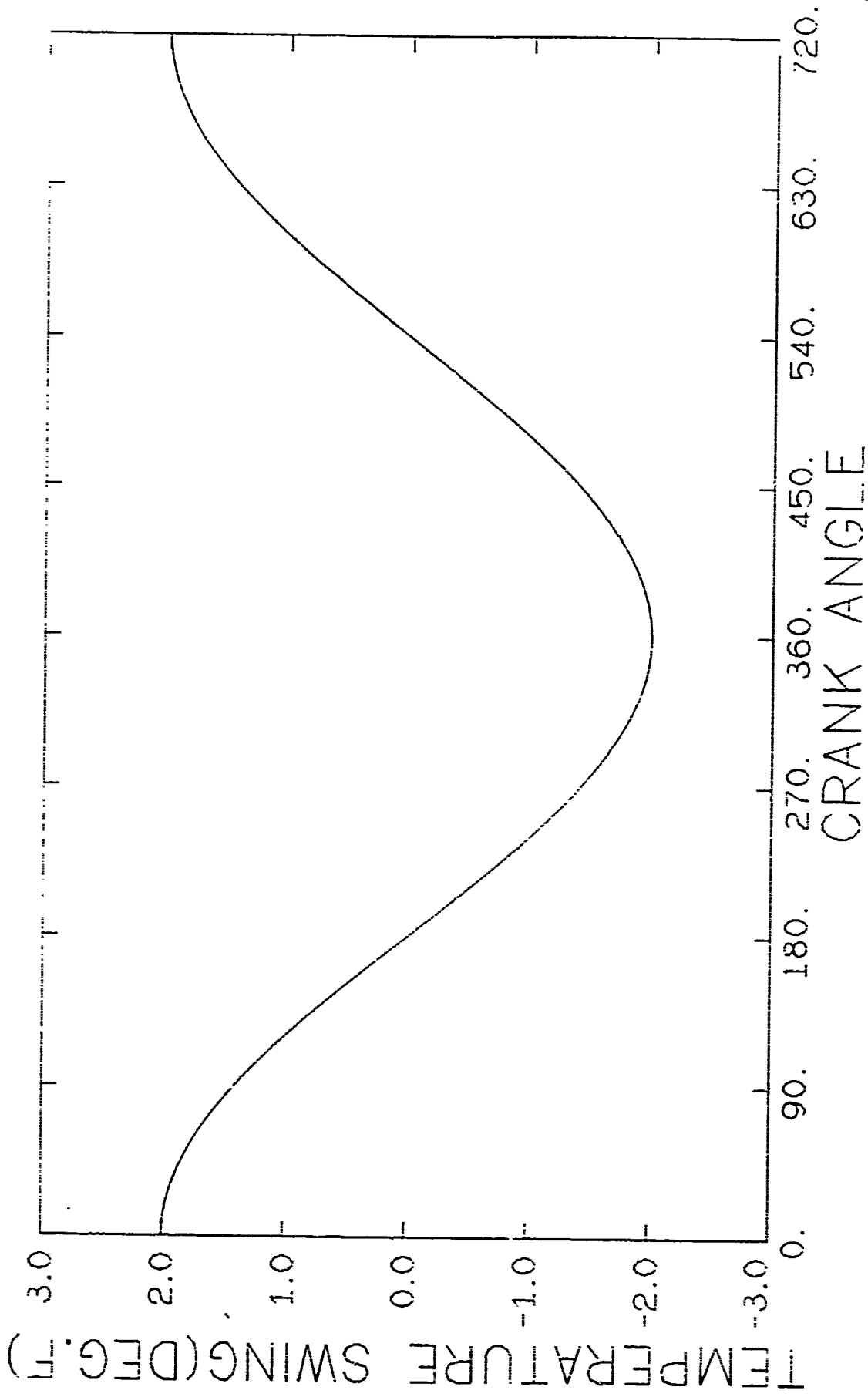


Figure 6.3 Gas side wall temperature swing expressed as a cosine function

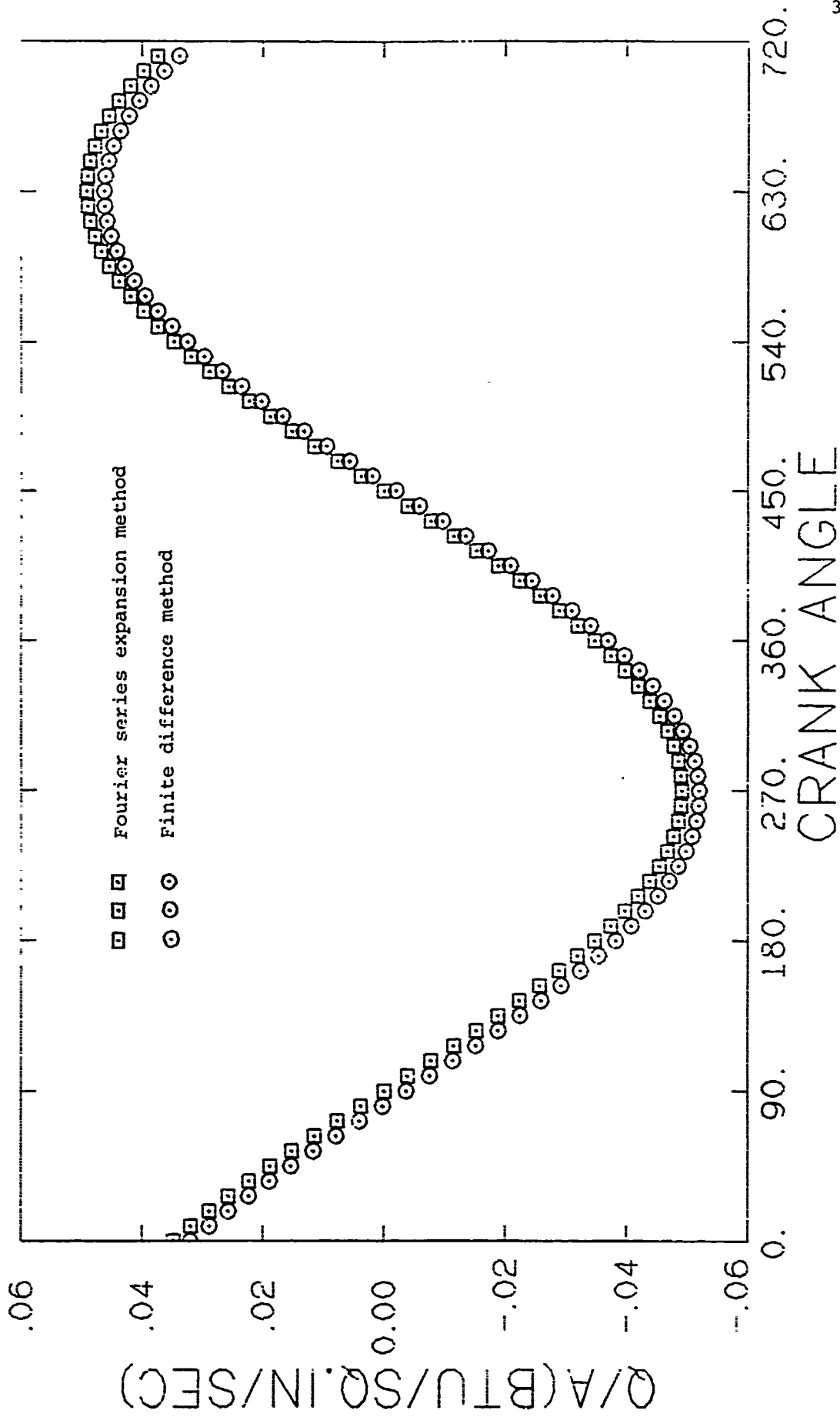


Figure 6.4 The instantaneous heat flux through a flat plate with one surface temperature expressed as a cosine function computed by both the finite difference and Fourier series expansion method.

$$\frac{(\Delta x)^2}{\alpha \Delta t} > 2$$

Since the gas wall temperature was measured at every 3 degrees crank rotation, the time step  $\Delta t$  was selected to be the time required to rotate the crank by 3 degrees. Thus the time step selected was a function of the engine rpm.

$$\Delta t = \frac{1}{2 \times (\text{rpm})} \quad \text{seconds}$$

Thus the stability condition required

$$\Delta x > \left( \frac{\alpha}{\text{rpm}} \right)^{1/2}$$

Assuming that the lowest engine rpm required for the experimental study was about 1000 rpm and also as

$$\alpha = 0.0055 \frac{\text{in}^2}{\text{sec}}$$

Then for stability

$$\Delta x > \left( \frac{0.0055}{1000} \right)^{1/2} = 0.0023 \text{ inch}$$

A safe value of  $\Delta x = 0.003$  inch was selected. The thickness of the wall was 0.156 inch. Then,

$$\text{Number of one dimension grids} = 0.156/0.003 = 52$$

$$\text{Number of Nodal points in the wall} = 53.$$

## 7. EXPERIMENTAL RESULTS AND DISCUSSION

The measured and calculated results of this study are presented and discussed in this chapter.

### 7.1 TYPICAL SET OF DATA

Figure 7.1 shows the gas side wall temperature swing and exhaust gas mass flow rate as a function of the crank rotation typically for one complete engine cycle measured at a single position in the test section. The gas side wall temperature swing and the exhaust gas temperature also as functions of the crank rotation for one engine cycle are shown in Figure 7.2. The trends of these curves can be best explained by looking at what happens during the exhaust period of the engine. As the exhaust valve opens, about  $55^\circ$  before BDC, the hot burnt gases at high pressure in the cylinder rush through the exhaust port into the test section displacing the volume of gas from the previous exhaust stroke. The movement of this relatively constant temperature volume of gas causes the initial rise in the wall temperature. The piston then pushes the remaining burnt gases in the cylinder through the test section on the exhaust stroke. The trends of the exhaust gas temperature correspond to the exhaust gas flow relatively closely. As the exhaust valve closes, at about  $40^\circ$  after TDC, the exhaust gas temperature starts to drop as thermal energy is being lost to the walls of the test section. The wall temperature then starts to drop after reaching its peak value and continues to do so till another pulse of hot gas drives it up again.,

Figure 7.3 displays the traces of the pressures from the upstream and downstream pressure transducers, the gas side wall temperature and the TDC pulses for one engine cycle. After the exhaust valve closes the pressures continue to oscillate due to reflected pressure waves in the exhaust pipe. At

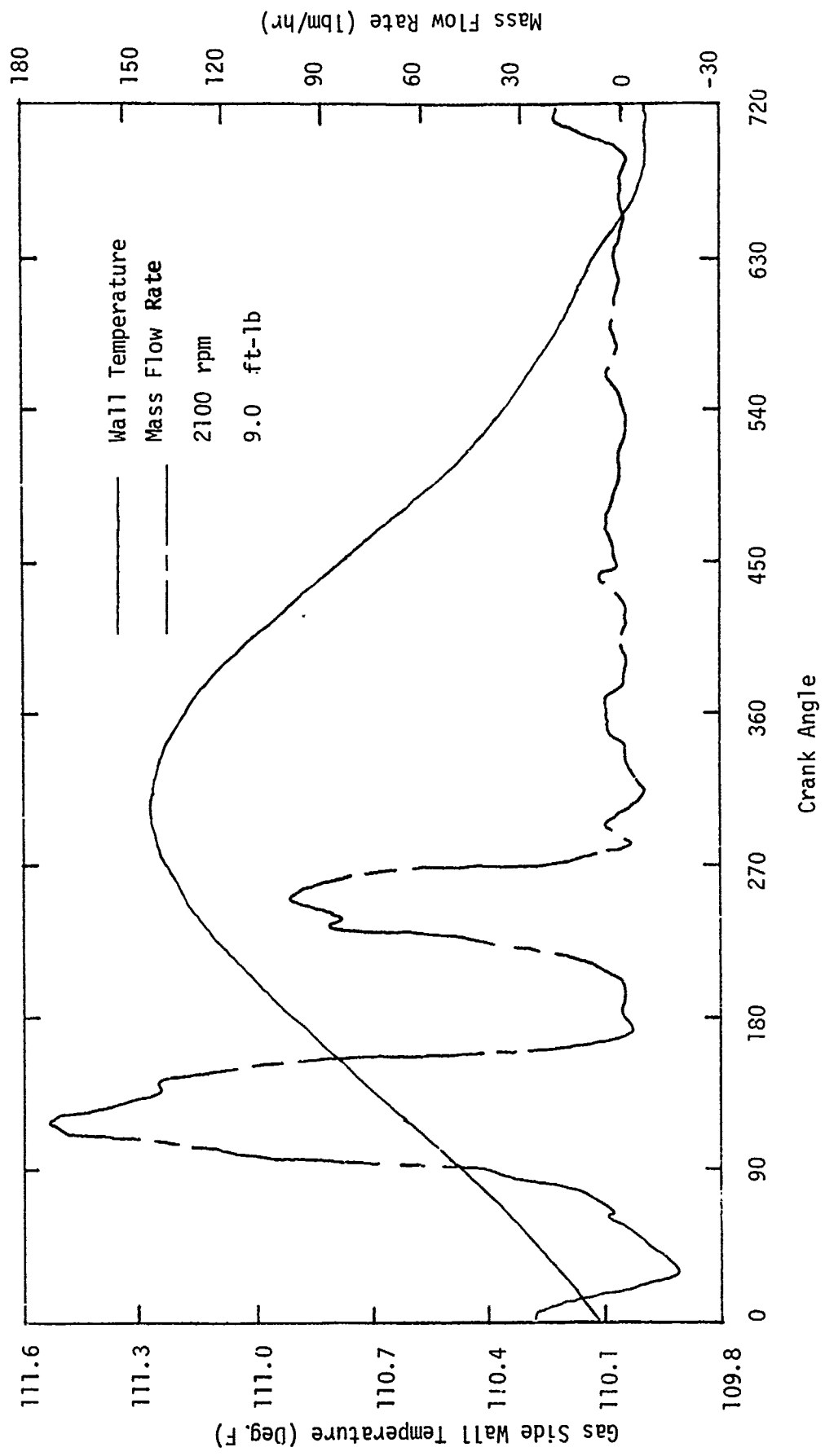


Figure 7.1 A typical plot of the gas side wall temperature swing and the exhaust gas mass flow rate as a function of the crank angle

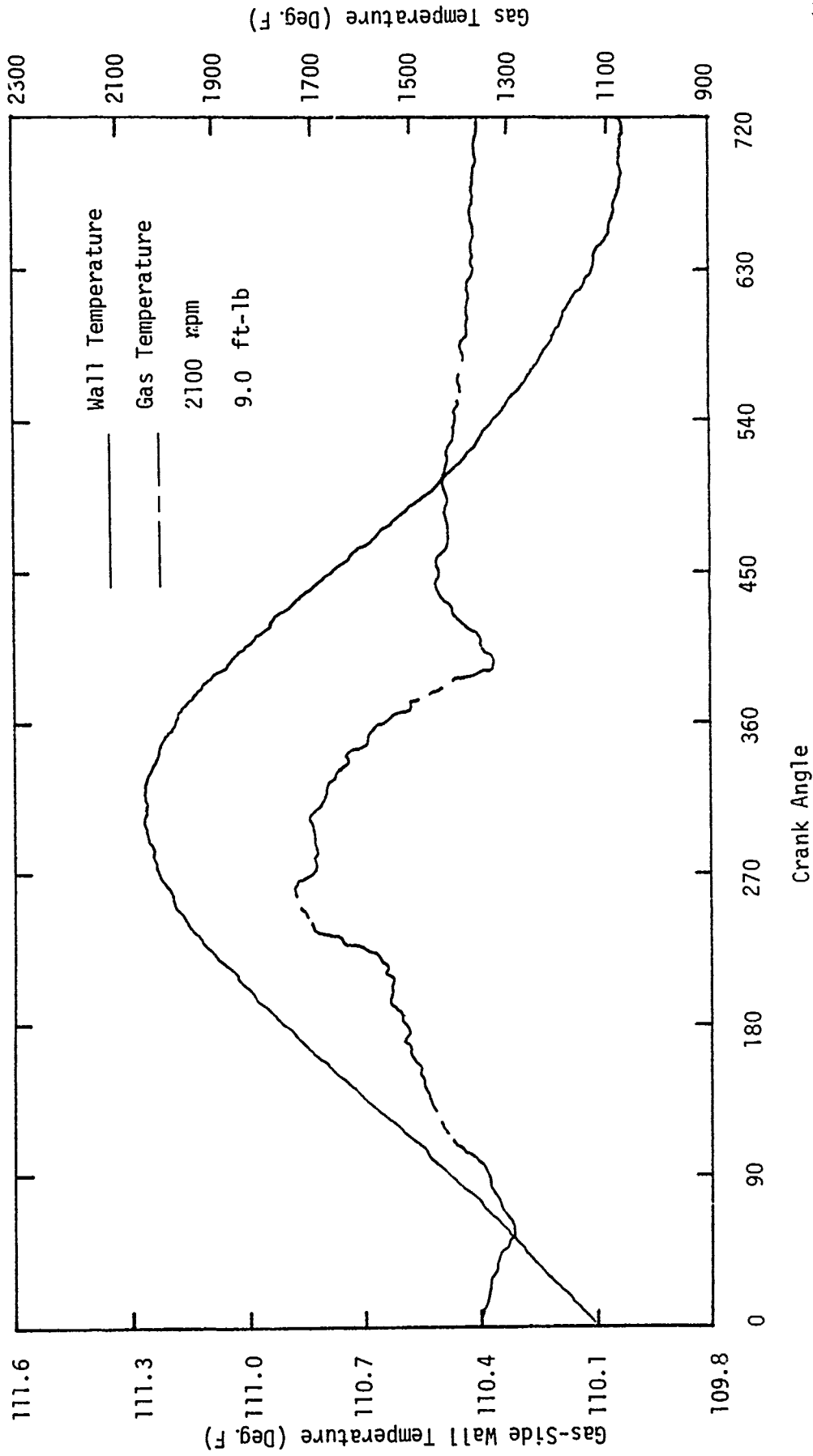


Figure 7.2 A typical plot of the gas side wall temperature swing and the exhaust gas temperature as a function of the crank angle

the engine rpm of 2100 the period of these pulsations was noticed to be about 75 degrees of crank rotation. For a pressure pulse at sonic velocity  $c$ , to travel the pipe length,  $\ell$ , and return, the time required,  $t$  secs, or equivalently the crank rotation,  $\theta$ , in degrees can be computed

$$t = \frac{2\ell}{c} \text{ sec}$$

$$\theta = \frac{2\ell}{c} \times 6 \times (\text{rpm})$$

The pipe length,  $\ell$ , was approximately 3.5 ft. For a gas temperature of  $600^{\circ}$  F, the sonic velocity  $c$  is approximately 1590 ft./sec.

$$\theta = \frac{2(3.5)}{1590} \times 6 \times 2100 = 56^{\circ}$$

The calculated period was thus found to differ from the observed period of pulsation slightly.

Figure 7.4 shows the consistency in the pressure, gas side wall temperature and exhaust gas temperature data for a number of engine cycles. Both Figure 7.3 and Figure 7.4 are photographs of actual raw data as displayed on an oscilloscope before digitization. The precise measurement of relatively small changes in the gas wall temperature is extremely important in computing instantaneous heat fluxes at the gas side wall. A typical graph of the computed instantaneous heat flux that the test section wall as a function of the crank rotation for one engine cycle is depicted in Figure 7.5 for the same engine condition. The corresponding computed heat transfer coefficient as a function of the crank rotation is shown in Figure 7.6. The trends of both the instantaneous heat flux and the heat transfer coefficient are found to follow each other relatively closely. The heat transfer coefficient curve, however, tends to drop slightly earlier due to the increasing exhaust gas temperature.

## 7.2 WALL TEMPERATURE RISE DUE TO MOVEMENT OF VOLUME OF GAS IN TEST SECTION

### FROM PREVIOUS EXHAUST STROKE

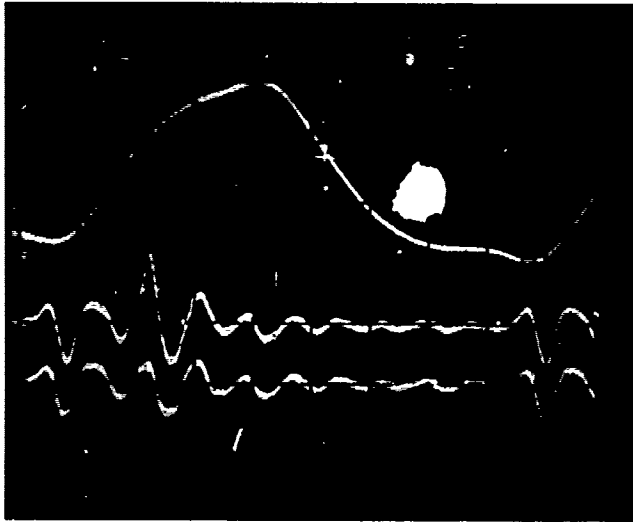


Figure 7.3 A typical oscilloscope trace of the gas side wall temperature and the upstream and downstream pressures

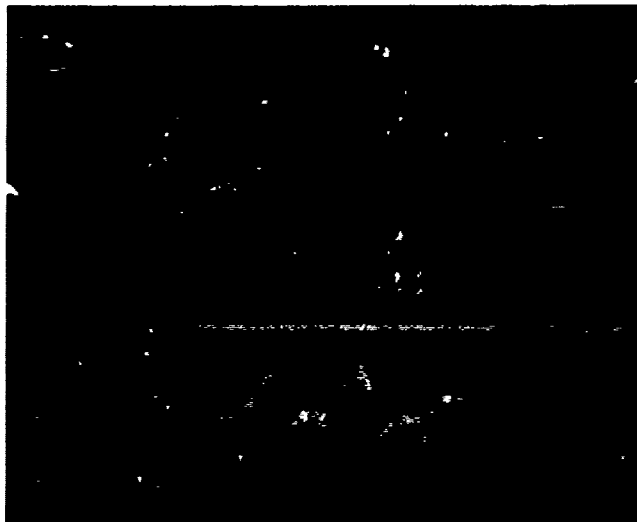


Figure 7.4 Oscilloscope trace showing the consistency in the upstream pressure, gas side wall temperature data for 6 consecutive engine cycles

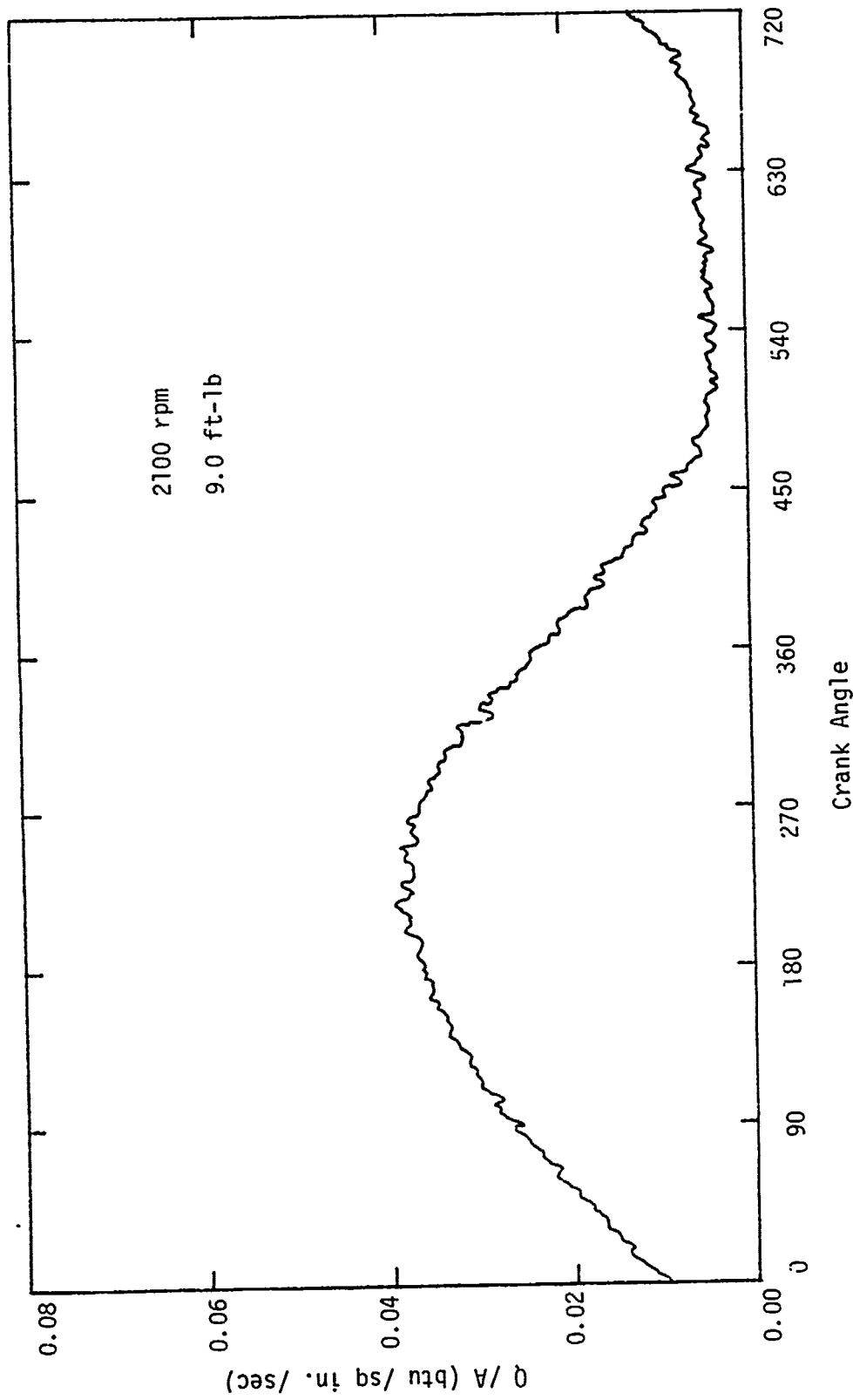


Figure 7.5 A typical plot of the instantaneous heat flux as a function of the crank angle

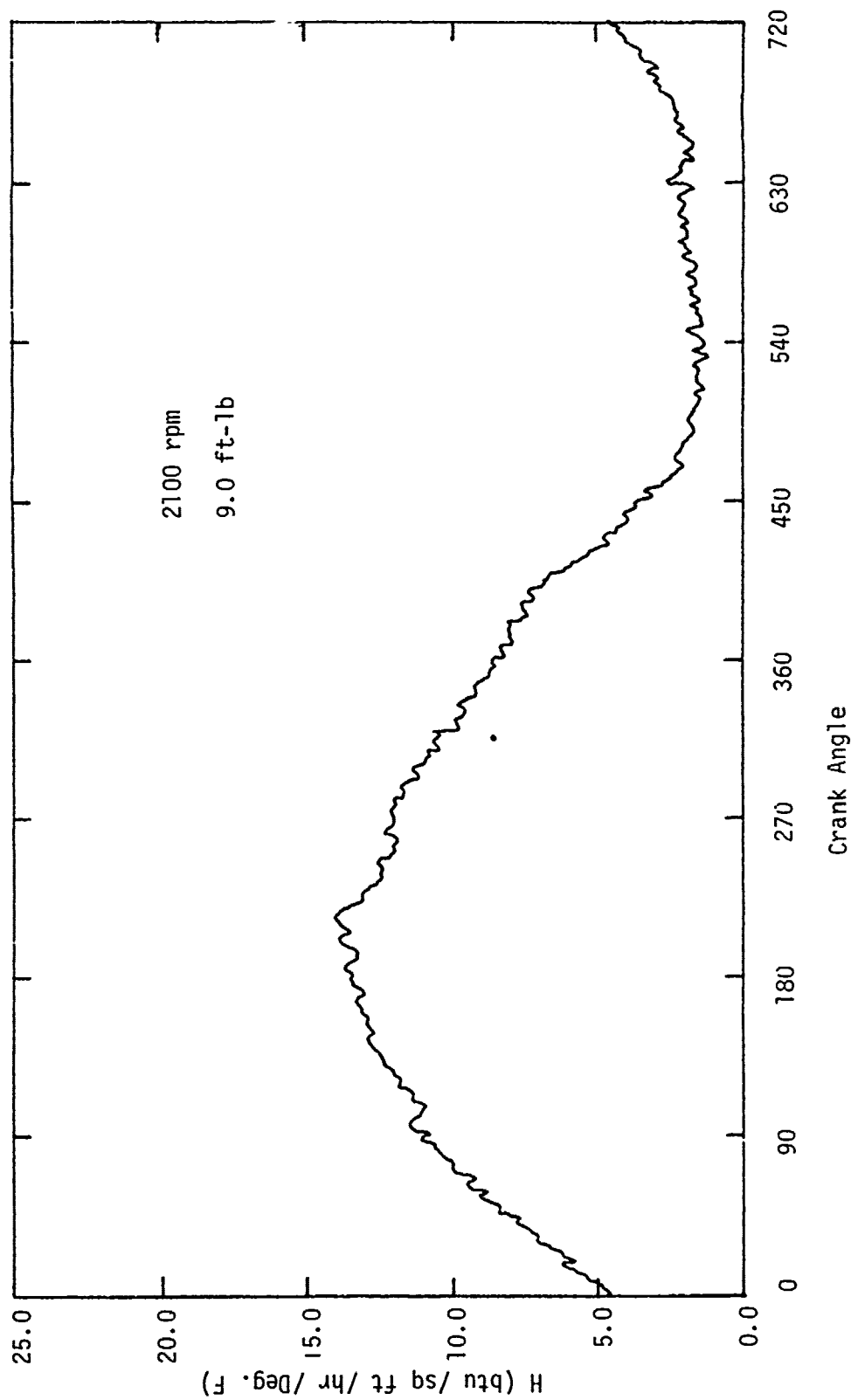


Figure 7.6 A typical plot of the instantaneous heat transfer coefficient as a function of the crank angle

Figures 7.7 and 7.8 display the traces of the gas side wall temperature and the exhaust gas temperature as a function of time for a single engine cycle. It was observed that for very low engine speeds, the rise in the gas side wall temperature begins even before the exhaust gas temperature starts to rise. (Figure 7.7). On the other hand at high engine speeds the rise in the wall temperature follows closely with the rise in the exhaust gas temperature. This phenomenon can first be physically explained by observing what happens during the periods the exhaust valve is closed and open. When the exhaust valve is closed, there is a cold boundary layer of gas insulating the wall from the volume of gas from the previous exhaust stroke resulting in a little or no temperature rise in the wall. As the exhaust valve opens, the high pressure gases from the cylinder rush out through the exhaust port into the test section displacing the volume of gas. The large increase in the gas velocity then causes the rise in the wall temperature even before the hot gas pulse from the cylinder actually reaches that particular location in the test section. At high engine speeds the time required to displace the volume of gas until the hot exhaust gas pulse arrives at the particular location in the test section is reduced. As a result the rise in the gas side wall temperature due to the movement of this volume of gas is also reduced.

The above result was confirmed by carrying out a simulation of the gas side wall temperature rise in the test section due to a sudden flow of gas at a constant temperature using a stepwise function for the heat transfer coefficient. (See Appendix E). The simulation was carried out for various engine speeds. For an engine speed of 1700 rpm and a constant gas temperature of  $1000^{\circ}$  F, the wall temperature was found to rise  $0.87^{\circ}$ F over a crank rotation of  $180^{\circ}$ . At the same position in the test section, for an engine speed of 3400 rpm and a constant gas temperature of  $1000^{\circ}$  F, the wall

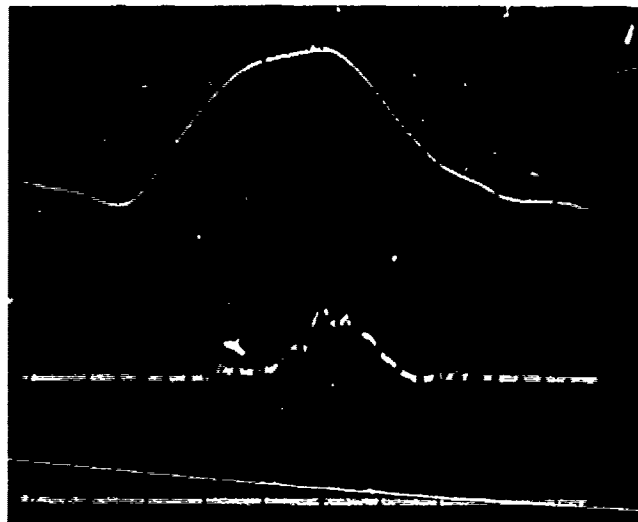


Figure 7.7 Oscilloscope trace of the gas side wall temperature and the exhaust gas temperature for an engine speed of 1700 rpm and under no load conditions



Figure 7.8 Oscilloscope trace of the gas side wall temperature and the exhaust gas temperatures for an engine speed of 3000 rpm and engine load of 20 ft-lb

temperature was found to actually decrease  $0.02^{\circ}\text{F}$  over a period of  $180^{\circ}$  of crank rotation. These results from the simulation agree quite well with the experimental data confirming the physical reasoning.

### 7.3 EFFECT OF TEST SECTION GEOMETRY

Figure 7.9 shows the gas side wall temperature swing at each of the four positions in the test section plotted as a function of the crank angle for the same engine run. The highest temperature swings were observed at positions 4 and 2, while the lowest temperature swings were recorded at positions 1 and 3. These results can be attributed to the curved geometry of the flow region, where the highest gas velocities occur near the wide radius of the curve. Moreover, a higher degree of turbulent mixing takes place near position 4 resulting in higher heat transfer to the wall.

Figure 7.10 shows the exhaust gas temperature as a function of the crank rotation at the two locations of measurement in the test section for the same engine conditions. An average decrease of approximately  $250^{\circ}\text{F}$  in the gas temperature, between the upstream and downstream location, was observed. The computed instantaneous heat flux and the instantaneous heat transfer coefficient at each of the four positions for the same engine run are shown in Figure 7.11 and 7.12 respectively. It can be seen that the trends of these two curves follow closely with those of the wall temperature swings at the various positions in the test section. The heat flux was found to be the highest at position 4 and lowest at position 1. Moreover, the heat flux at the gas side wall at positions 2 and 3 was found to drop more rapidly and earlier during the engine cycle and remained at a low value for the remaining duration of the cycle. This trend was more pronounced at lower engine speeds. The instantaneous heat transfer coefficient curves were found to follow similar trends at the four different positions in the test section.

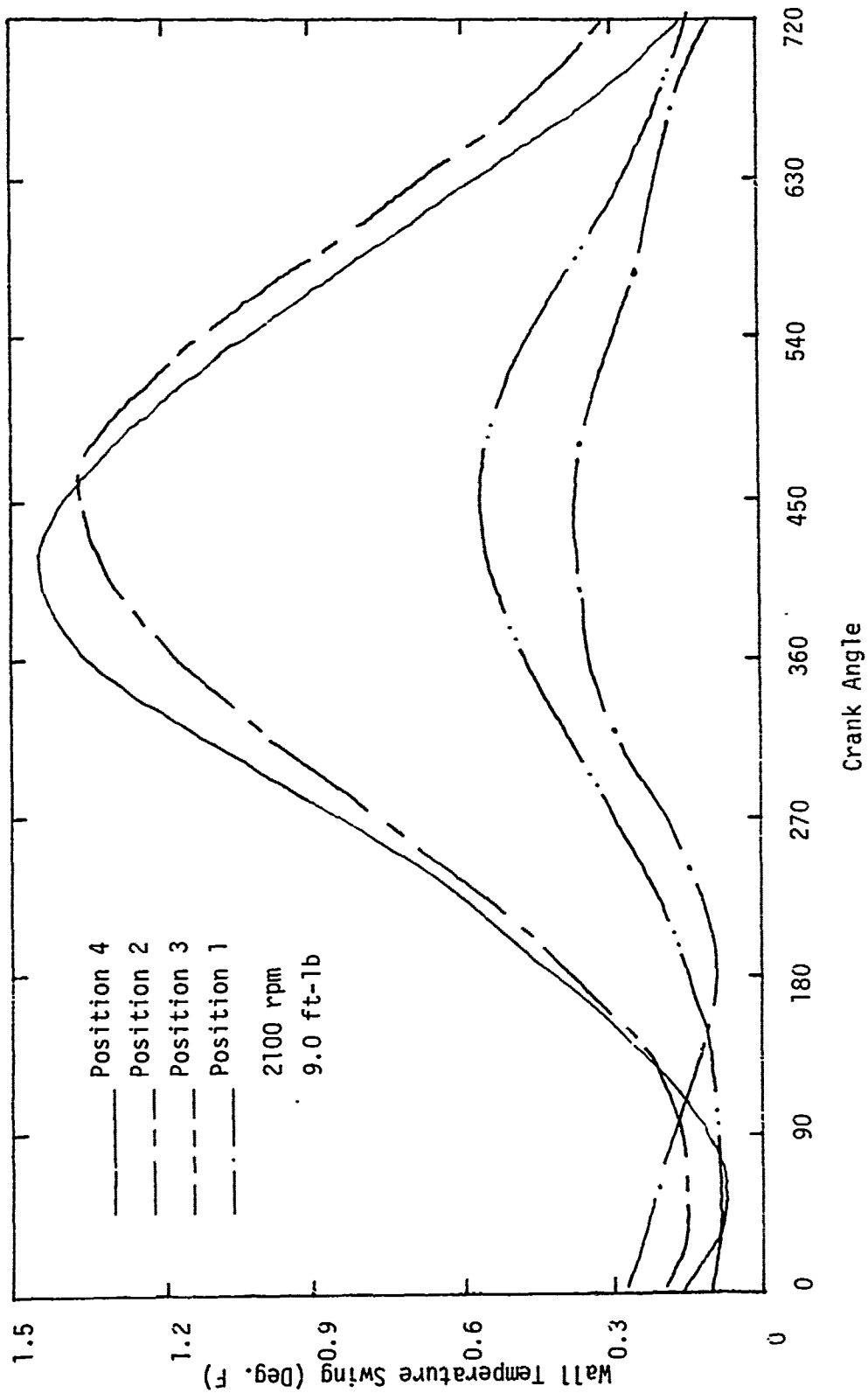


Figure 7.9 Effect of geometrical position in the test section on the gas side wall temperature swing

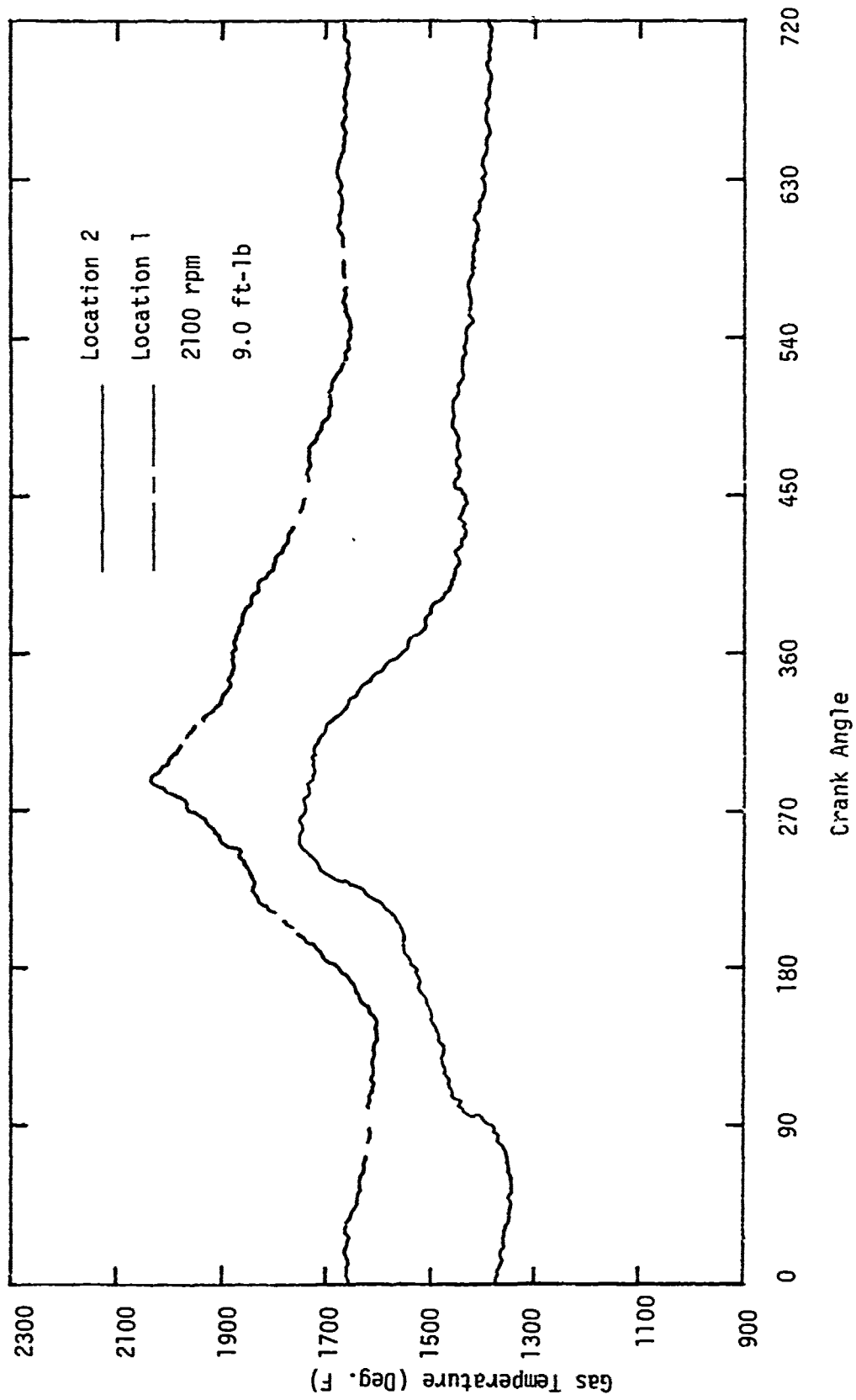


Figure 7.10 Effect of axial location in the test section on the exhaust gas temperature

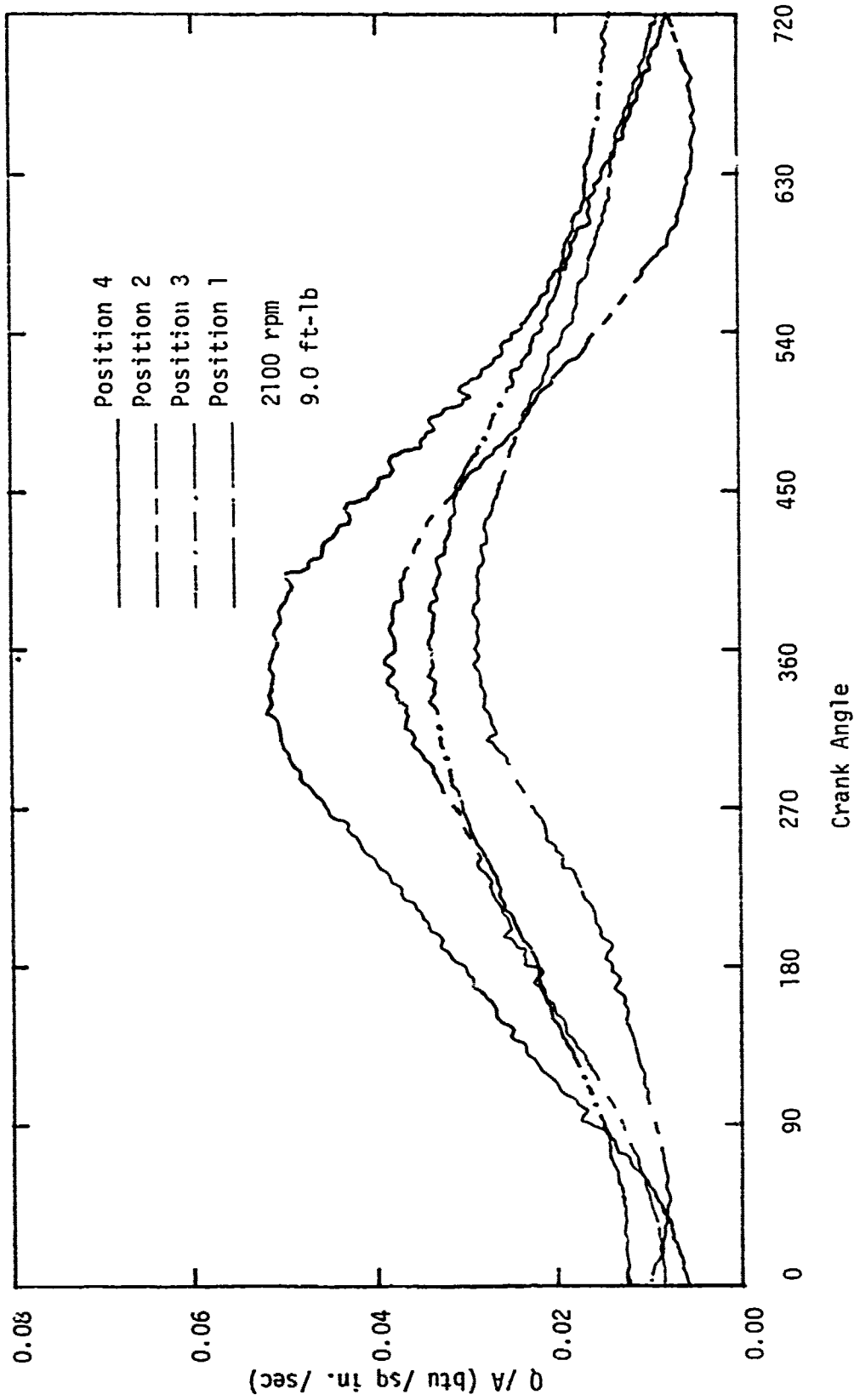


Figure 7.11 Effect of geometrical position in the test section on the instantaneous heat flux

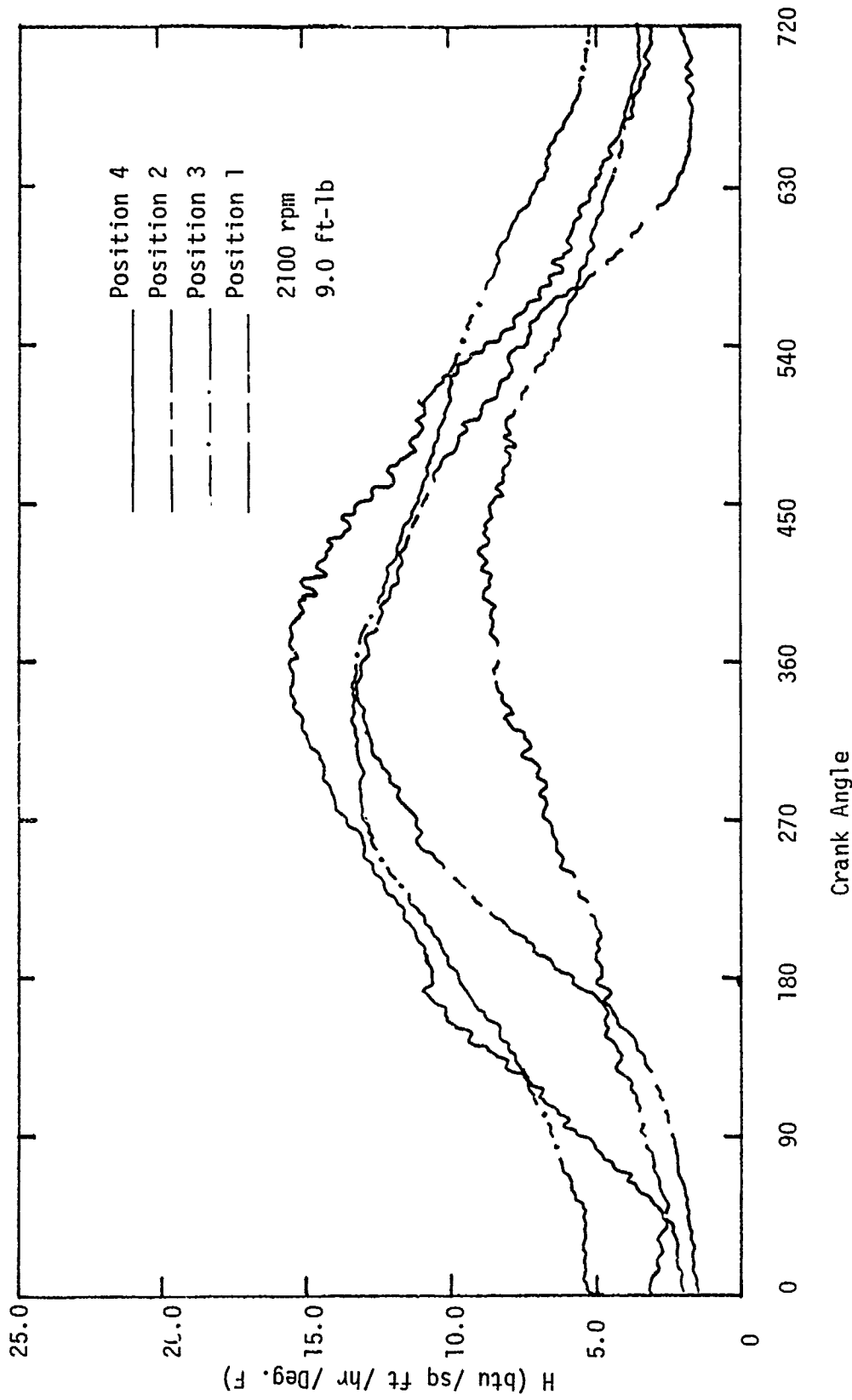


Figure 7.12 Effect of geometrical position in the test section on the instantaneous heat transfer coefficient

#### 7.4 EFFECT OF ENGINE SPEED AND ENGINE LOAD

The effect of engine speed and load on the instantaneous heat flux and the instantaneous heat transfer coefficient curves for a particular position in the test section can be best understood by looking at the gas side wall temperature swing and the exhaust gas temperature curves measured at various engine speeds and loads at that position. The effect of increasing engine speed and load on the wall temperature swing at position 4 is shown in Figure 7.13. The effect of increasing the engine speed is to reduce the temperature swing of the gas side wall and also to shift the peak of the gas side wall temperature curve to a later point of time in the engine cycle. This is because at higher engine speeds the time for the wall temperature to rise, i.e., the rise time, is reduced resulting in a larger fraction of the heat energy to be lost in the exhaust and consequently a decrease in the wall temperature swing during the engine cycle. These trends were also confirmed by carrying out a simulation as explained in the previous section. For more details see Appendix E.

The effect of increasing the engine load is to increase the mean temperature of the gas side wall and hence the mean temperature difference between the gas side wall and the water side wall resulting in a higher heat flux at the wall. This reaction is expected as the engine must consume more fuel and air to accommodate the increased load causing an increase in the exhaust gas mass flow rates and exhaust gas temperatures. The wall temperature swing curves were found to follow similar trends at the other positions in the test section for increasing engine speeds and loads as shown in figure 7.14, 7.15 and 7.16 for position 3, 2 and 1 respectively.

The effect of increasing engine speed and load on the exhaust gas temperature during the engine cycle is shown in figures 7.17 and 7.18 for the

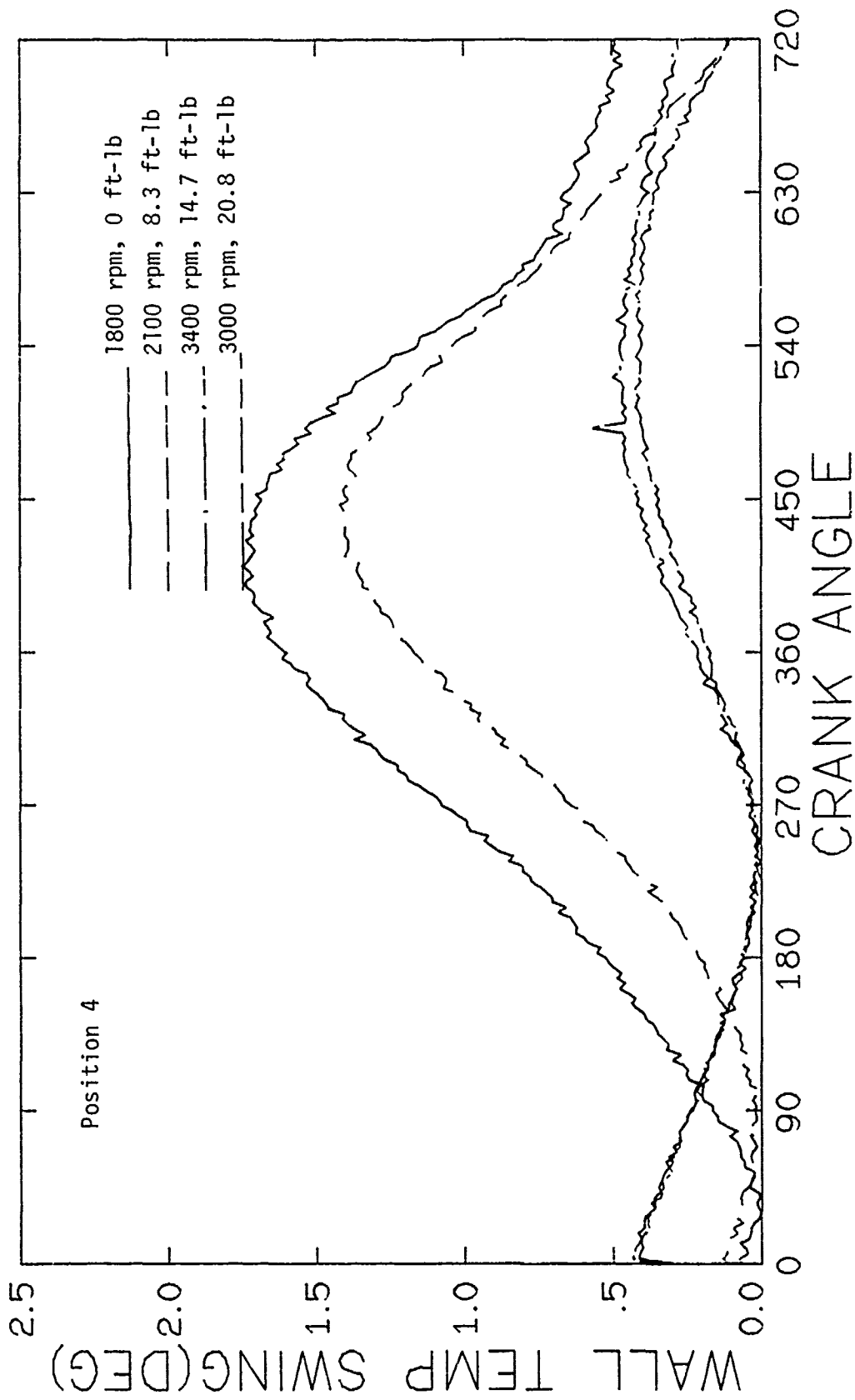


Figure 7.13 Effect of engine speed and load on the gas side wall temperature swing at position 4 in the test section

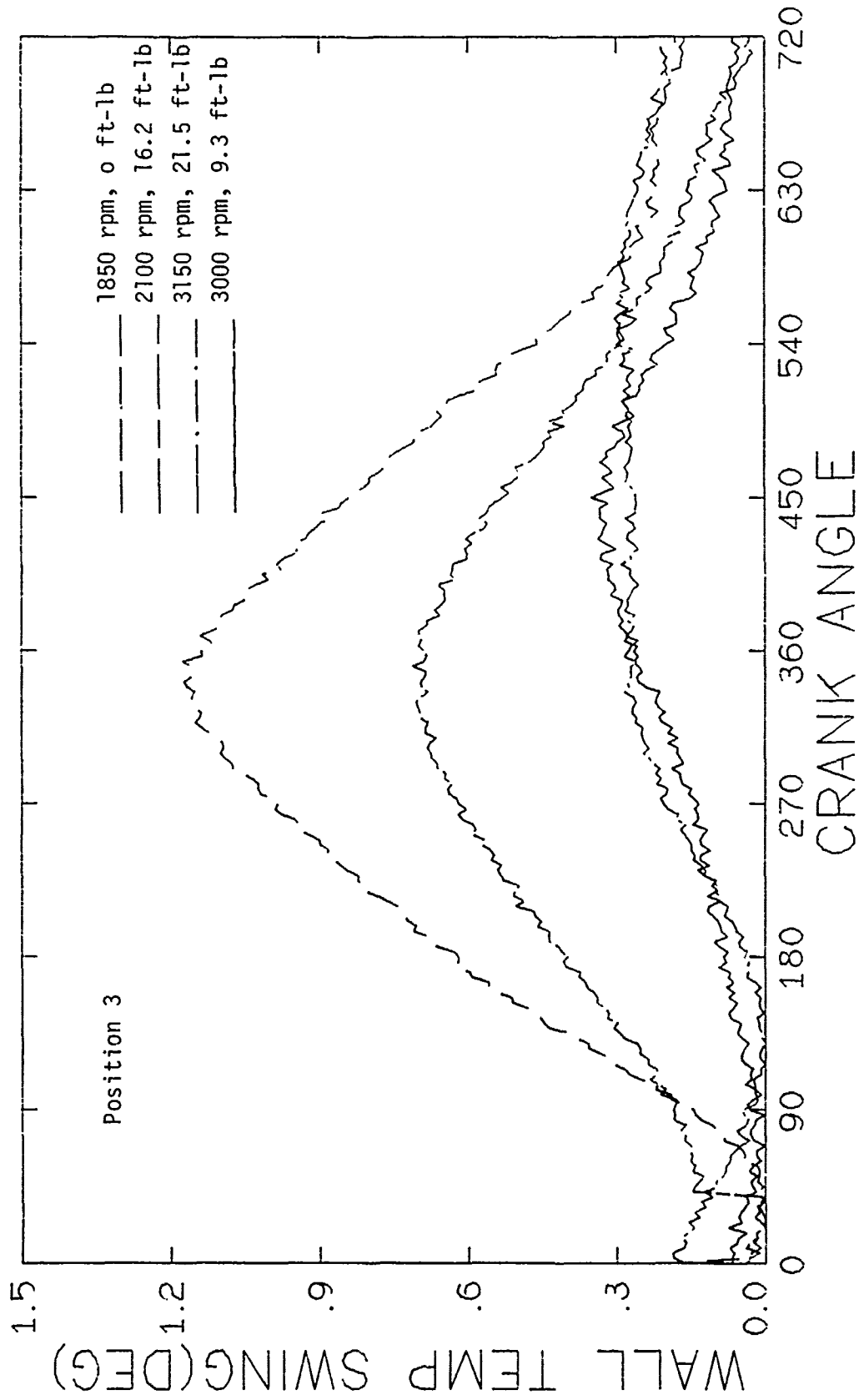


Figure 7.14 Effect of engine speed and load on the gas side wall temperature swing at position 3 in the test section

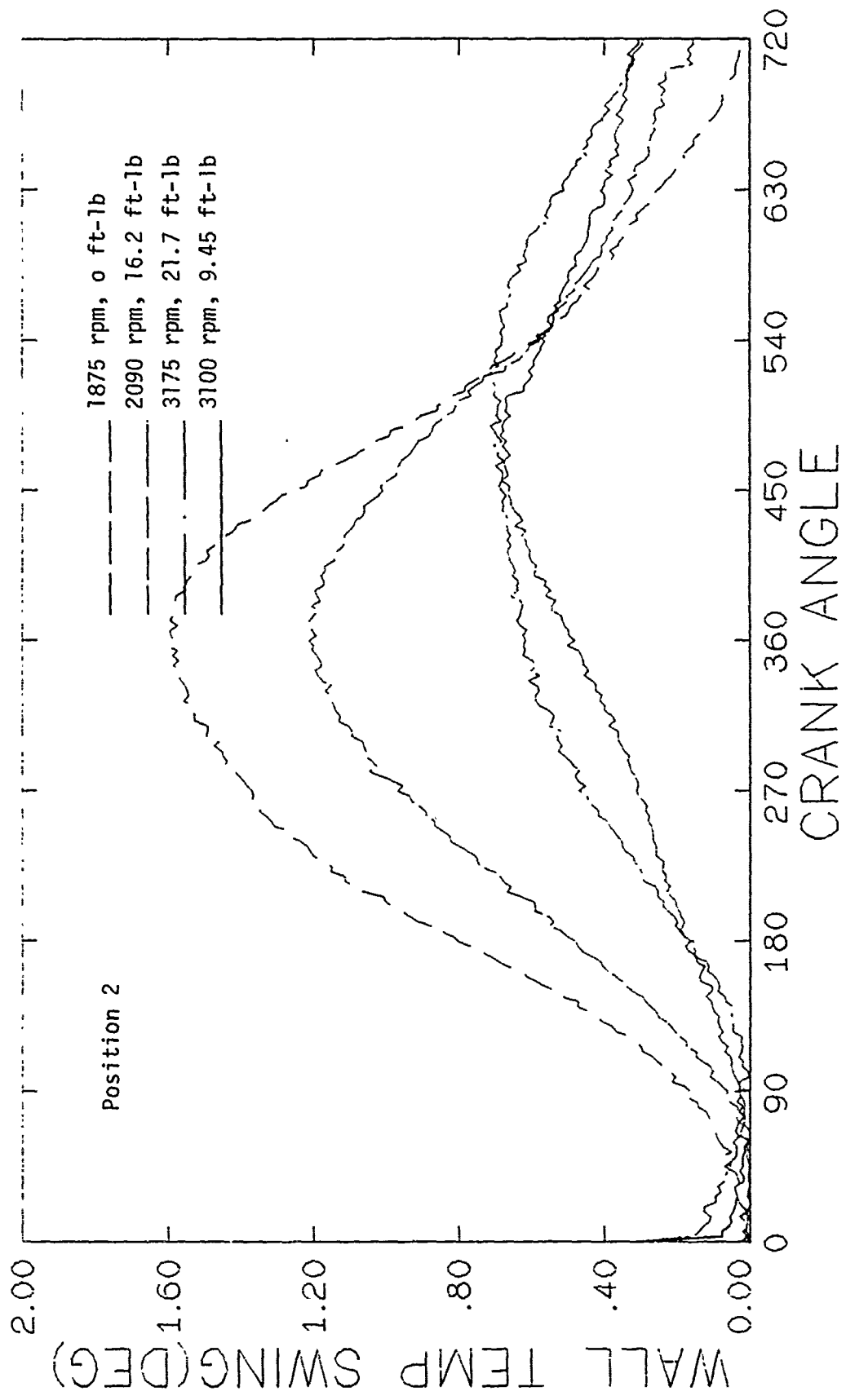


Figure 7.15 Effect of engine speed and load in the gas side wall temperature swing at position 2 in the test section

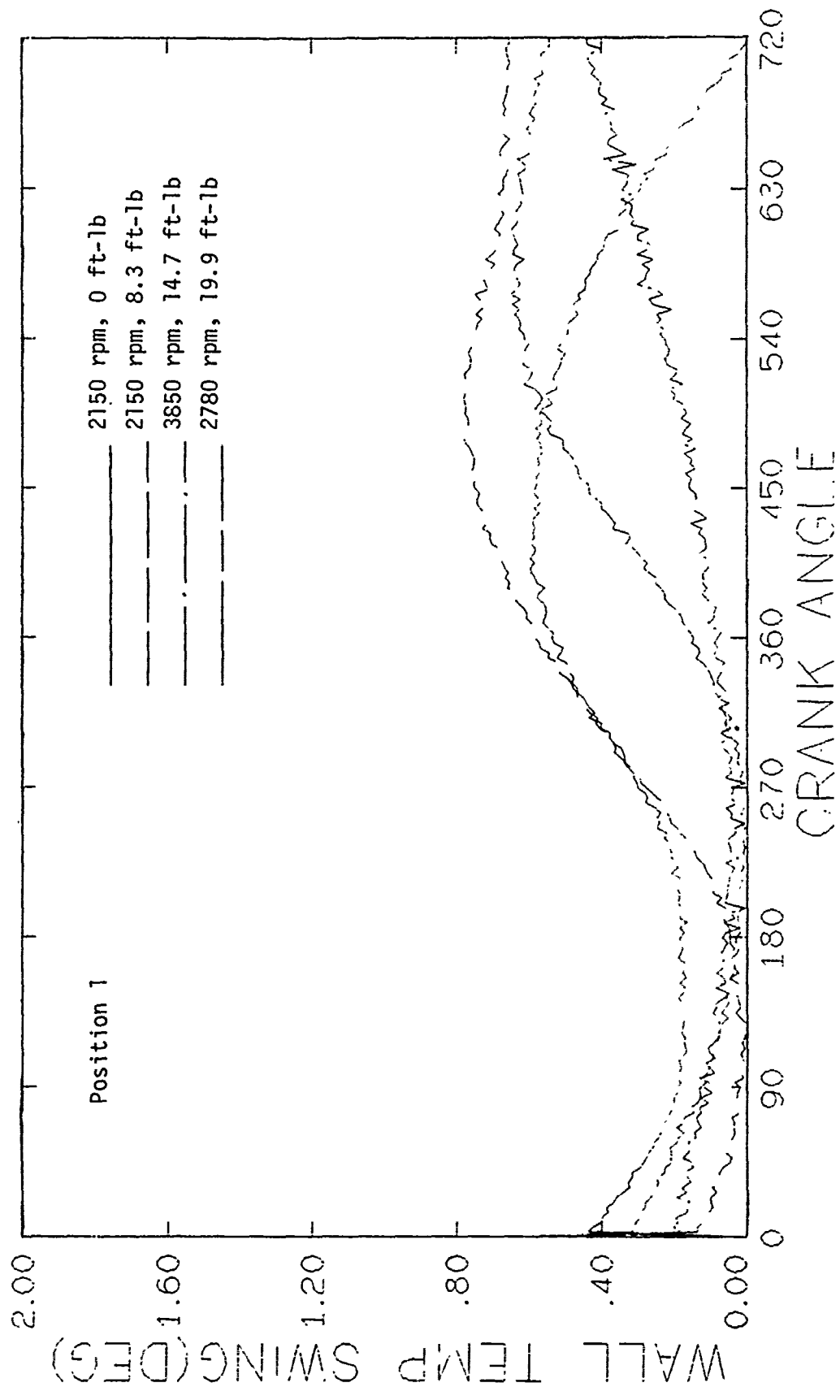


Figure 7.16 Effect of engine speed and load on the gas side wall temperature swing at position 1 in the test section

upstream and downstream locations in the test section. The exhaust gas temperature, while on one hand was little effected by the engine speed, increased with an increase in the engine load. As can be seen the exhaust gas temperature was more sensitive to change in engine loads at the upstream location (location 1) as compared to the downstream location. (location 2).

The trends of the computed instantaneous heat flux curves depend on the instantaneous temperature distribution in the wall, and thus follow closely with the gas side wall temperature swing. The heat flux at the wall, however, starts dropping before the gas side wall temperature reaches its maximum. The effects of engine speed and load on the instantaneous heat flux curves at each of the four positions in the test section are shown in Figures 7.17, 7.18, 7.19 and 7.20. At higher engine speeds and loads the heat flux curves tend to remain flat and high during the engine cycle. With a decrease in engine speed and load the heat flux was found to drop more rapidly and earlier during the engine cycle. Similar trends were observed for the computed instantaneous heat transfer coefficient curves as shown in Figures 7.21, 7.22, 7.23 and 7.24 for each of the four positions.

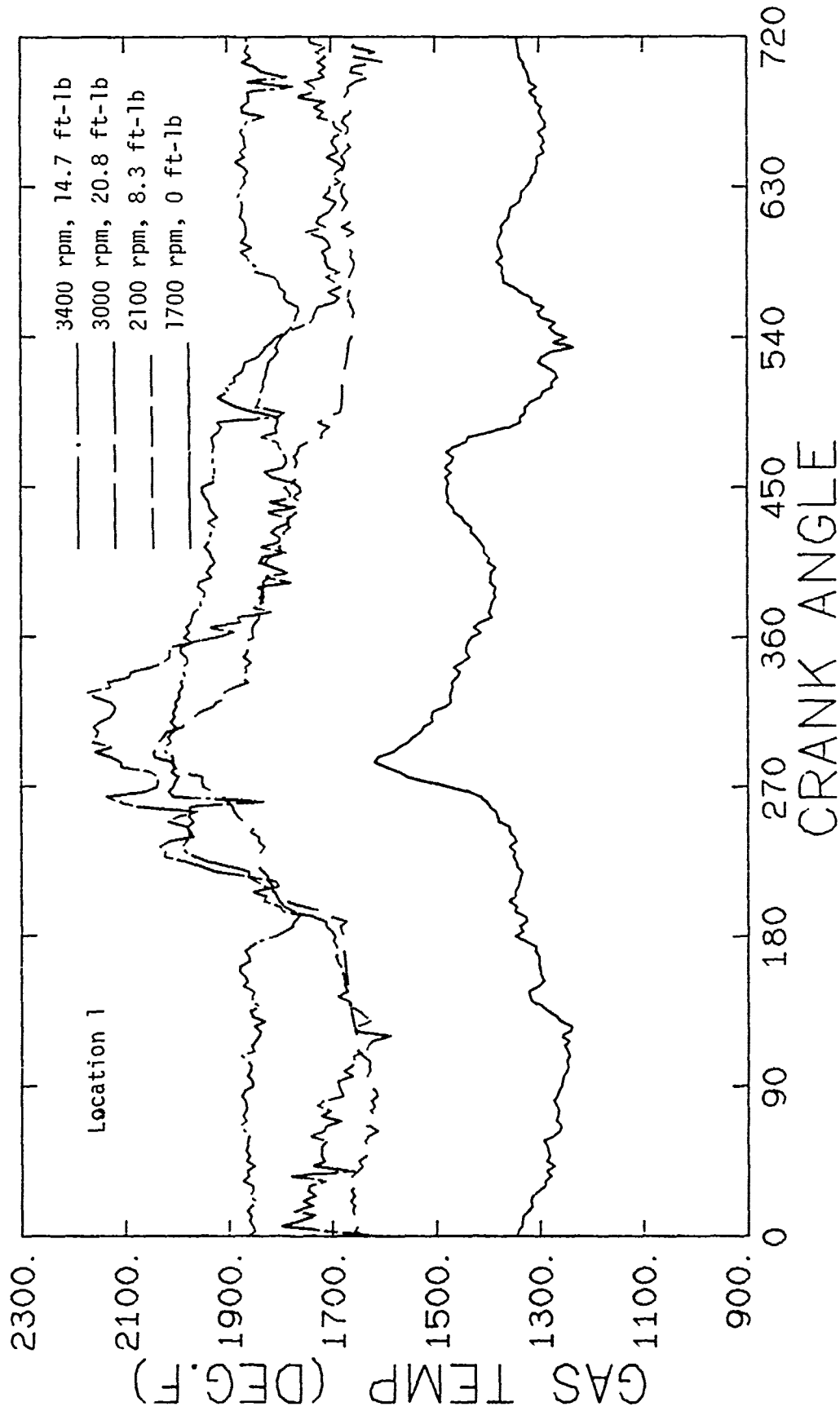


Figure 7.17 Effect of engine speed and load on the exhaust gas temperature at location 1 in the test section

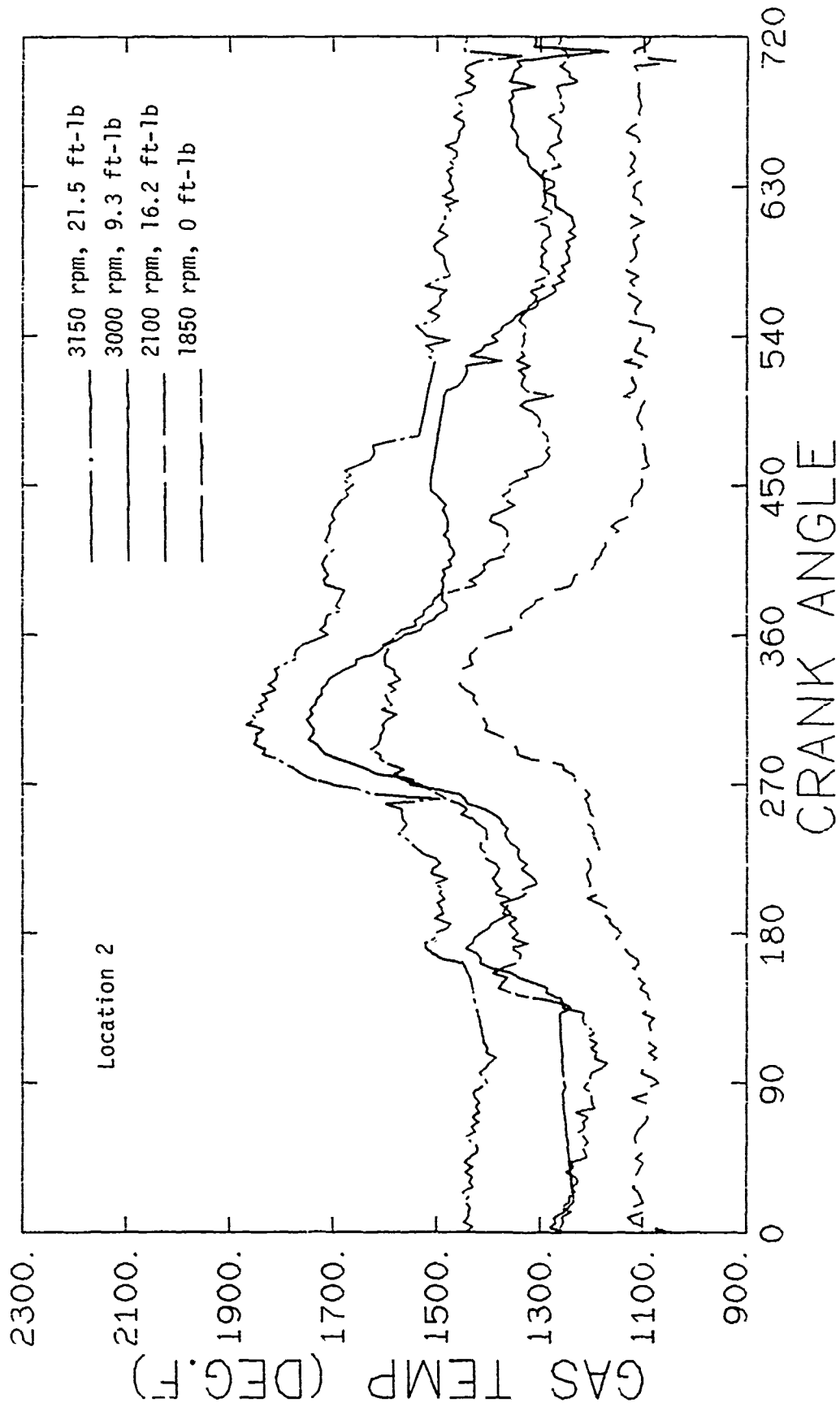


Figure 7.18 Effect of engine speed and load on the exhaust gas temperature at location 2 in the test section

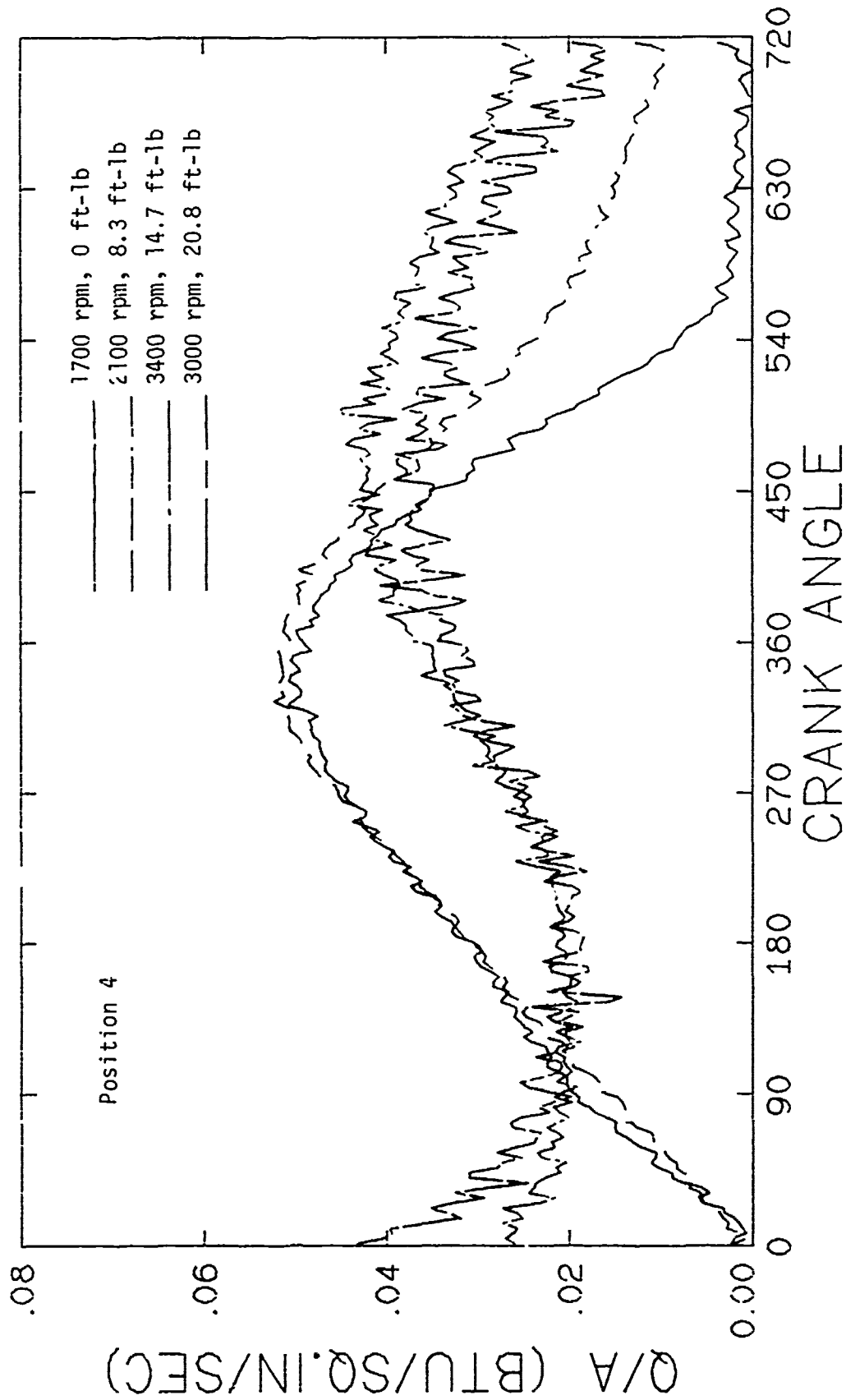


Figure 7.19 Effect of engine speed and load on the instantaneous heat flux at position 4 in the test section

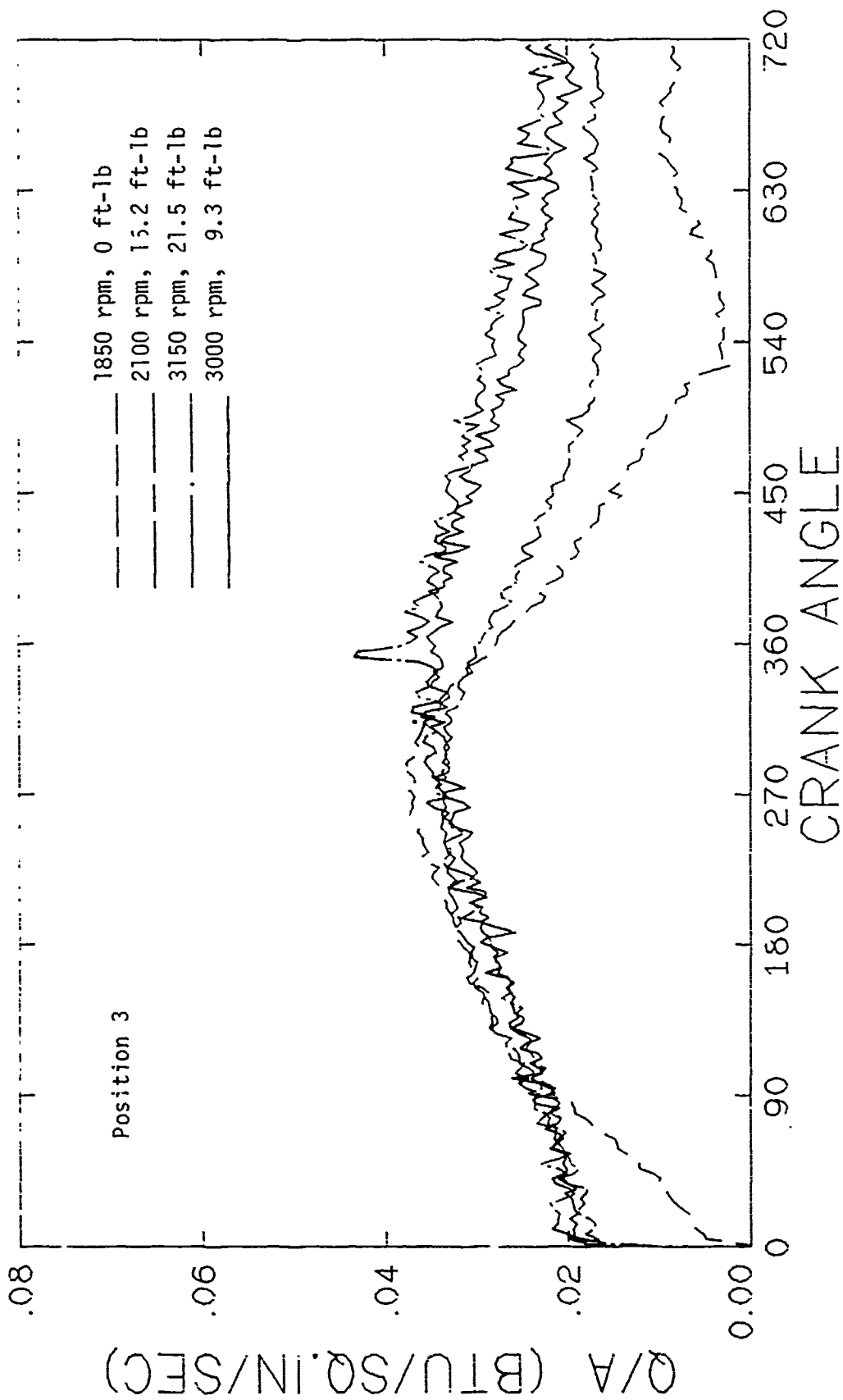


Figure 7.20 Effect of engine speed and load on the instantaneous heat flux at position 3 in the test section

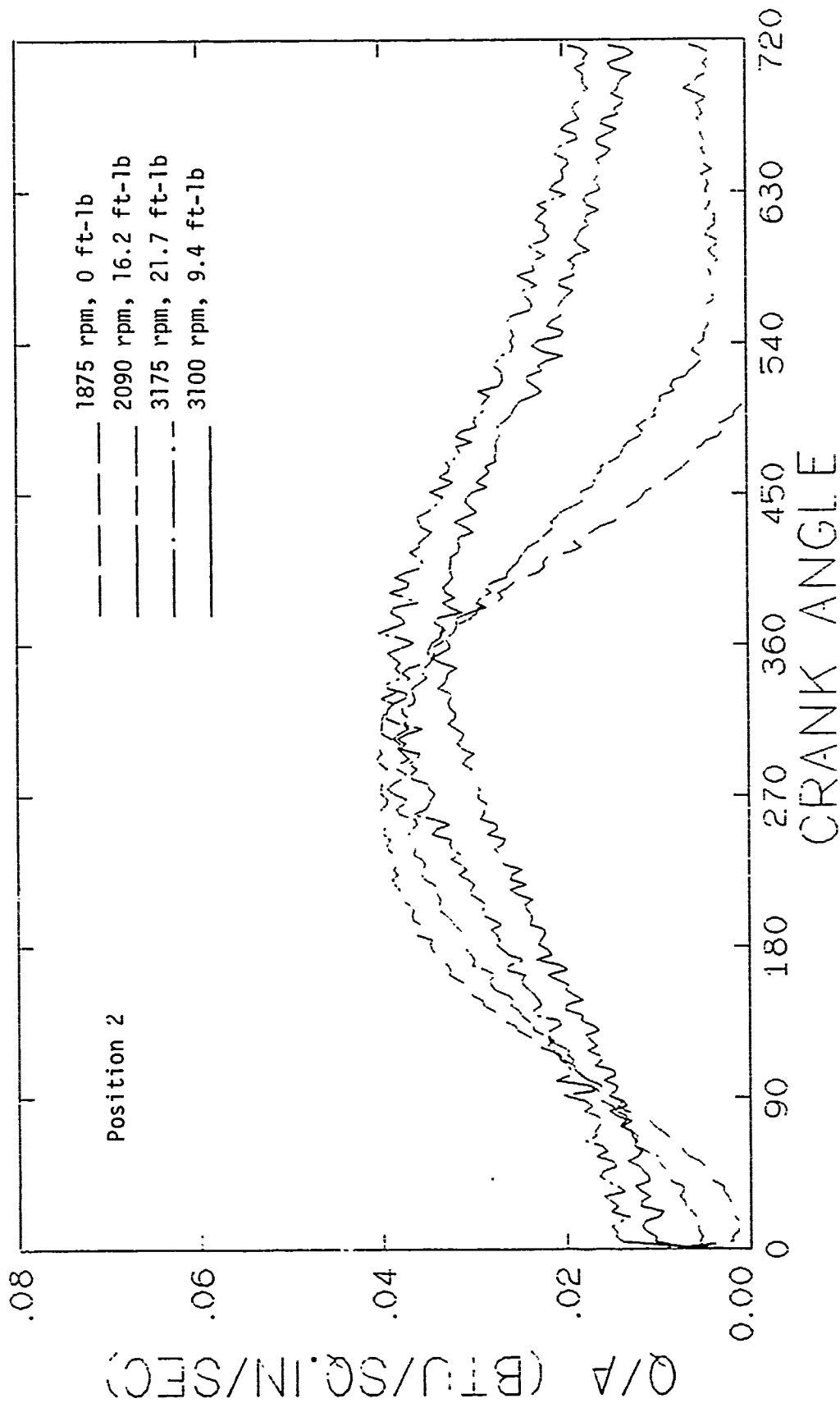


Figure 7.21 Effect of engine speed load on the instantaneous heat flux at position 2 in the test section

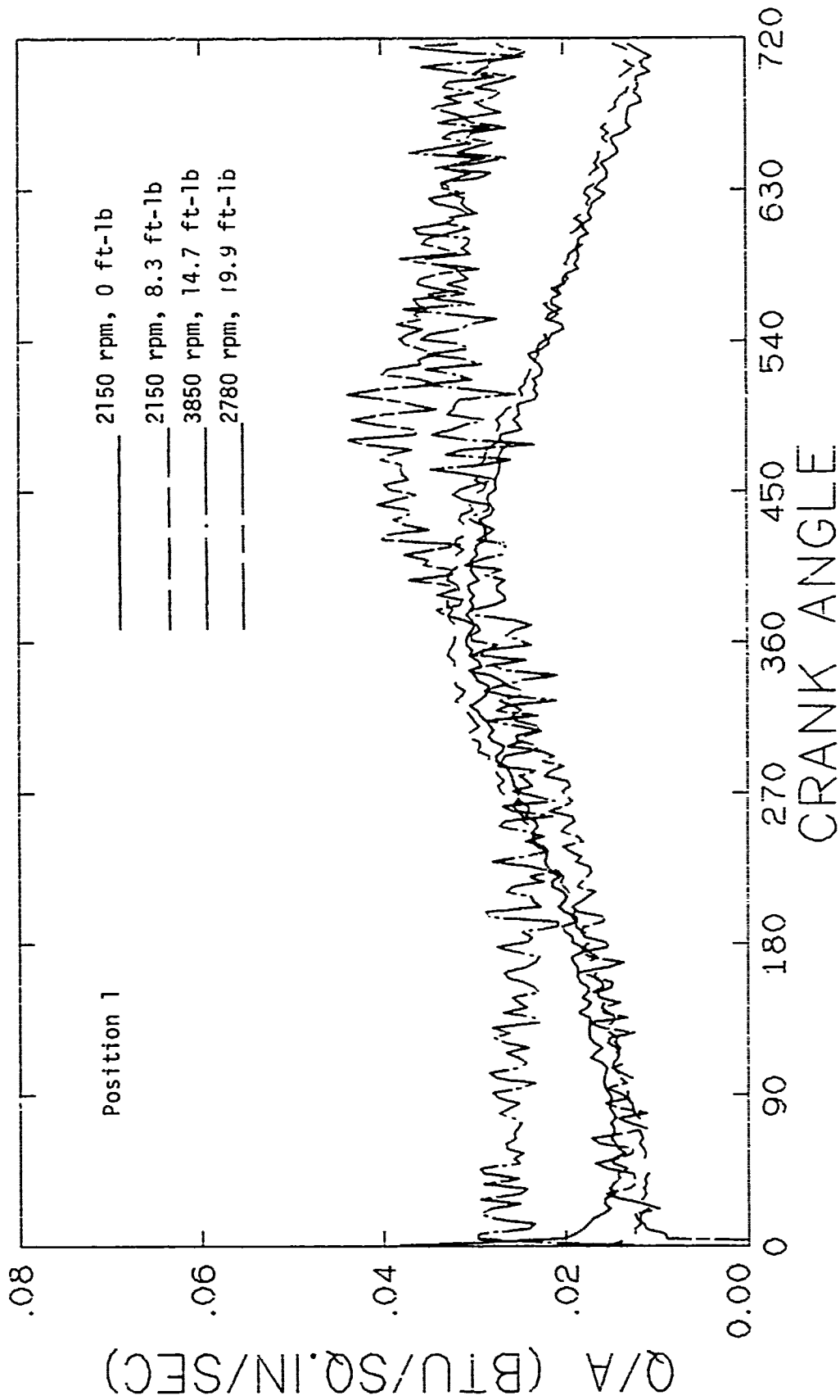


Figure 7.22 Effect of engine speed and load on the instantaneous heat flux at position 1 in the test section.

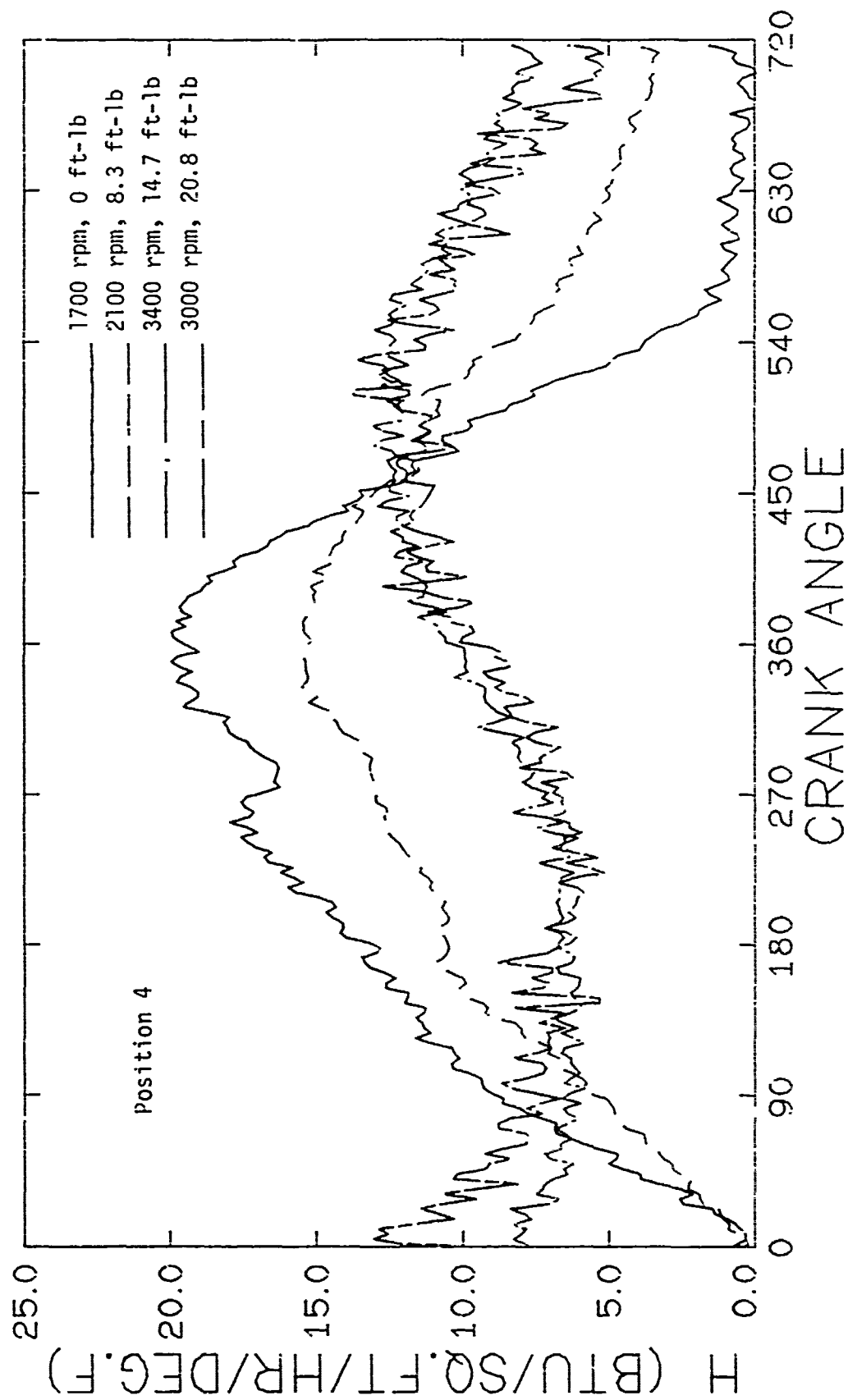


Figure 7.23 Effect of engine speed and load on the instantaneous heat transfer coefficient at position 4 in the test section

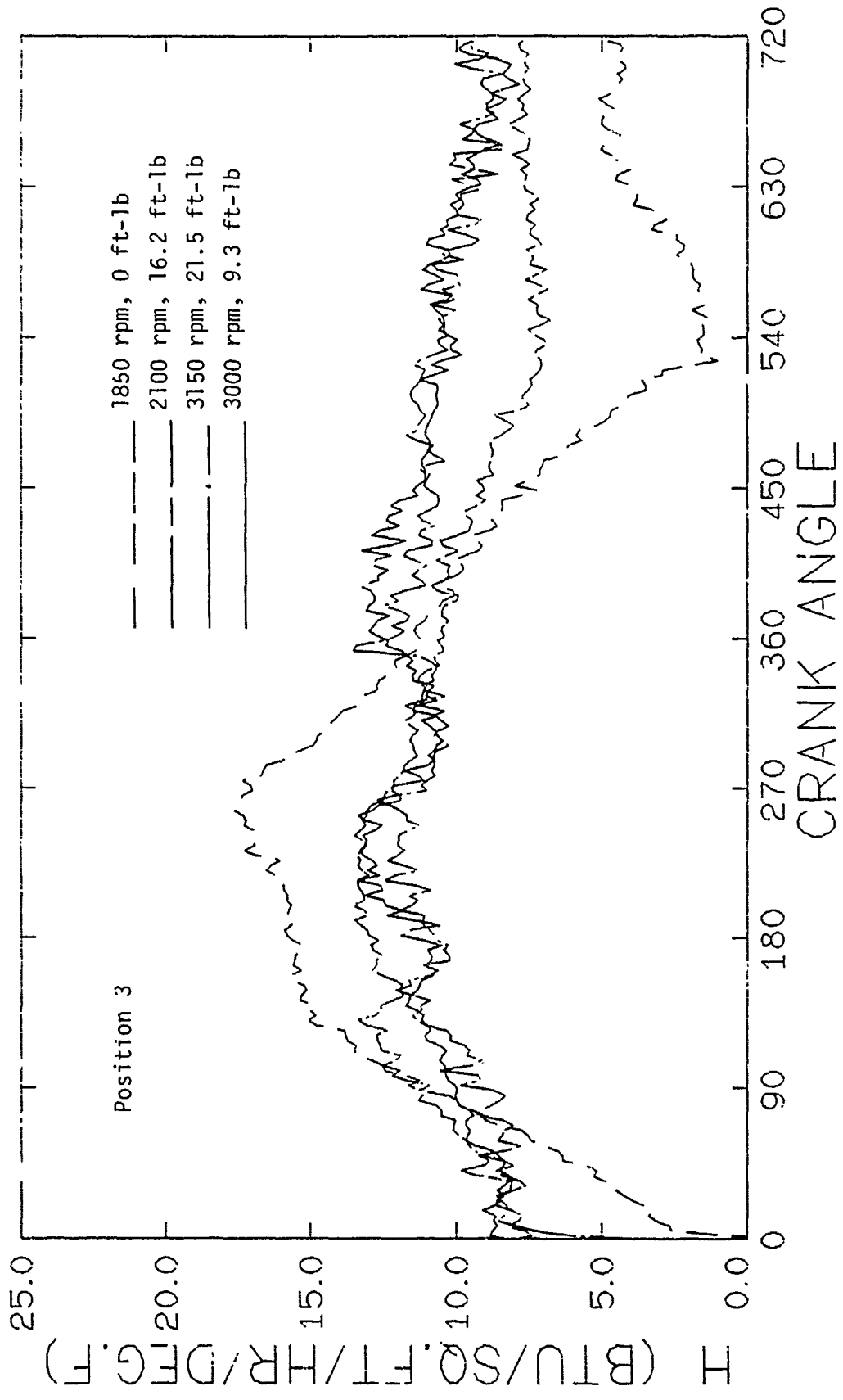


Figure 7.24 Effect of engine speed and load on the instantaneous heat transfer coefficient at position 3 in the test section

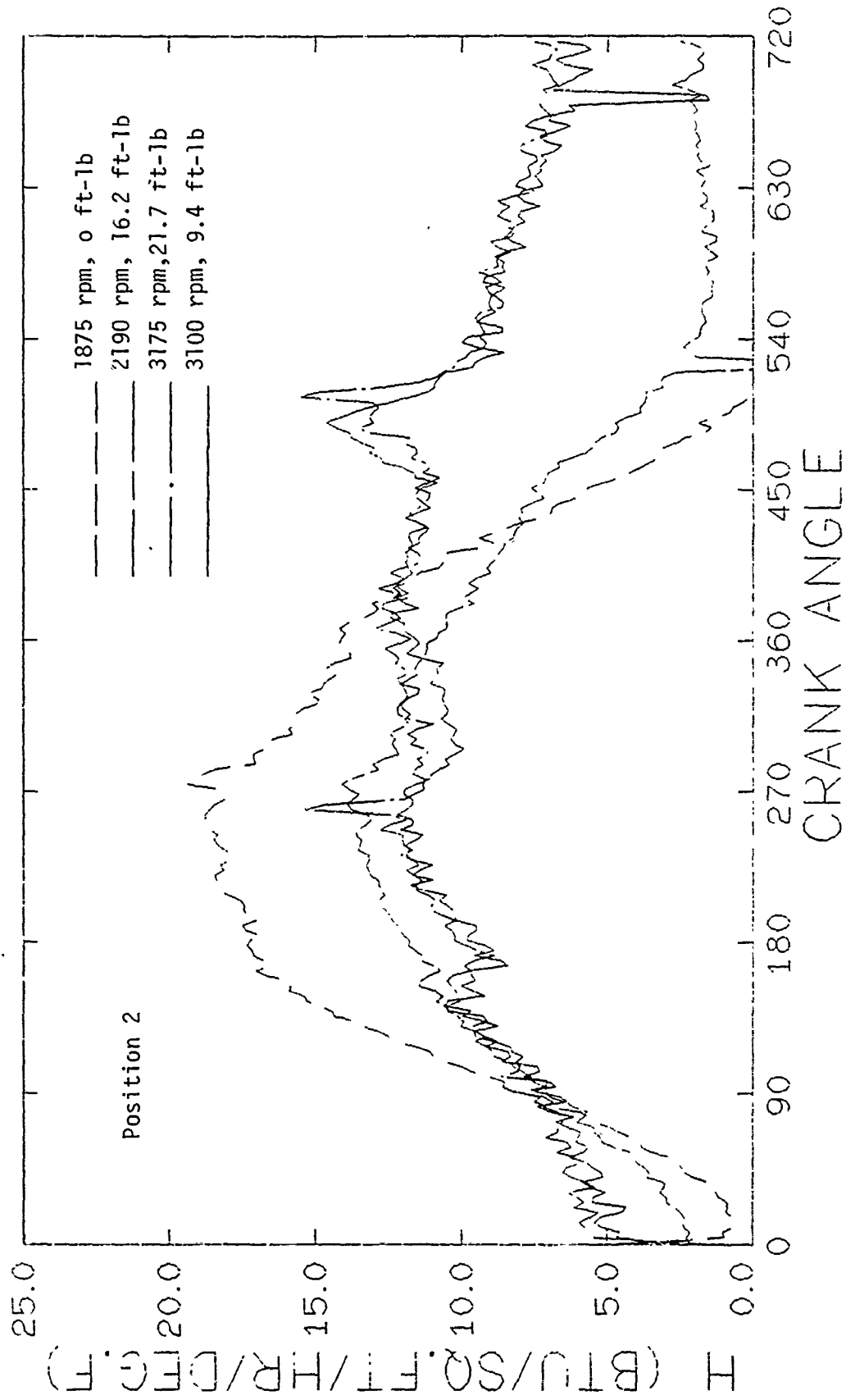


Figure 7.25 Effect of engine speed and load on the instantaneous heat transfer coefficient at position 2 in the test section

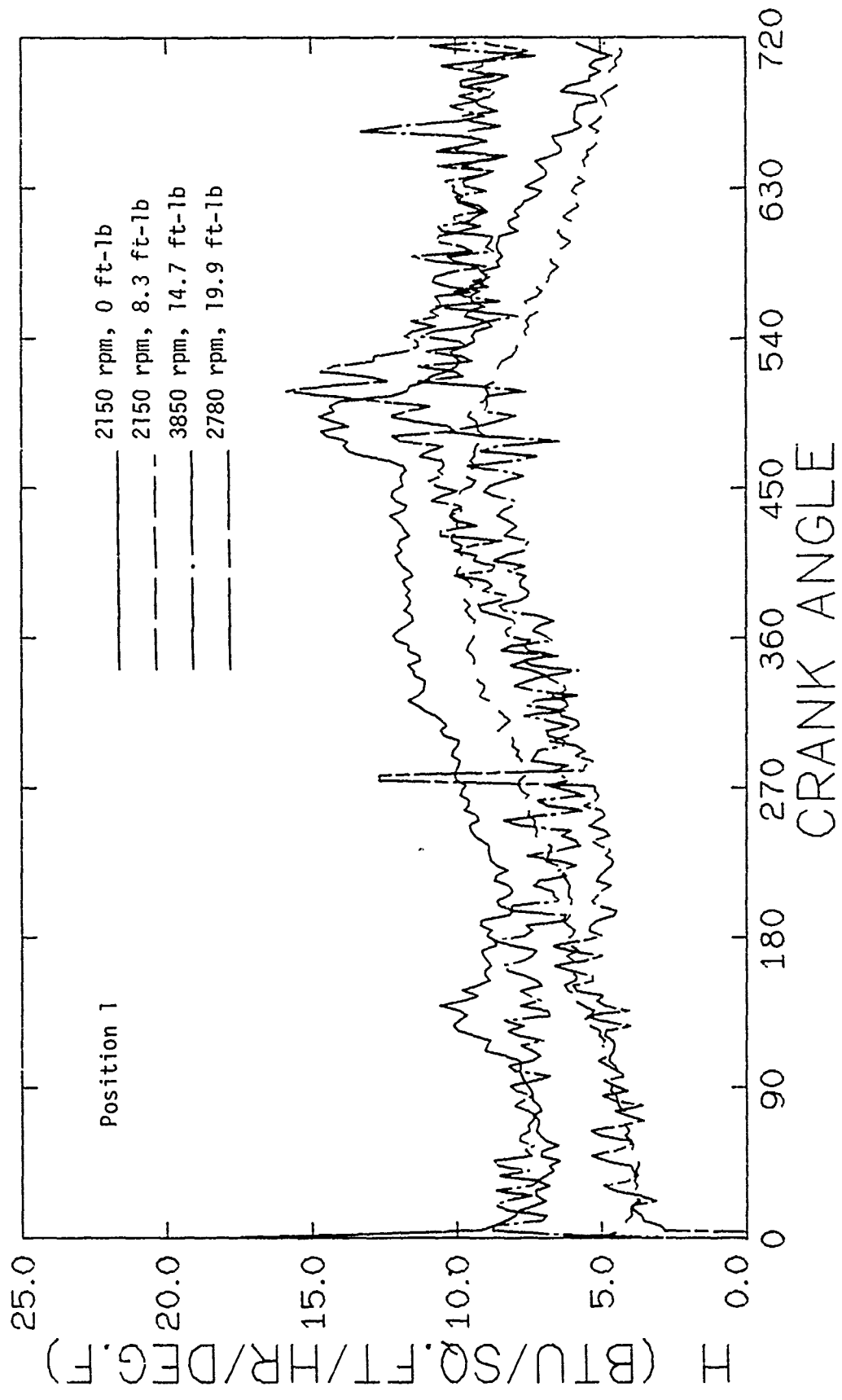


Figure 7.26 Effect of engine speed and load on the instantaneous heat transfer coefficient at position 1 in the test section

## 8. CONCLUSIONS

The current efforts achieved the objective of measuring and collecting transient heat transfer data in the straight portion of the exhaust port of a spark ignition engine. The following conclusions can be drawn from the experimental data.

1. The temperature of the gas side wall in the test section was found to be dependent on the engine speed, engine load, geometrical position and time. At lower engine speeds the magnitude of the gas side wall temperature swing increases and it is found to peak at an earlier time in the engine cycle. With an increase in the engine load the mean temperature of the gas side wall and hence the mean temperature difference across the wall increases. The largest temperature differentials were observed closest to the exhaust valve and along the large radius of the flow path.
2. The exhaust gas temperature was a function of time, engine load and location in the test section. Engine speed was found to have little effect. At a location 4 inches from the valve seat, temperature differences as high as 600°F were recorded during the engine cycle and exhaust gas temperature drops of 250°F over an axial distance of 4 inches were measured. Also, the exhaust gas temperature was more sensitive to change in engine loads at the location closer to the exhaust valve as compared to the downstream location.
3. The computed instantaneous heat flux at the test section wall was found to follow closely with, and showed similar trends to the wall temperature swing curves. The engine speed, engine load and geometrical position were found to effect the heat flux in a manner similar to the wall temperature. With an increase in the engine speed, the heat flux at the

wall is reduced. An increase in the engine load increases the heat flux at the wall. Thus at both higher engine speeds and loads the heat flux curves tend to remain high and flat during the engine cycle and tend to drop more rapidly and earlier during the engine cycle with the lowering of the engine speed and load. Moreover, the highest heat fluxes were observed at the position in the test section at the location closer to the exhaust valve and along the large radius of the flow path. The computed heat transfer coefficient values during the engine cycle displayed similar trends as the instantaneous heat flux curves along with the added effect of the exhaust gas temperature tending to smoothen the curves during the period the exhaust temperature was high.

4. The exhaust gas mass flow rate is seen to be the driving factor governing the convective heat transfer from the exhaust. However, it seems that no one simple correlation correlating the instantaneous Nusselt number with the instantaneous-exhaust gas mass flow rate or equivalently the Reynolds number can be formulated. This was not completely analysed and needs further examination.

## REFERENCES

1. W. Nusselt, "Der Wärmeübergang in der Verbrennungs-Kraftmaschine," V.D.I.-Forschungsheft, 264 (1923).
2. G. Eichelberg, "Some New Investigations on Old Combustion Engine Problems," *Engineering* (1939).
3. W. J. D. Annand, "Heat Transfer in the Cylinders of Reciprocating Internal Combustion Engines," *Proc. Inst. Mech. Eng.*, Vol. 177, No. 36 (1963).
4. G. Woschni, "A Universally Applicable Equation for the Instantaneous Heat Transfer Coefficient in the Internal Combustion Engine," *S. A. E. Trans.* Vol. 76, Paper 670931 (1967).
5. T. LeFeuvre; P. S. Myers, and O. A. Uyehara, "Experimental Instantaneous Heat Fluxes in a Diesel Engine and their Correlation," *S. A. E. Trans.* Vol. 78, Paper 690464 (1969).
6. J. P. Holman, "Heat Transfer," McGraw Hill, New York, 2nd Edition, 1963, p. 98.
7. I. T. El'perin, Galershteyn, D. M. and Levental', "Influence of Surface Effects and Unsteadiness on Transfer Processes in Heterogeneous Systems," *Inzh.-fiz. zhur*, 7,8, 1964.
8. G. B. Darling, "Heat Transfer to Liquids in Intermittent Flow," *Petroleum*, 22, 1959.
9. V. V. Mamayev, V. S. Nosov and N. I. Syromyatnikov, "Investigation of Heat Transfer in Pulsed Flow of Air in Pipes," *Heat Transfer-Soviet Research*, Vol. 8, No. 3, May-June, 1976.
10. G. G. Agadzhanian, "Convective Heat Transfer in Pipes with Pulsed Gas Flow," In: *Teoriya podobiya i modelirovaniya (Similitude and Modeling Theory)*. Press of USSR Academy of Sciences, 1951.
11. F. B. West, A. T. Taylor, "The Effect of Pulsation on Heat Transfer," *Chemical Eng. Prog.*, Vol. 48, 1952, p. 39.
12. R. R. Morris, Univ. of Washington, M.S. Thesis, 1950.
13. R. P. Webb, Univ. of Washington, M.S. Thesis, 1949.
14. D. O. Barnett, R. I. Vachon, "An Analysis of Convective Heat Transfer for Pulsating flow in Tube," 4th International Heat Transfer Conference, Paris, France, 1970, p. FC9.1.
15. H. Havemann, R. Narayan, "Heat Transfer in Pulsating Flow," *Nature*, Vol. 174, 1954, p. 41.
16. V. Chalibhan, "Effect of Longitudinal Pulsations on Heat Transfer," Ph.D. Thesis, Univ. of Texas, 1959.

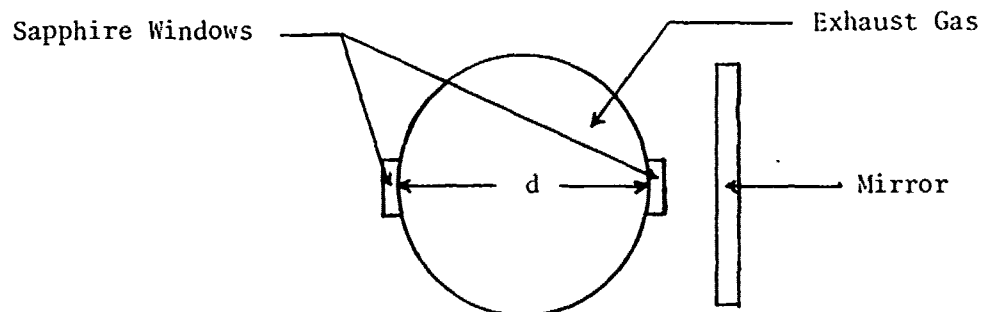
17. V. K. Koshlin, Y. I. Danilov, G. A. Dreitser, B. M. Gulikseysky, E. K. Kalinin, V. K. Isosinov, "Unsteady Heat Transfer in Tubes Resulting from Changes in Heat Flow, Gas Mass Flow Rate and Acoustic Resonance," Proc. 3rd International Heat Transfer Conf., Vol. 3, 1966, p. 57.
18. K. Hwu, "The Effect of Vibrations on Forced Convective Heat Transfer," Univ. of Cinn., Ph.D. Thesis, 1968.
19. R. W. Goluba, "The Effect of Periodic Shock Fronted Pressure Waves on the Instantaneous Heat Flux at the End Wall of a Tube," Univ. of Wis., Ph.D., Thesis, 1968.
20. F. J. Bayley, P. A. Edwards, P. P. Singh, "The Effect of Flow Pulsations on Heat Transfer by Forced Convection from a Flat Plate," Second International Heat Transfer Conference, Aug. 1961, p. 499.
21. D. Bendersky, "A Special Thermocouple for Measuring Transient Temperatures," Mechanical Engineering, Vol. 75, 1953, p. 117.
22. P. F. Flynn, "An Experimental Determination of the Instantaneous Potential Radiant Heat Transfer within an Operating Diesel Engine," Univ. of Wisconsin, Ph.D. Thesis, 1971.
23. T. LeFeuvre, P. S. Myers, D. A. Uyehara, J. H. Shipinski, "A Tape Recording and Computer Processing System for Instantaneous Engine Data," Paper 680133, presented at SAE Automotive Engineering Congress, Detroit, January 1968.
24. S. S. Penner, "Quantitative Molecular Spectroscopy and Gas Emissivities," Reading, Mass., Addison-Wesley, 1959.
25. L. M. K. Boelter, V. H. Cherry, H. A. Johnson, R. C. Martinelli, "Heat Transfer Notes," Univ. of Calif. Press, Berkely and Los angeles, 1946.
26. D. P. Eckman, "Industrial Instrumentation," John Wiley and Sons, New York, 1950, p. 270.
27. G. L. Malchow, "An Experimental Heat Transfer Study of the Straight Portion of the Exhaust Port of a Spark Ignition Engine," Univ. of Illinois, Ph.D. Thesis, 1978.

## APPENDIX A

## OPTICAL TECHNIQUE FOR THE DETERMINATION OF GAS TEMPERATURE

The two-path method:

The two path method for the measurement of temperatures is an optical technique that permits temperature measurements on systems in which the intensity of radiation emitted varies rapidly (and aperiodically) with time (24). The method depends upon a comparison of spectral temperatures when two different path lengths are viewed separately.



For a volume of gas enclosed in a chamber the path length may be conveniently doubled by placing a mirror at one end of the field of view. Neglecting transmission losses through the windows and multiple reflection from the chamber walls, the observed radiancy of the gas for a path length  $d$  in the wavelength  $\lambda$  and  $\lambda + d\lambda$  is,

$$R^{\circ}(\lambda, T_{br1}) d\lambda = R^{\circ}(\lambda, T_F) [1 - \exp(-K_{\lambda} \rho d)] d\lambda \quad (1)$$

where  $T_{br1}$  represents the apparent brightness temperature corresponding to a path length  $d$ ;  $R^{\circ}(\lambda, T_F)$  is the blackbody radiancy at the true temperature  $T_F$ ;  $K_{\lambda}$  equals the spectral main absorption coefficient and  $\rho$  is the density of the gas. When the path length is doubled by placing a mirror at one end of the field of view, the observed radiancy corresponding to the apparent brightness temperature  $T_{br2}$  is

$$R^{\circ}(\lambda, T_{br2}) d\lambda = R^{\circ}(\lambda, T_F) [1 - \exp(-K_{\lambda} \rho d)] [1 + r_{\lambda} \exp(-K_{\lambda} \rho d)] d\lambda \quad (2)$$

where  $r_\lambda$  is the spectral reflection coefficient of the front-surface reflecting mirror. From Eqs. (1) and (2) it follows that

$$\frac{R^0(\lambda, T_{br2})}{R^0(\lambda, T_{br1})} = 1 + r_\lambda \exp(-K_\lambda \rho d) \quad (3)$$

From Eq. (1)

$$\exp(-K_\lambda \rho d) = 1 - \frac{R^0(\lambda, T_{br1})}{R^0(\lambda, T_F)} \quad (4)$$

Therefore,

$$1 - \frac{R^0(\lambda, T_{br2})}{R^0(\lambda, T_{br1})} = -r_\lambda \left[ 1 - \frac{R^0(\lambda, T_{br1})}{R^0(\lambda, T_F)} \right]$$

If the path length is large enough to make the exponential term in Eqs. (3) and (4) negligible, it follows that

$$R^0(\lambda, T_{br2}) = R^0(\lambda, T_{br1}) = R^0(\lambda, T_F)$$

Thus the experimental determination of  $R^0(\lambda, T_{br})$  permits calculation of  $R^0(\lambda, T_F)$  and, therefore, determines the gas temperature  $T_F$  uniquely.

## APPENDIX B

## VOLTAGE CALIBRATION OF F.M. TAPE RECORDER

Step by Step Voltage Calibration Procedure:

The procedures below is for calibration without tape motion. This procedure was found to be the easiest to apply.

1. For greatest accuracy, set the speed selection to the speed to be used for recording. The highest tape speed, 60 inches per second, was selected as the recording speed.
2. Remove the panel on the upper left side of the recorder and switch the squelch toggle to the position marked "D" (disable).
3. Connect the "To Recorder" BNC on the voltage calibrator to the input BNC of the channel to be calibrated, and connect the output BNC of the channel to the "From Recorder" BNC on the calibrator.
4. Connect a jumper cable from the yellow tip jack on the record board marked "CAR" to the yellow tip jack on the reproduce board marked "IN." This bypasses the record head, tape, reproduce head pathway.
5. Connect the Simpson DVM to the calibrator and adjust the "VOLTS ADJ" knob on the calibrator to the desired setting.

6. Depress the "Record" button.
7. Move the range switch on the record board to "TEST", the output of the reproduce board, as measured with the DVM (calibrator "READ" switch on "OUT") should be within  $\pm 50$  mV of zero. If it is not, adjust the "ZERO" potentiometer on the reproduce board to achieve this result.
8. Move the "RANGE" switch on the record board to the appropriate range (.2 - 1.5 vrms) or (1.5 - 10 vrms).
9. Adjust the "IN" potentiometer on the record board until the output of the reproduce board reaches the desired value. When the "POLARITY" switch on the calibrator is thrown, the output should reverse in polarity. Some adjustment of the "IN" pot may be needed to achieve the best compromise setting. If the difference in the absolute values of the two output values is greater than 10 mv, the system is malfunctioning and should be repaired.
10. Return the "POLARITY" switch on the calibrator to the "NORM" setting, remove the jumper from the record to the reproduce board, switch the "squench" toggle off of "D" and start the tape by pressing FWD and RECORD simultaneously (release FORWARD first). This will record the reference voltage on the tape for checking calibration on later reproduction. Observe the output of the reproduce board. After the tape is up to speed, and the recorded data has moved from the record heads to the reproduce heads (this takes a while at low tape speeds), the output reading should be within a few mv of that obtained above with the tape stationary. If it is not, the system is malfunctioning and should be repaired.

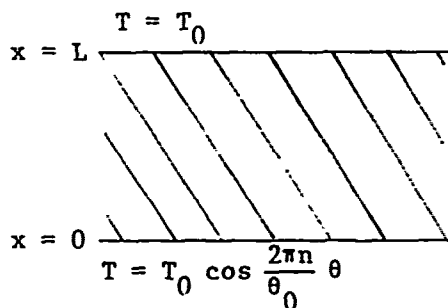
11. Repeat the procedure for all channels to be calibrated.

Transducer	Channel Number	Input (volts)	Output (volts)	Gain
Upstream Pressure Transducer	1	0.5	1.0	2.0
Downstream Pressure Transducer	2	0.5	1.0	2.0
Gas Wall Temperature Thermocouple	3	3.0	1.0	0.33
Detector for Exhaust Gas Temperature	5	4.0	1.0	0.25
TDC pulse Generator	6	3.5	1.0	0.286
CA pulse generator	7	3.5	1.0	0.286

Table B-1 Voltage calibration values for all channels  
used on the F.M. Tape Recorder

## APPENDIX C

## TEMPERATURE DISTRIBUTION IN A FLAT PLATE WITH ONE SURFACE TEMPERATURE A PERIODIC FUNCTION OF TIME (STEADY STATE SOLUTION)



Expressing the periodic surface temperatures of a flat plate by a Fourier series of cosine (either by an even function or with phase angles) gives the temperature distribution as the combined sum of two or more series of cosine terms. The procedure in the derivation is to superimpose arbitrarily a series of hypothetical temperature waves by considering the  $n^{\text{th}}$  harmonic, which will give the desired boundary conditions for that harmonic (25). The "n" harmonics are then summed to obtain the resultant periodic temperature distribution which is superimposed upon the mean temperature gradient which exists within the solid. The derivations are based upon the  $n^{\text{th}}$  harmonic. Calculations are carried out for each harmonic of the boundary conditions and the resultant temperature found at any point and any time by algebraic addition.

For the semi-infinite solid where the surface temperature is given by

$$T = T_0 \cos \frac{2\pi n}{\theta_0} \theta \quad (1)$$

the periodic temperature distribution within the solid is:

$$T_{1,x} = T_0 e^{-\frac{\pi n}{\alpha \theta_0} x} \cos \left[ \frac{2\pi n}{\theta_0} \theta - \frac{\pi n}{\alpha \theta_0} x \right]$$

Let  $\frac{n\pi L^2}{\alpha \theta_0} = b$ , then

$$T_{1,x} = T_0 e^{-\frac{b}{L} x} \cos \left[ \frac{2\pi n}{\theta_0} \theta - b \frac{x}{L} \right] \quad (2)$$

However, this problem involves a plate of finite thickness  $L$  and equation (2) indicates that the temperature at the plane  $x = L$  is

$$T_{1,L} = T_0 e^{-b} \cos \left[ \frac{2\pi n}{\theta_0} \theta - b \right]$$

A temperature wave

$$T_{2,x} = -T_0 e^{-b} e^{-b \frac{L-x}{L}} \cos \left[ \frac{2\pi n}{\theta_0} \theta - b - b \frac{(L-x)}{L} \right] \quad (3)$$

is arbitrarily superimposed to cancel that temperature variation of equation (2) which penetrates to the plane  $x = L$ . Then the temperature variation given by equation (3) becomes, at the surface  $x = 0$

$$T_{2,0} = -T_0 e^{-b} e^{-b} \cos\left[\frac{2\pi n}{\theta_0} \theta - b - b\right]$$

which is cancelled by arbitrarily imposing the temperature wave:

$$T_{3,x} = T_0 e^{-b} e^{-b} e^{-\frac{b x}{L}} \cos\left[\frac{2\pi n}{\theta_0} \theta - b - b - b \frac{x}{L}\right] \quad (4)$$

Similarly a fourth wave

$$T_{4,x} = -T_0 e^{-3b} e^{-\frac{b(L-x)}{L}} \cos\left[\frac{2\pi n}{\theta_0} \theta - 3b - b \frac{(L-x)}{L}\right] \quad (5)$$

which cancels the effect of the 3<sup>rd</sup> wave upon the surface  $x = L$ .

Thus, a sufficient number of waves when added will give finally, a periodic temperature distribuion in the slab such that the surface  $x = 0$  has the temperature variation expressed by equation (1) while the surface  $x = L$  will have a constant surface temperature  $T_0$ . That is adding equations (2), (3), (4), (5) etc. gives:

$$T_{1x} = T_0 \left\{ e^{-\frac{b x}{L}} \cos\left[\frac{2\pi n}{\theta_0} \theta - \frac{b x}{L}\right] - e^{-b\left(2 - \frac{x}{L}\right)} \cos\left[\frac{2\pi n \theta}{\theta_0} - b\left(2 - \frac{x}{L}\right)\right] \right\}$$

$$+ e^{-b(2 + \frac{x}{L})} \cos[\frac{2\pi n}{\theta_0} \theta - b(2 + \frac{x}{L})] + e^{-b(4 - \frac{x}{L})} \cos[\frac{2\pi n}{\theta_0} \theta - b(4 - \frac{x}{L})] + \dots\}$$

or writing this equation as the sum of a general term

$$T_{1x} = T_0 \sum_{N=0}^{\infty} (-1)^N e^{-b[N+\delta+(-1)^N \frac{x}{L}]} \cos[\frac{2\pi n}{\theta_0} \theta - b(N+\delta+(-1)^N \frac{x}{L})] \quad (6)$$

where  $\delta = 0$  when  $N$  is even and  $\delta = 1$  when  $N$  is odd; which is the temperature distribution in a plate of thickness  $L$  where the temperature at the surface  $x = 0$  is  $T_0 \cos[\frac{2\pi n}{\theta_0} \theta]$  and at the surface  $x = L$  temperature variation is zero.

The instantaneous heat flux through the wall would then be

$$\frac{Q}{A} = -k \frac{\partial T_{1x}}{\partial x} \quad x = 0$$

$$\frac{Q}{A} = \frac{-kT_0}{L} \sum_{N=0}^{\infty} b e^{-b[N+\delta]} \{ \sin[\frac{2\pi n}{\theta_0} \theta - b(N + \delta)]$$

$$- \cos[\frac{2\pi n}{\theta_0} \theta - b(N + \delta)] \}$$

## APPENDIX D

## FLOW RATE OF AN IDEAL GAS THROUGH AN ORIFICE

Assuming an adiabatic flow through an orifice and neglecting the potential energy, the First law of Thermodynamics can be expressed as:

$$p_2 v_2 + \frac{v_2^2}{2g} + u_2 = p_1 v_1 + \frac{v_1^2}{2g} + u_1 \quad (1)$$

where subscripts 1 and 2 denote the downstream and upstream locations with respect to the orifice and,

$p$  = Absolute pressure

$V$  = Velocity

$v$  = specific volume

$u$  = specific internal energy

Rearranging eqn. (1)

$$v_2^2 - v_1^2 = 2[(p_1 v_1 + u_1) - (p_2 v_2 + u_2)]$$

or, 
$$v_2^2 - v_1^2 = 2(h_1 - h_2) \quad (2)$$

where the specific enthalpy  $h$  is defined as

$$h = u + pv$$

For an ideal gas with constant specific heats

$$C_p = \frac{\gamma R}{(\gamma - 1)}$$

where  $C_p$  = Specific heat at constant pressure

$\gamma$  = Ratio of specific heats

$R$  = Gas constant

For an ideal adiabatic gas flow

$$T_2/T_1 = (P_2/P_1)^{\gamma-1/\gamma}$$

where  $T$  is the absolute temperature. Also,

$$h_1 - h_2 = C_p(T_1 - T_2)$$

or

$$h_1 - h_2 = \frac{\gamma R}{(\gamma-1)} T_1 [1 - (p_2/p_1)^{\gamma-1/\gamma}]$$

Substituting in Eqn. (2)

$$v_2^2 - v_1^2 = \frac{2\gamma R}{(\gamma-1)} T_1 [1 - (p_2/p_1)^{\gamma-1/\gamma}] \quad (3)$$

From conservation of mass, the mass flow rate  $\dot{M}$  is

$$\dot{M} = \frac{A_2 v_2}{v_2} = \frac{A_1 v_1}{v_1}$$

Incorporating the above in eqn. (3)

$$\frac{\dot{M}^2 v_2^2}{A_2^2} - \frac{\dot{M}^2 v_1^2}{A_1^2} = \frac{2\gamma R T_1}{(\gamma-1)} [1 - (p_2/p_1)^{\gamma-1/\gamma}]$$

$$\text{or, } \dot{M}^2 = \frac{2\gamma R}{(\gamma-1)} T_1 \left[ \frac{1 - (p_2/p_1)^{\gamma-1/\gamma}}{v_2^2/A_2^2 - v_1^2/A_1^2} \right]$$

Noting that  $A_2/A_1 = D_2^2/D_1^2 = \beta^2$  where  $\beta$  is the diameter ratio the above expression can be simplified

$$\dot{M} = A_2 \left( \frac{2\gamma R T_1}{(\gamma-1) v_1^2} \right)^{1/2} \left( \frac{1 - (p_2/p_1)^{\gamma-1/\gamma}}{(v_2/v_1)^2 - \beta^4} \right)^{1/2} \quad (4)$$

Since for an adiabatic flow of an ideal gas

$$\frac{v_2}{v_1} = \left( \frac{p_1}{p_2} \right)^{1/\gamma}$$

and  $p_1 v_1 = RT_1$ , eqn (4) can be simplified to

$$\dot{M} = A_2 \left( \frac{2\gamma p_1^2}{(\gamma-1)RT_1} \right)^{1/2} \left( \frac{(p_2/p_1)^{2/\gamma} - (p_2/p_1)^{\gamma+1/\gamma}}{1 - \beta^4 (p_2/p_1)^{2/\gamma}} \right)^{1/2}$$

Finally with the use of a flow coefficient,  $C_v$ , to account for vena contracta effects the above equation can be written as: (26)

$$\dot{M} = C_v A_2 \left( \frac{2 \gamma P_1^2}{(\gamma-1)RT_1} \right)^{1/2} \left( \frac{(P_2/P_1)^{2/\gamma} - (P_2/P_1)^{\gamma+1/\gamma}}{1 - \beta^4 (P_2/P_1)^{2/\gamma}} \right)^{1/2} \quad (5)$$

## APPENDIX E

SIMULATION OF WALL TEMPERATURE RISE IN TEST SECTION DUE TO SUDDEN FLOW OF GAS  
AT CONSTANT TEMPERATURE

With an increase in the flow velocity of gas in a pipe, an increase in the heat transfer coefficient of the gases is expected. This has been confirmed by many heat transfer studies carried out for both laminar and turbulent flow in smooth tubes. Generally the simplest type of relation used to correlate the experimental data by the use of the principles of dimensional analysis and physical similarity is of the form

$$\text{Nu}_D = C \text{Re}_D^m \text{Pr}^n$$

where  $\text{Nu}_D$  = Nusselt number based on the tube diameter  $D$

$\text{Re}_D$  = Reynolds number based on the tube diameter  $D$

$\text{Pr}$  = Prandtl number

and  $C$ ,  $m$  and  $n$  are constants determined from the experimental data. In a previous study (27), a correlation of the steady state heat transfer data was established in the form

$$\text{Nu}_D = 0.066 \text{Re}_D^{0.76}$$

Since  $\text{Nu}_D = \frac{hD}{K}$

$$\text{Re}_D = \frac{4\dot{M}}{\pi\mu D}$$

where  $h$  = heat transfer coefficient

$K$  = thermal conductivity of the gas

$\mu$  = absolute viscosity of the gas

$\dot{M}$  = gas mass flow rate

Then,

$$h = 0.079 \frac{K}{D} \left( \frac{\dot{M}}{\mu D} \right)^{0.76}$$

For flow of gas at a constant temperature, the gas properties will remain fairly constant and hence corresponding to the gas mass flow rate an approximate value for the heat transfer coefficient can be obtained. Thus it seemed feasible to determine the effect on the wall temperature due to a sudden flow of gas at a constant temperature by using a stepwise function for the heat transfer coefficient and neglecting flow acceleration.

A computer program using the finite difference approach was used to determine the gas side wall temperature when subjected to a stepwise function of the heat transfer coefficient of the gas. A transient energy balance can be made on a node,  $m$ , on the surface of wall (See Figure 6.2) by setting the sum of the energy conducted and convected into the node equal to the increase in the internal energy of the node

$$kA \left( \frac{T_{m-1}^j - T_m^j}{\Delta x} \right) + h^j A (T_g^j - T_m^j) = \rho CA \frac{\Delta x}{2} \frac{(T_m^{j+1} - T_m^j)}{\Delta t}$$

Rearranging,

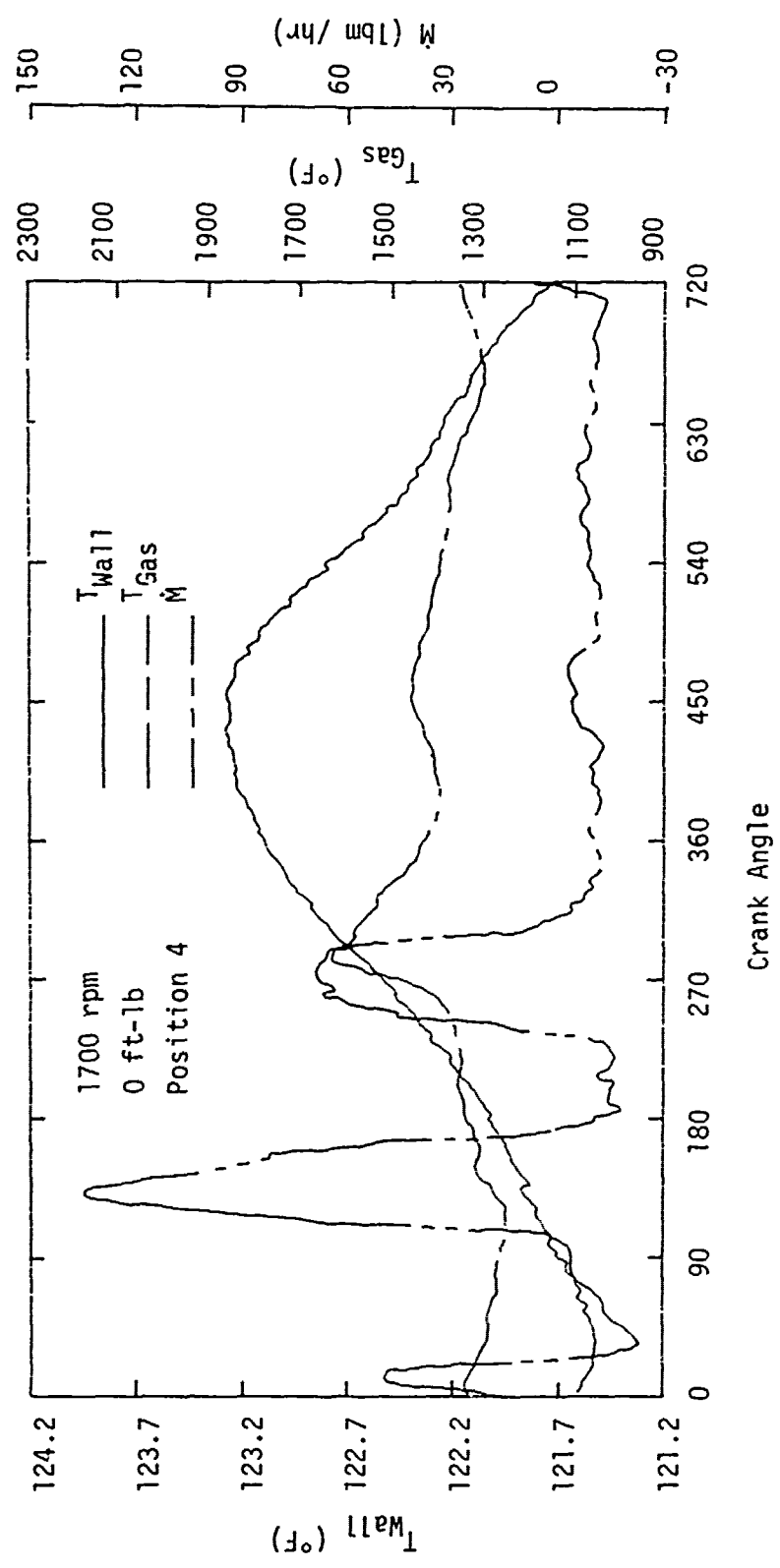
$$T_m^{j+1} = \frac{\alpha \Delta t}{(\Delta x)^2} \left[ \frac{2 h^j \Delta x}{k} T_g^j + 2 T_{m-1}^j + T_m^j \left\{ \frac{(\Delta x)^2}{\alpha \Delta t} - \frac{2 h^j \Delta x}{k} - 2 \right\} \right]$$

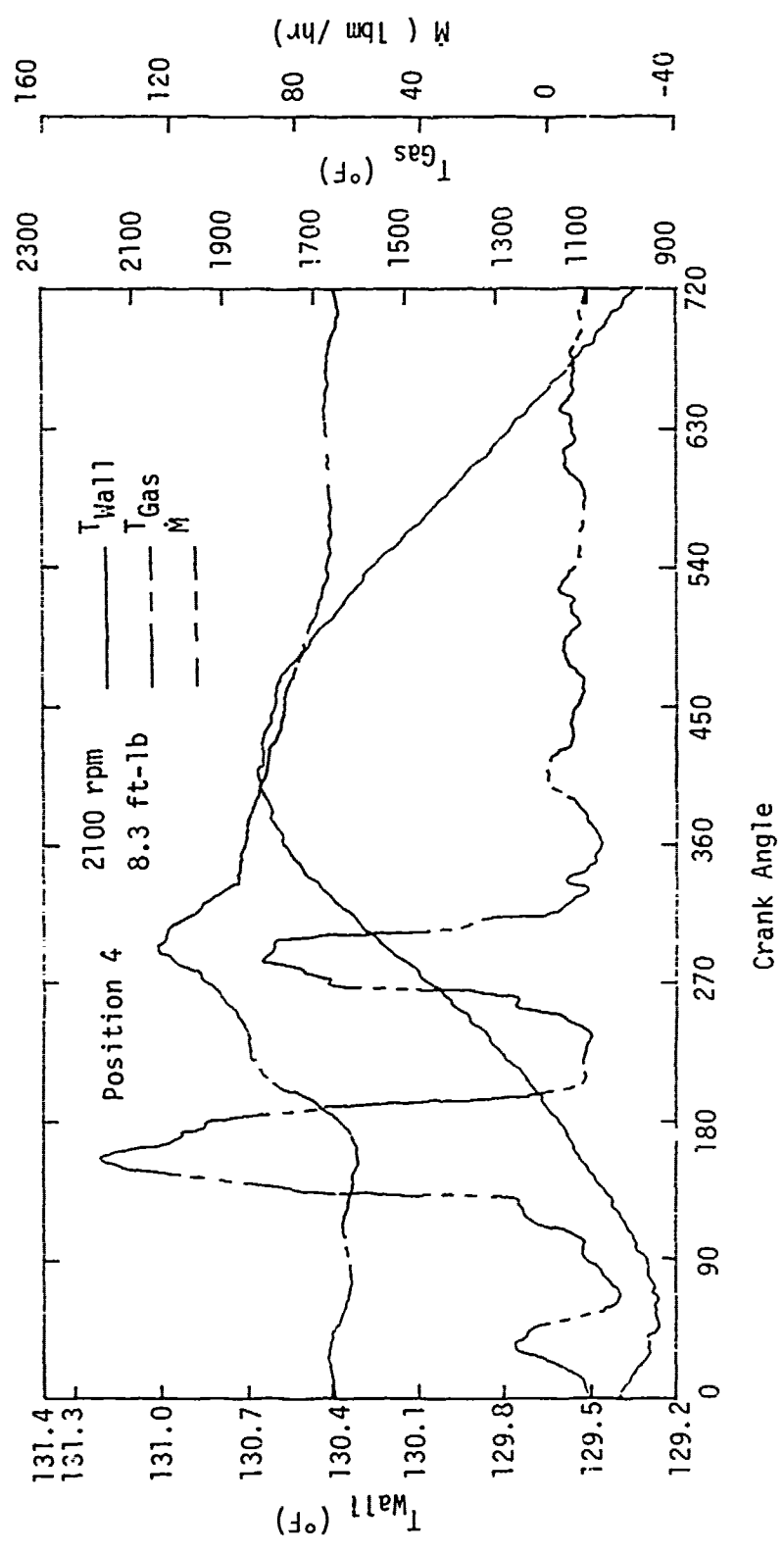
Thus the gas side wall temperature can be determined as a function of time given the stepwise function for the heat transfer coefficient and the initial temperature distribution in the wall. The simulation was carried out for various engine speeds and the effect on the wall temperature determined up to the desired crank angle in the engine cycle. The initial temperature distribution in the wall required by the simulation program was calculated from the actual experimental data.

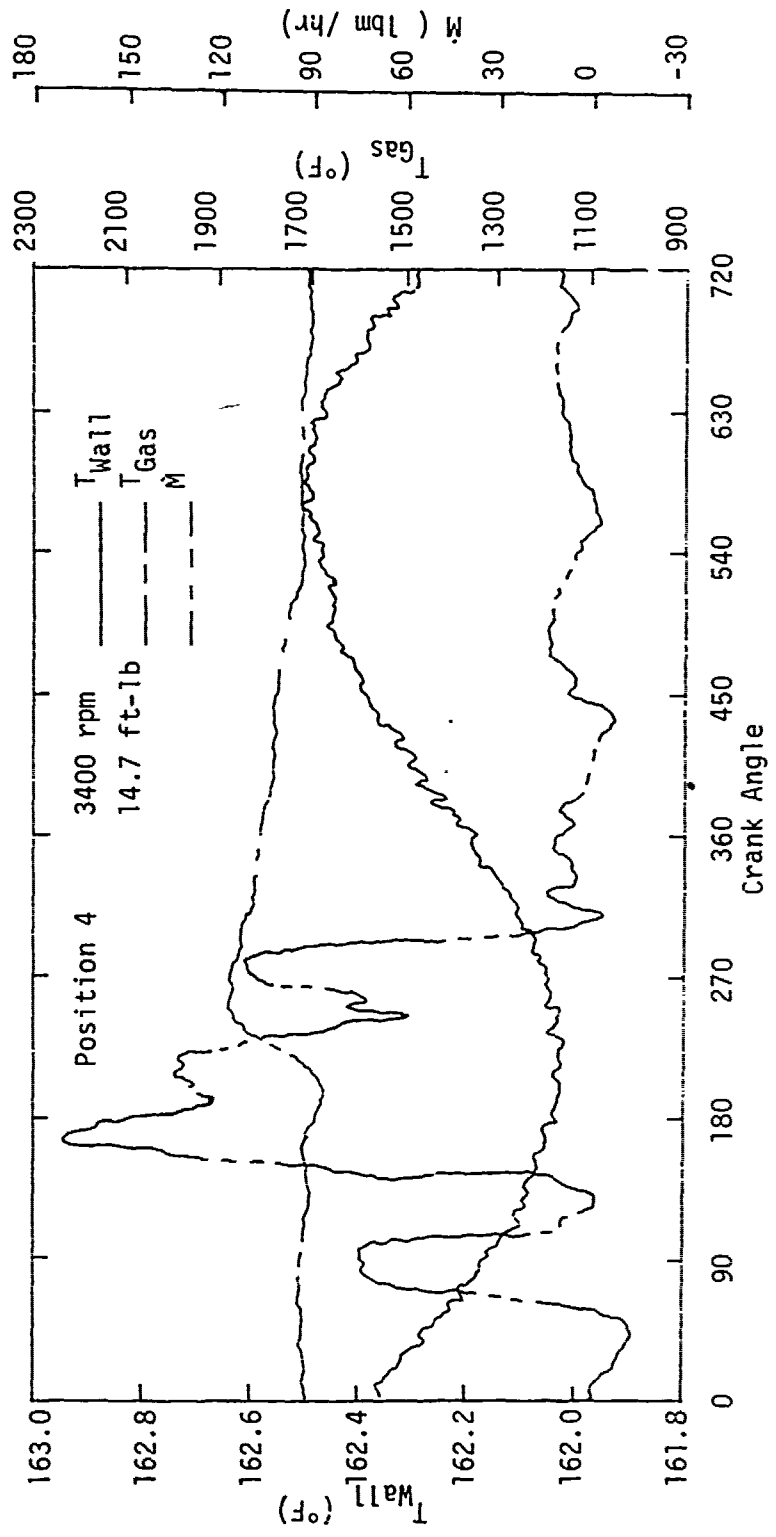
## APPENDIX F

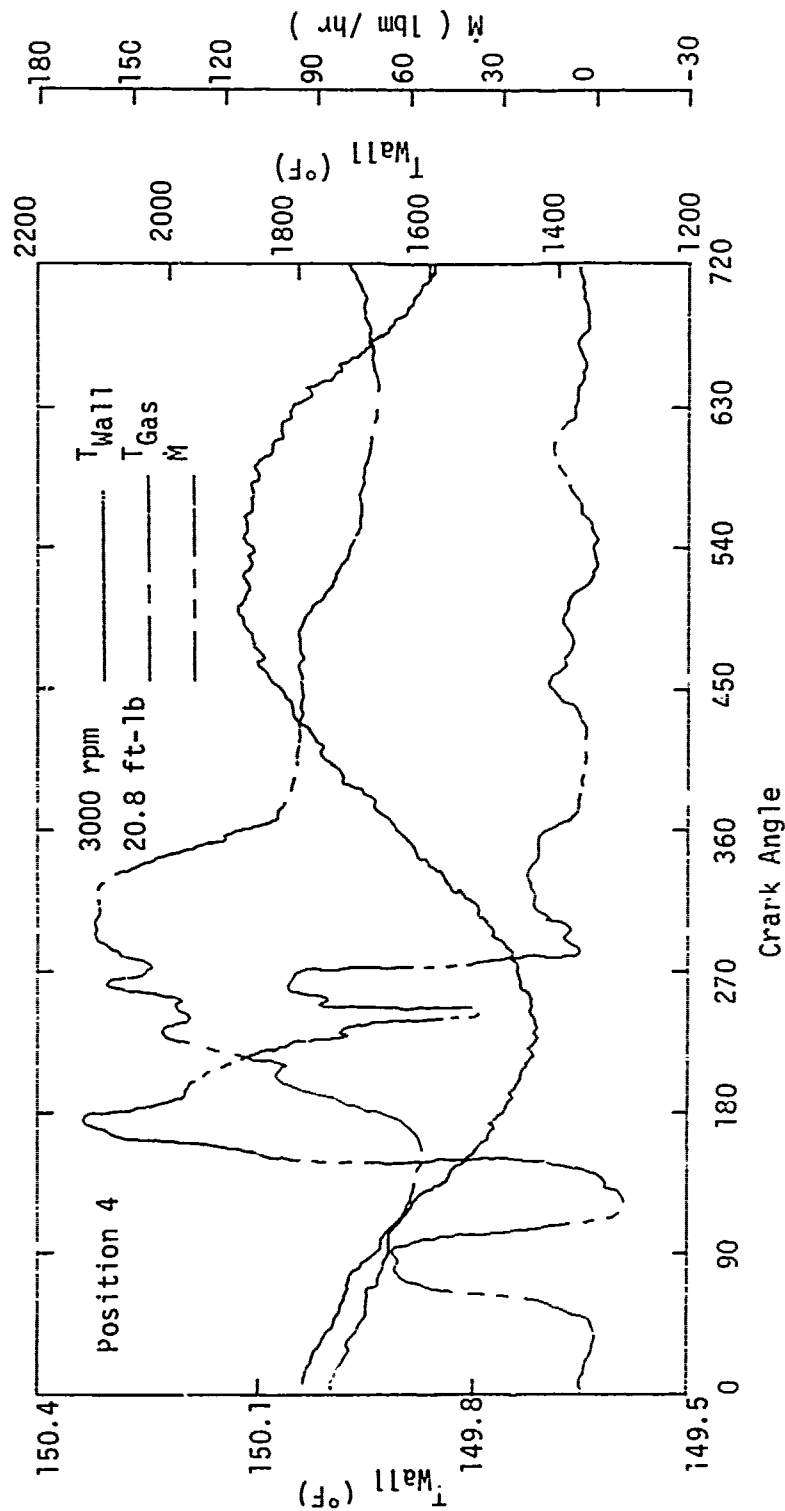
## GRAPHS OF MEASURED AND CALCULATED DATA

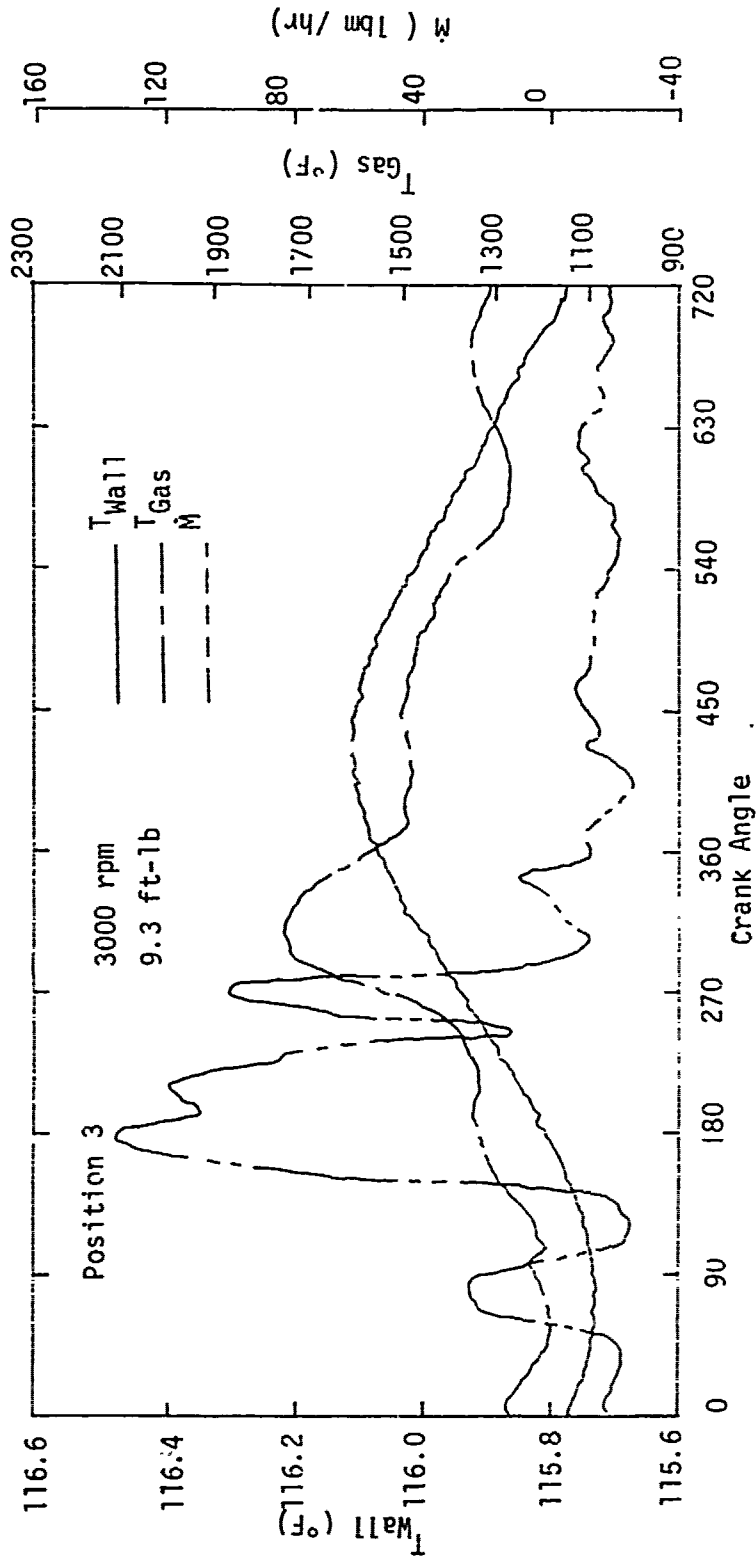
The graphs presented in this appendix depict the gas side wall temperature,  $T_{\text{wall}}$ , the exhaust gas temperature,  $T_{\text{gas}}$  and the exhaust gas mass flow rate  $\dot{M}$  as a function of the crank angle for different engine conditions at each of the four positions in the test section. The gas temperature was ensemble averaged over ten engine cycles while the wall temperatures curve plotted was obtained from a single engine cycle for the same engine conditions.

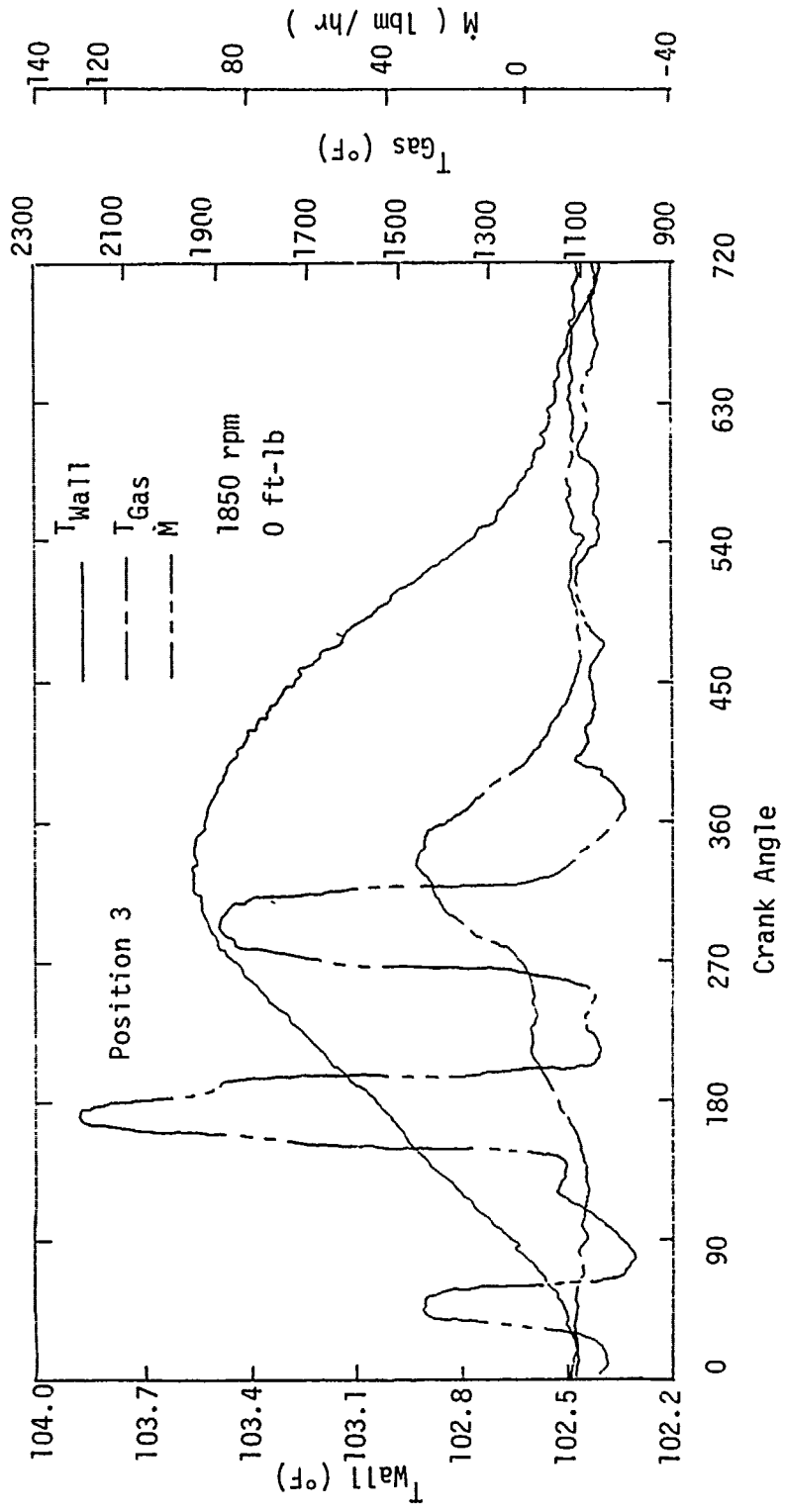


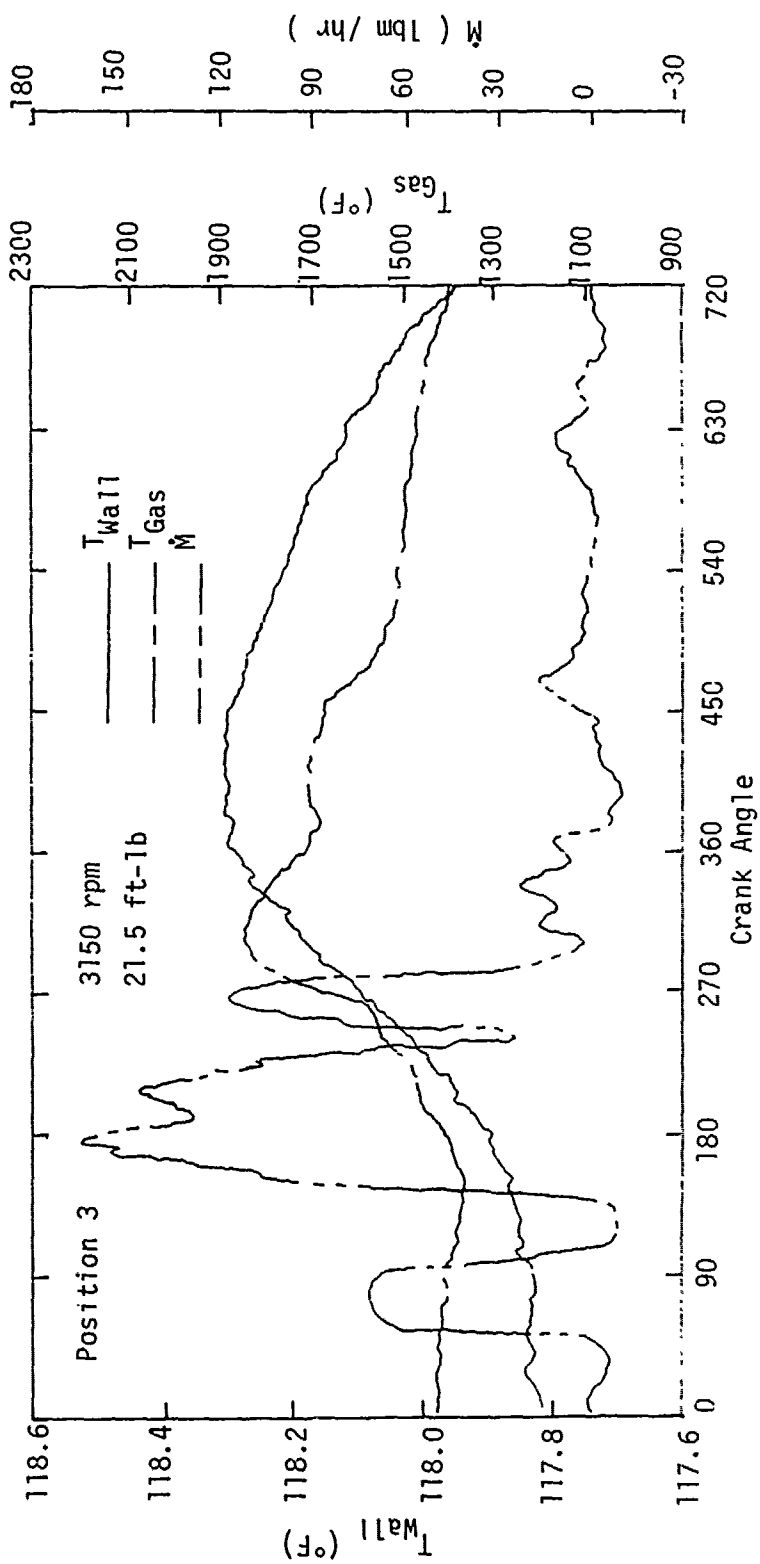


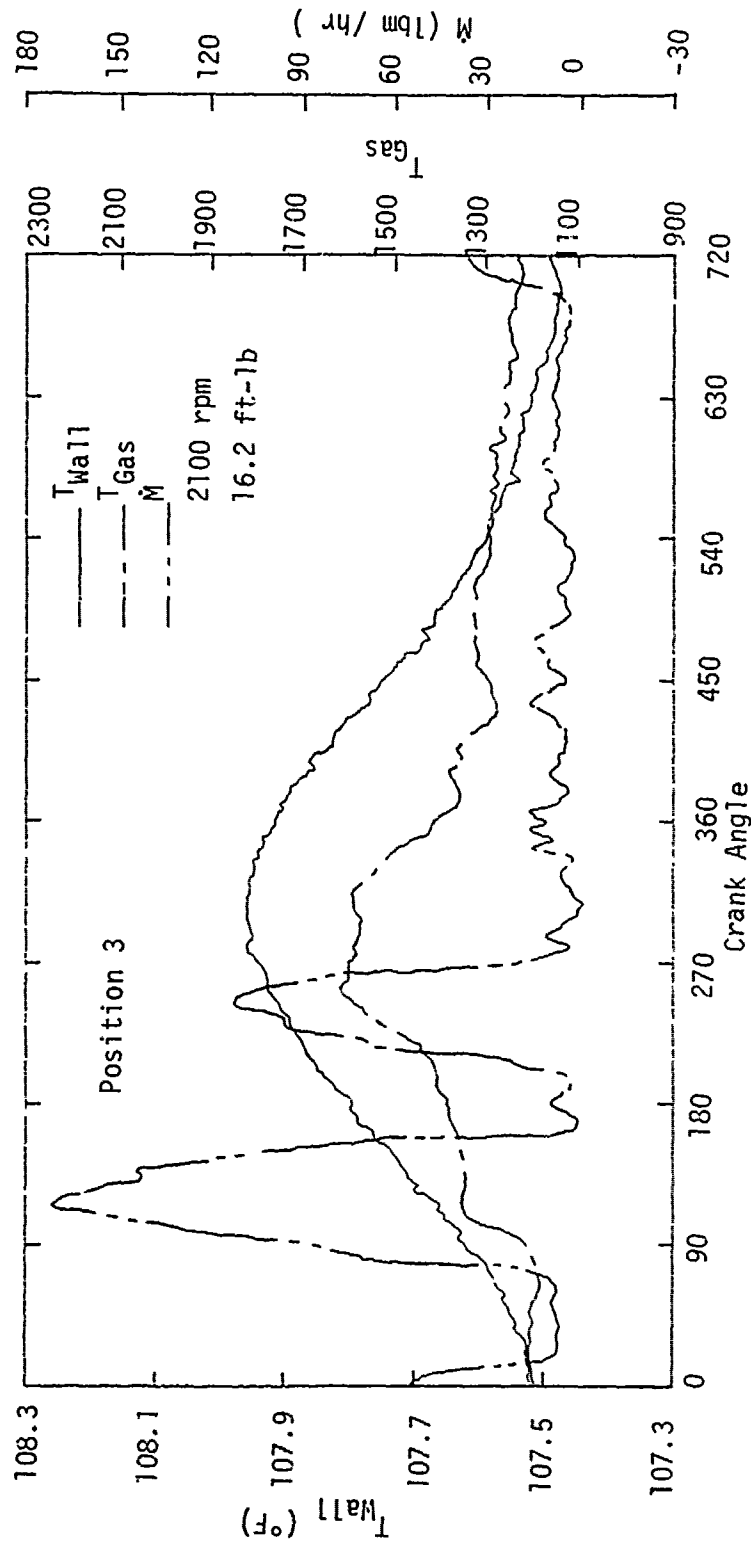


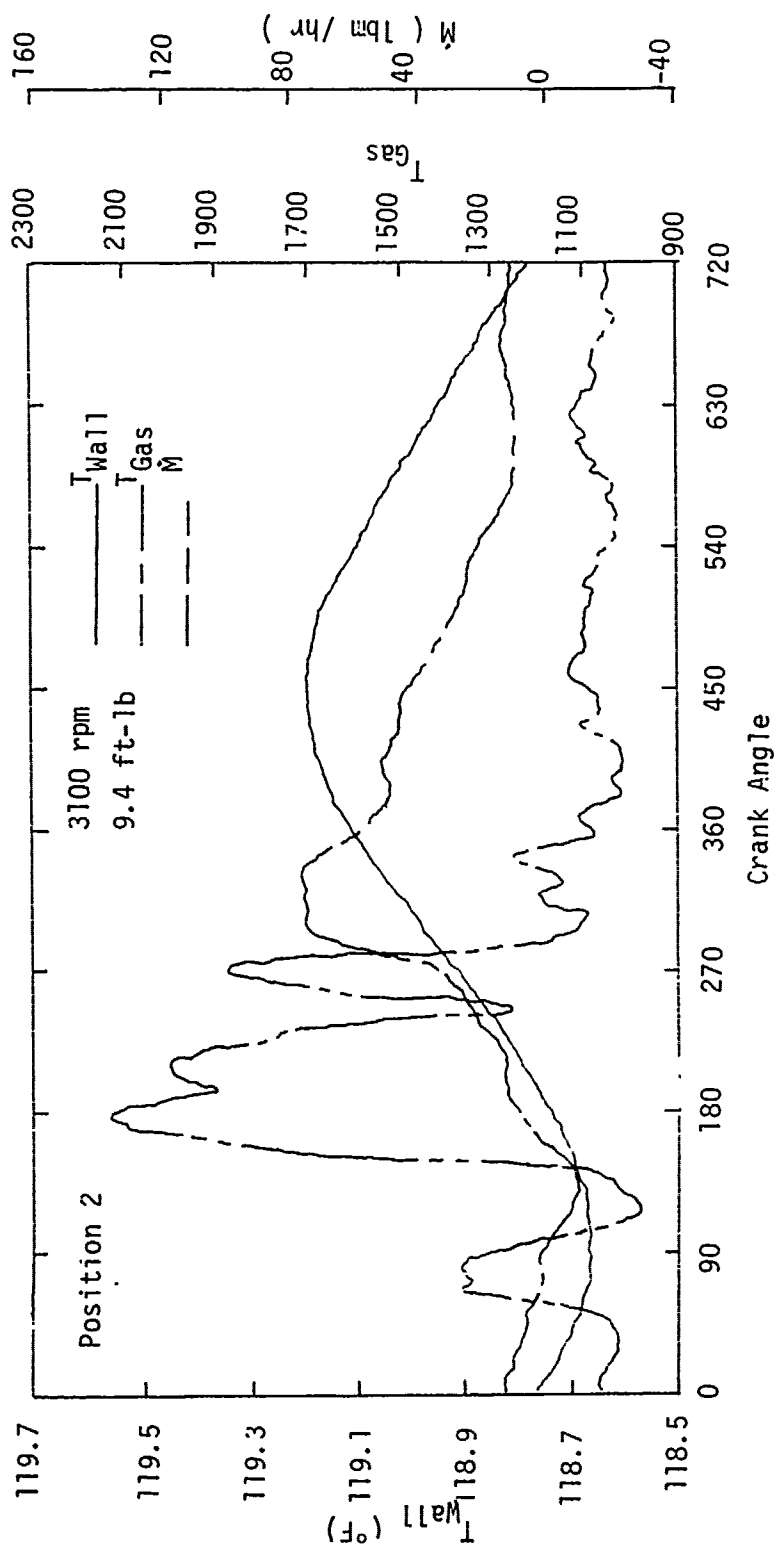


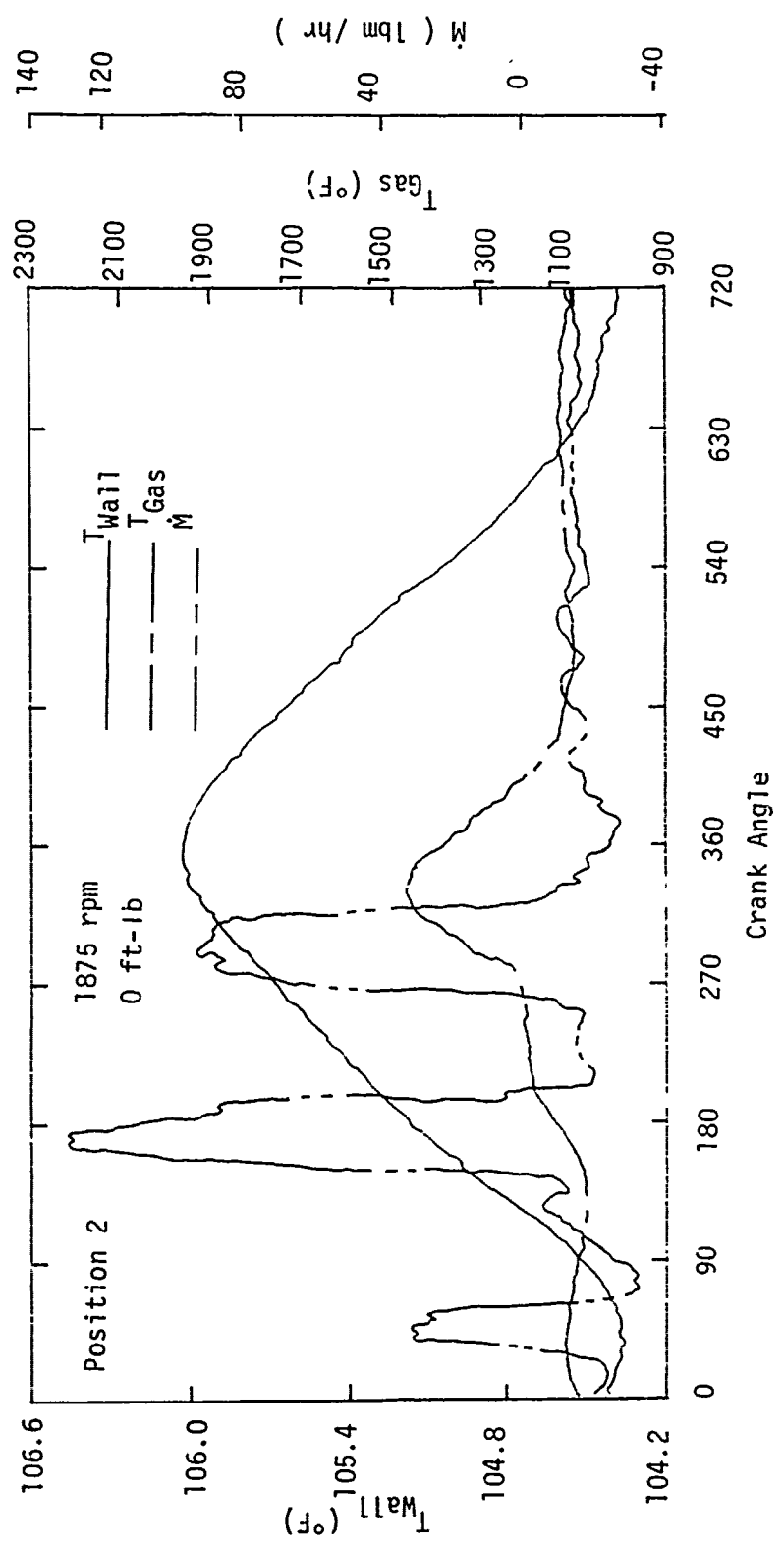


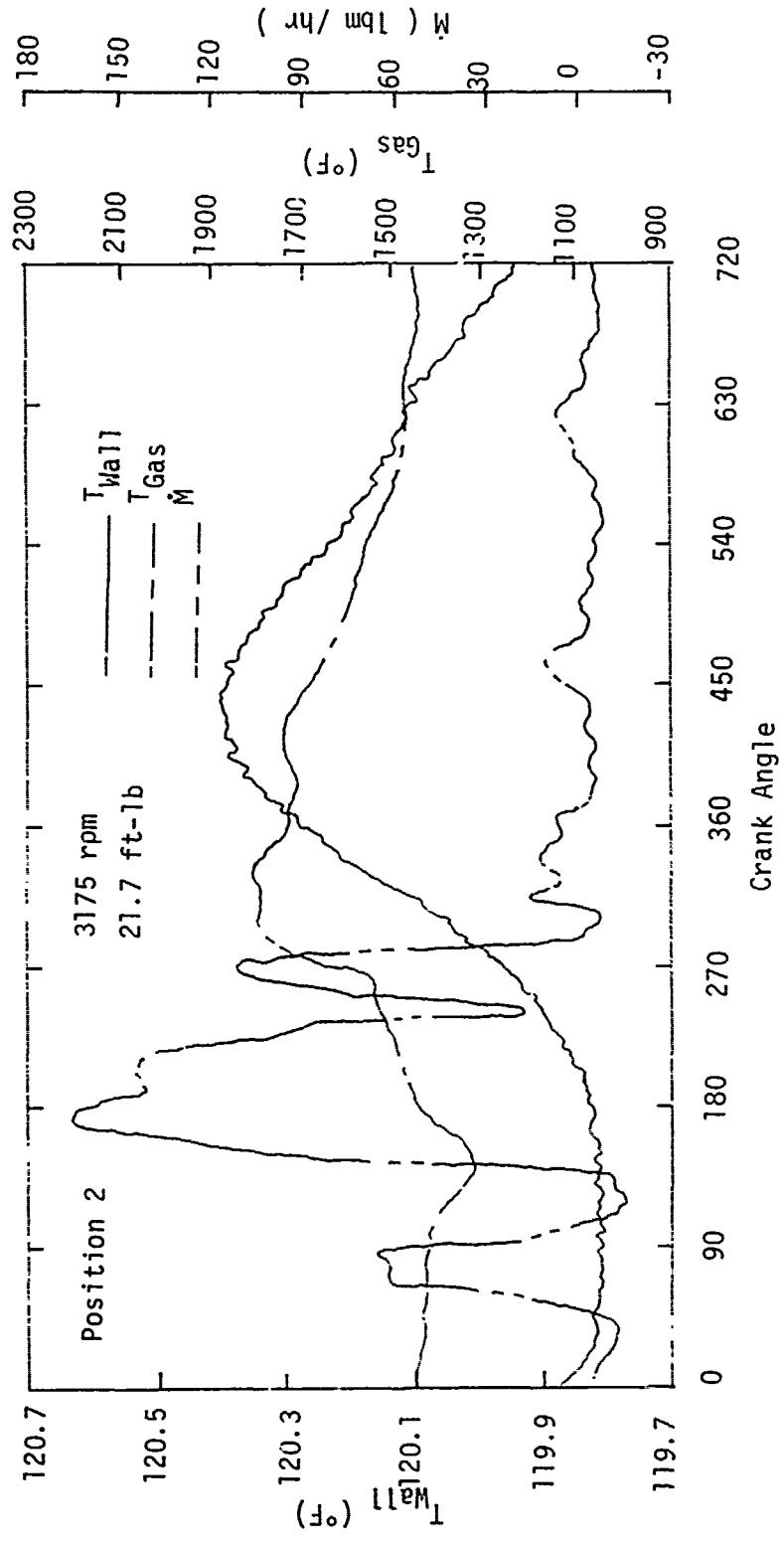


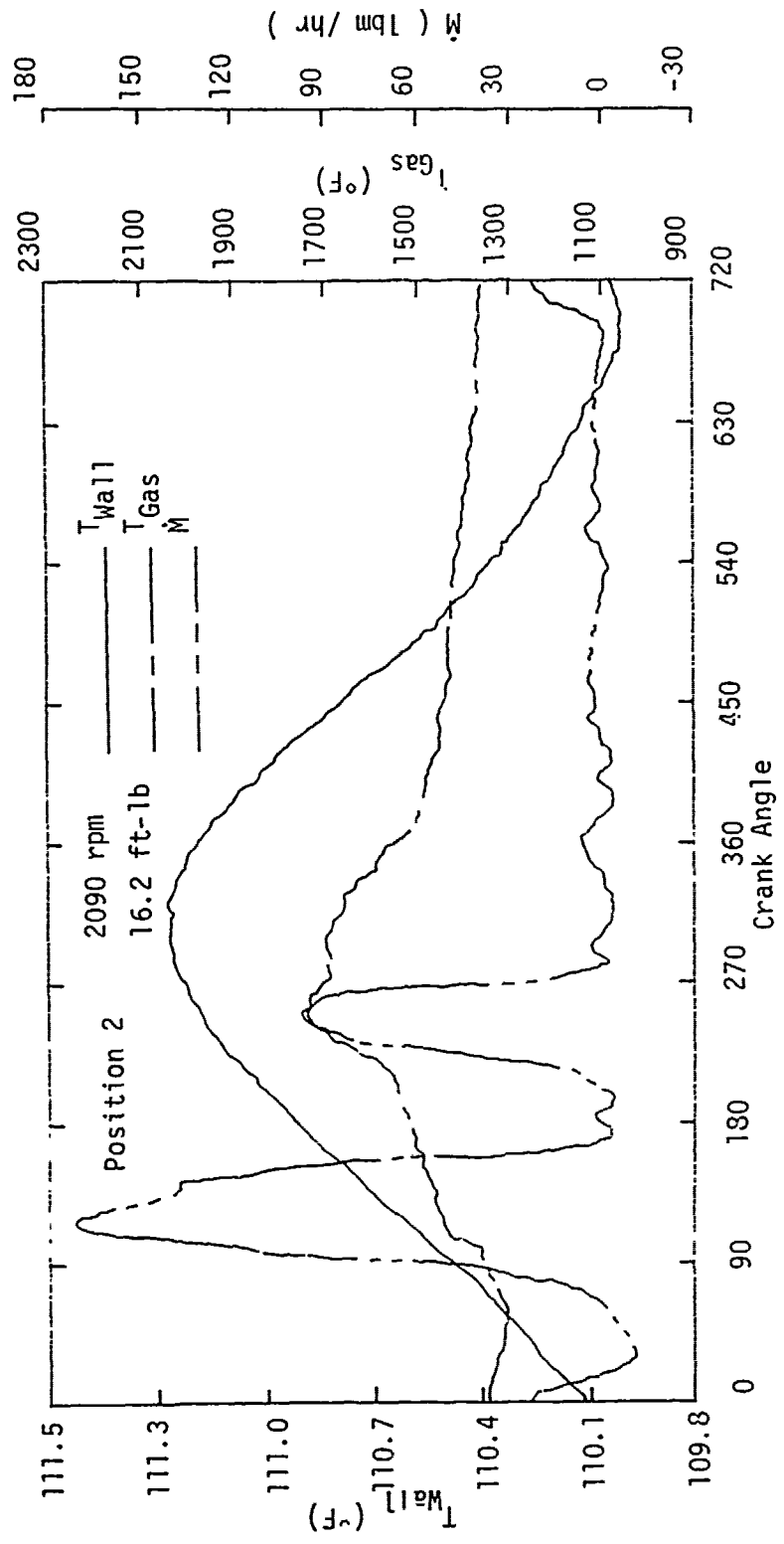


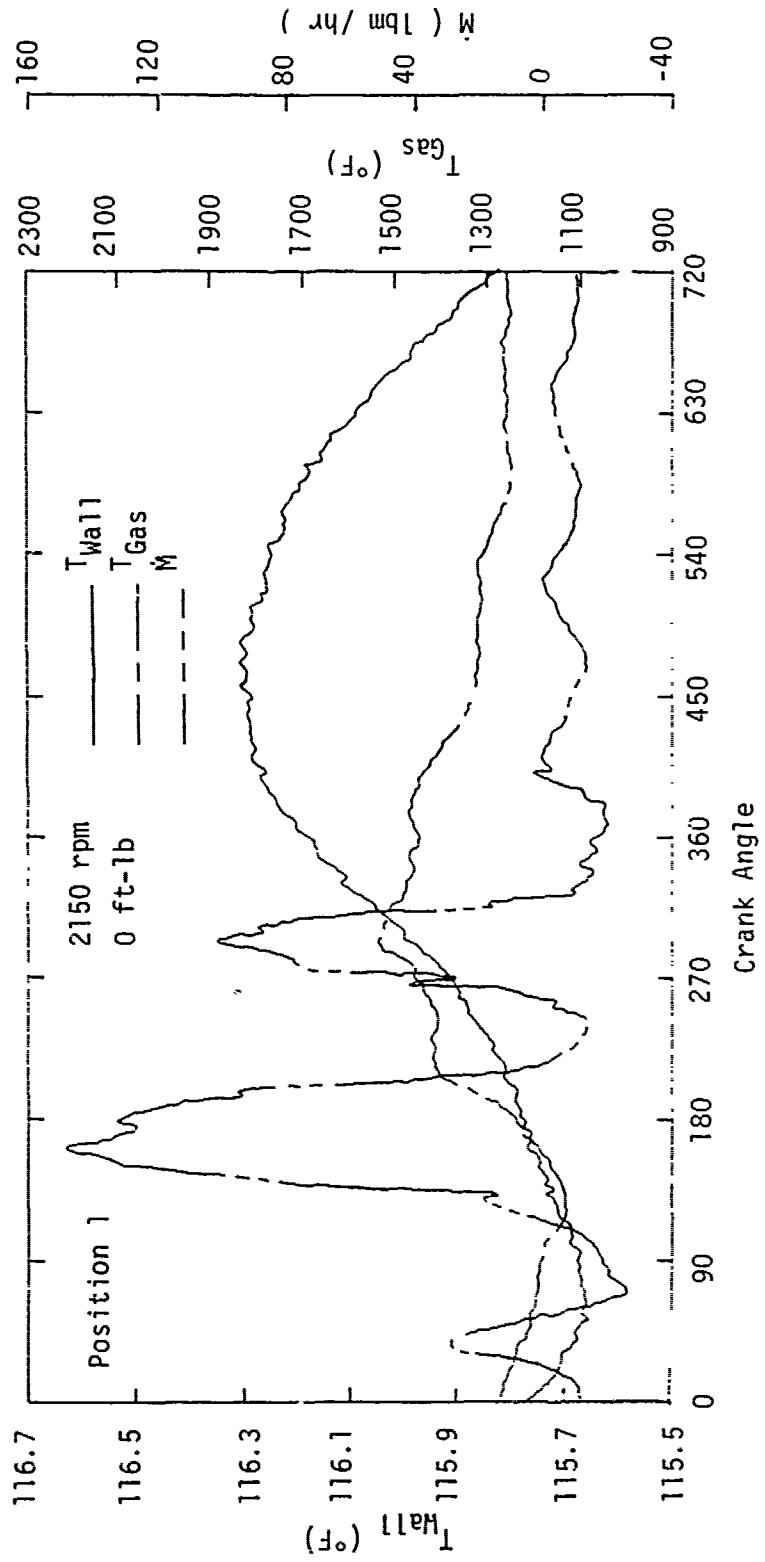


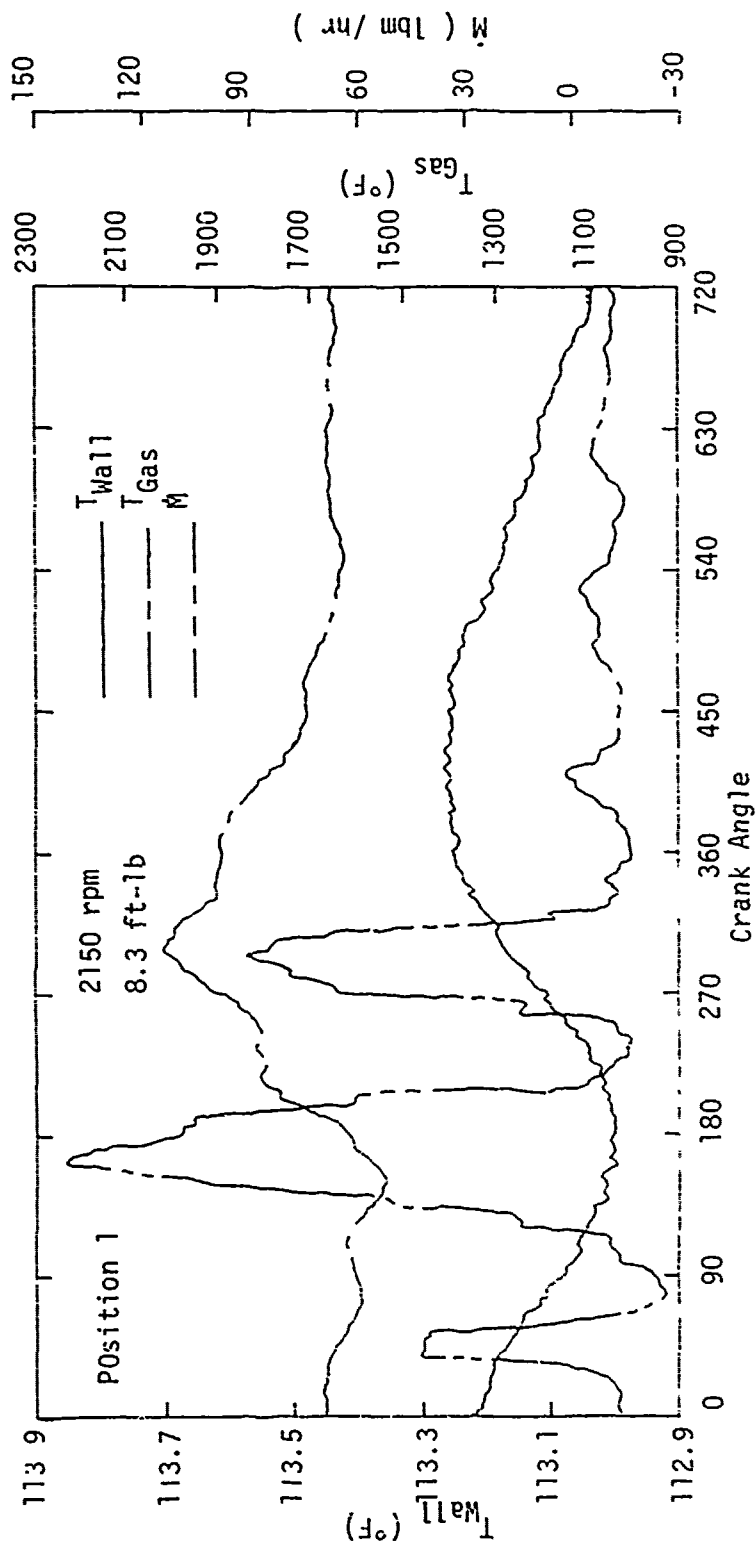


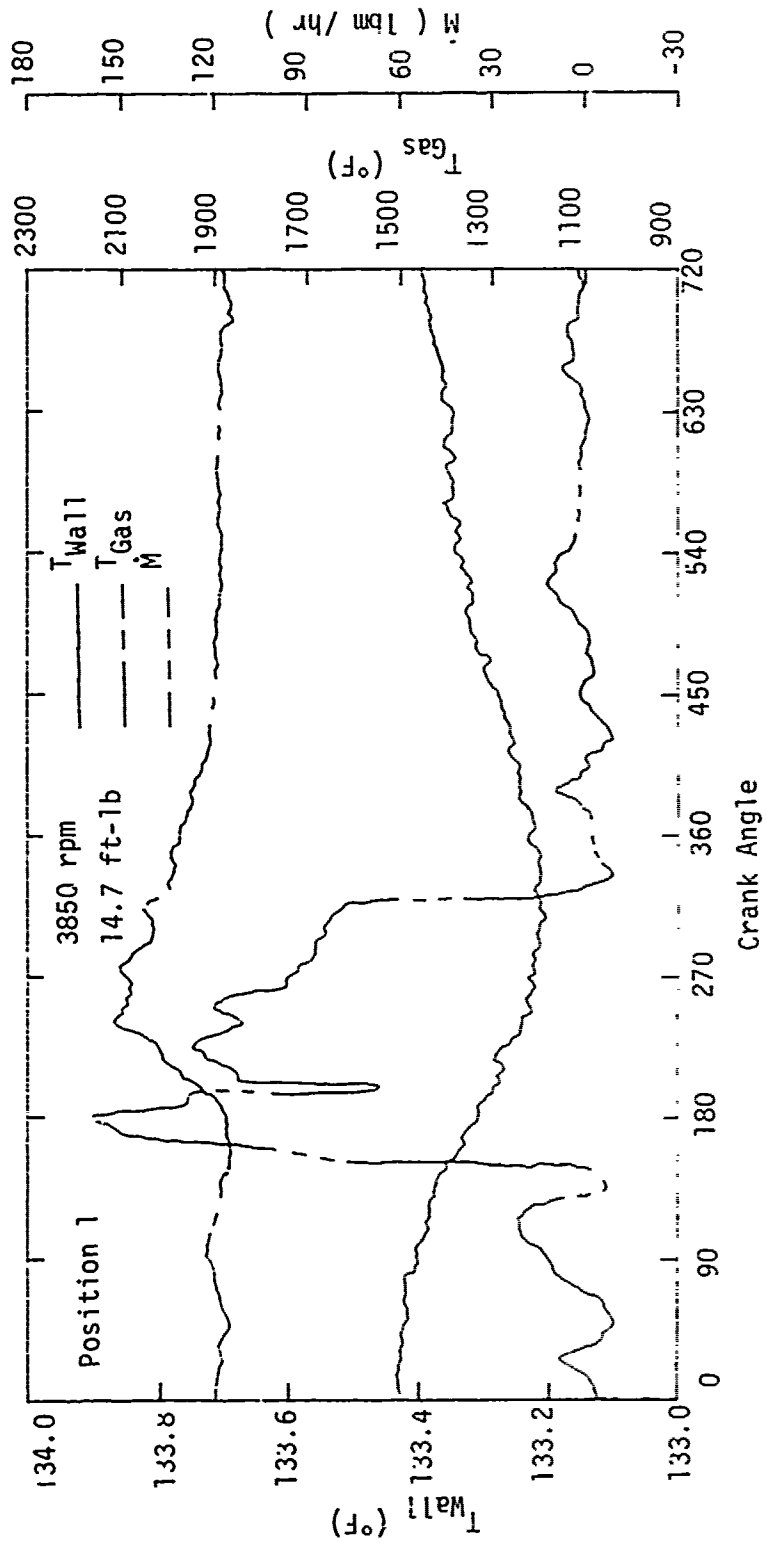


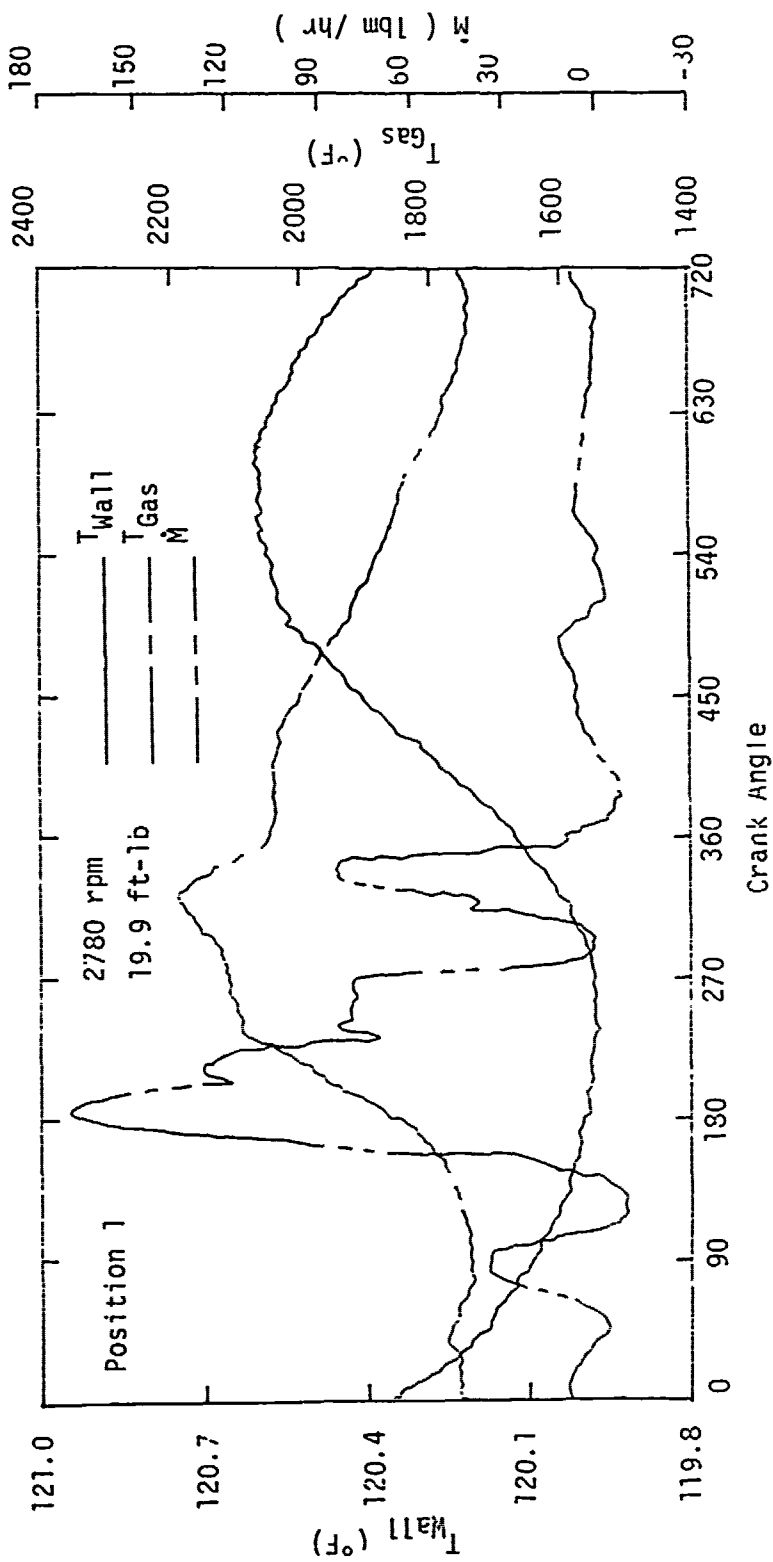












## APPENDIX G

## COMPUTER PROGRAMS

C THE FOLLOWING PROGRAM USES CRANK ANGLE PULSES TO EXTERNALLY  
 C TRIGGER THE DIGITISATION OF THE ANALOG SIGNALS WITH THE AID  
 C OF A REAL TIME SAMPLING (RTS) ROUTINE ON A PDP 11 MINI-  
 C COMPUTER.

```

MAIN PROGRAM
DIMENSION IBUF(12000)
DATA K/1/
TYPE 5
5  FORMAT(2X,'NAME OUTPUT DATA FILE')
   CALL ASSIGN(1,'DUM',-1,'NEW',,)
C   SET THE FLAG
   ICMF=0
C   SAMPLING DRIVEN BY S.T.#1
   CALL RTS(IBUF,12000,,2400,,5,,0,ICMF,IBEF)
C   WAIT FOR COMPLETION
   CALL LWAIT(ICMF,0)
   TYPE 10
10  FORMAT(//,5X,'ICHAN1',2X,'ICHAN2',2X,'ICHAN3',
        12X,'ICHAN4',2X,'ICHAN5')
   DO 30 J=1,2400
   WRITE(1,20) IBUF(K),IBUF(K+1),IBUF(K+2),IBUF(K+3),IBUF(K+4)
20  FORMAT(5(I5))
   TYPE 25,IBUF(K),IBUF(K+1),IBUF(K+2),IBUF(K+3),IBUF(K+4)
25  FORMAT(5X,5(2X,I5))
   K=K+5
30  CONTINUE
   CALL CLOSE(1)
   STOP
   END

```

C THE FOLLOWING PROGRAM SCANS THE DIGITISED DATA FOR  
 C ENGINE CYCLES, COMPILES THEM, DELETES THE DEFECTIVE  
 C CYCLES AND THEN PROCESSES THEM INTO THEIR ACTUAL VALUES.  
 C PROGRAM VALUE THEN USES A FINITE-DIFFERENCE METHOD  
 C TO DETERMINE THE INSTANTANEOUS HEAT FLUX AND HEAT  
 C TRANSFER COEFFICIENT FOR EACH INDIVIDUAL ENGINE CYCLE  
 C AND THEN FINALLY ENSEMBLE AVERAGES THEM TO OBTAIN ONE  
 C AVERAGED ENGINE CYCLE.

```

PROGRAM VALUEC(INPUT,OUTPUT,TAPE7,TAPE6)
DIMENSION IBUF3(53,241),IBUF4(241),IBUF5(241),SUM1(241)

```

```

1,SUM2(241),SUM4(241),Q(241),H(241),X(21),Y(21),A(53,241)
  REAL K,IBUF3,IBUF4,IBUF5
  DATA X/2.0,2.1,2.2,2.3,2.4,2.5,2.6,2.7,2.8,2.9,3.0,3.1
1,3.2,3.3,3.4,3.5,3.6,3.7,3.8,3.9,4.0/
  DATA Y/520., 725.,932.,1105.,1235.,1350.,1445.,1540.,
C1635.,1720.,1805.,1895.,1995.,2090.,2180.,2260.,2340.
C,2430.,2520.,2610.,2700./
  PRINT *,"NO OF CYCLES TO AVG="
  READ *,MM
  PRINT *,"FOR DELETING FIRST 120 PTS TYPE 1 ELSE 2"
  READ *,JP
  PRINT *,"GAS WALL TEMP(BIAS)="
  READ *,TWALLC
  PRINT *,"WATER WALL TEMP="
  READ *,TINIT
  PRINT *,"RPM="
  READ *,NN
  PRINT *,"IF GAS WALL TEMP AMPLIFIED X5 TYPE 1 ELSE 2"
  READ *,IP
  PRINT *,"IF GAS TEMP AMPLIFIED X5 TYPE 1 ELSE 2"
  READ *,IJK
  PRINT *,"ADDITIONAL GAS TEMP BIAS OVER 2V="
  READ *,AB
  PRINT *,"MAX ITERATIONS="
  READ *,KMAX
  KP=0
  TAVG=0.
  K=0.00023
  ALPHA=0.0055
  IF(IJK.EQ.1)GO TO 10
  AMP=1.
  GO TO 27
10  AMP=5.
27  IF(IP.EQ.1)GO TO 23
  GF=1.
  GO TO 29
28  GF=5.
29  DO 30 I=1,21
30  X(I)=X(I)+AB
31  DO 33 I=1,240
  READ(7,32)IBUF3(53,I),IBUF4(I),IBUF5(I)
32  FORMAT(10X,3F5.0)
  IF(I.LT.6)GO TO 33
  IF(IBUF5(I).GT.3000.)GO TO 34
33  CONTINUE
34  PRINT *,"DO LOOP 33 COUNTER SUFF"
  IF(JP.EQ.1)GO TO 36
  GO TO 37
36  JP=JP+5
  GO TO 31
37  KK=0

```

```

DO 40 I=1,240
READ(7,38) IBUF3(53,I),IBUF4(I),IBUF5(I)
38  FORMAT(10X,3F5.0)
    JJ=0
    IF(I.LT.10)GO TO 40
    IF(IBUF5(I).GT.3000.)GO TO 39
    GO TO 40
39  N=I
    GO TO 41
40  CONTINUE
41  IF(N.EQ.120)GO TO 42
    IF(N.GT.120)GO TO 37
    JJ=1
42  DO 45 I=1,240
    READ(7,43) IBUF3(53,I+120),IBUF4(I+120),IBUF5(I+120)
43  FORMAT(10X,3F5.0)
    IF(I.LT.10)GO TO 45
    IF(IBUF5(I+120).GT.3000.)GO TO 44
    GO TO 45
44  M=I
    GO TO 46
45  CONTINUE
46  IF(M.GT.120)GO TO 42
    IF(JJ.EQ.1)GO TO 37
    IF(M.EQ.120)GO TO 47
    GO TO 37
47  PRINT *,"240 PTS CHECK SUCESSFUL"
C
DO 52 I=1,240
IBUF3(53,I)=(IBUF3(53,I)-2048.)*0.0025
IBUF4(I)=(IBUF4(I)-2048.)*0.0025
IBUF3(53,I)=TWALLC+(IBUF3(53,I)*1000.*3./((0.0227*2000*28.
1*GF))
IBUF4(I)=IBUF4(I)*4./AMP
IF(IBUF4(I).GT.X(21))GO TO 74
IF(IBUF4(I).GE.X(1))GO TO 49
IBUF4(I)=Y(1)-((Y(2)-Y(1))/(X(2)-X(1)))*(X(1)-IBUF4(I))
IF(IBUF4(I).GT.0.)GO TO 52
IF(I.EQ.1)GO TO 80
IBUF4(I)=IBUF4(I-1)
GO TO 52
49  DO 51 J=1,21
    IF(IBUF4(I).EQ.X(J))GO TO 50
    GO TO 51
50  IBUF4(I)=Y(J)
    GO TO 52
51  CONTINUE
    M=1+(IBUF4(I)-X(1))/0.1
    IBUF4(I)=Y(M)+((IBUF4(I)-X(M))*(Y(M+1)-Y(M))/(X(M+1)-X(M)))
52  CONTINUE
    IBUF3(53,241)=IBUF3(53,240)

```

```

IBUF4(241)=IBUF4(240)
C
DO 53 J=1,241
TAVG=TAVG+IBUF3(53,J)
TAVG=TAVG/241.
DELTIM=1./(2.*NN)
DELX=.156/52
COEFF=ALPHA*DELTIM/(DELX**2)
ZZ=0.
DO 54 I=1,52
IBUF3(I,1)=TINIT+(TAVG-TINIT)*ZZ/.156
54 ZZ=ZZ+0.003
55 IBUF3(1,1)=TINIT
KK=KK+1
JK=0
DO 57 J=1,239
IBUF3(1,J+1)=TINIT
DO 56 I=2,52
IBUF3(I,J+1)=COEFF*(IBUF3(I+1,J)+IBUF3(I-1,J))
C+IBUF3(I,J)*(1-2*COEFF)
IF(KK.EQ.1)GO TO 25
IF(ABS((IBUF3(I,J+1)-A(I,J+1))/IBUF3(I,J+1)).GT..001)JK=1
25 A(I,J+1)=IBUF3(I,J+1)
56 CONTINUE
57 CONTINUE
IF(KK.EQ.1)GO TO 26
IF(KK.EQ.KMAX)GO TO 75
IF(JK.EQ.1)GO TO 26
GO TO 59
26 DO 58 I=1,53
IBUF3(I,1)=IBUF3(I,240)
58 CONTINUE
GO TO 55
59 QAVG=0.
DO 60 J=1,240
Q(J)=(IBUF3(53,J)-IBUF3(52,J))*K/DELX+(IBUF3(53,J+1)
C-IBUF3(53,J))*K/(DELX*2*COEFF)
H(J)=(144*3600.*Q(J)/(IBUF4(J)-IBUF3(53,J)))
QAVG=QAVG+Q(J)
60 CONTINUE
QAVG=QAVG/240.
PRINT *,"QAVG=",QAVG
PRINT *,"NO OF CYCLES FOR CONVERGENCE=",KK
IF(KP.GT.0)GO TO 63
DO 62 I=1,240
SUM1(I)=0.
SUM2(I)=0.
SUM4(I)=0.
62 CONTINUE
63 KP=KP+1
DO 64 I=1,240

```

```

SUM1(I)=SUM1(I)+Q(I)
SUM2(I)=SUM2(I)+H(I)
SUM4(I)=SUM4(I)+IBUF4(I)
64 CONTINUE
IF(KP.EQ.MM)GO TO 65
GO TO 37
65 PRINT *,"NO OF CYCLES TO AVG=",KP
DO 68 I=1,240
SUM1(I)=SUM1(I)/KP
SUM2(I)=SUM2(I)/KP
SUM4(I)=SUM4(I)/KP
68 CONTINUE
C DO 100 I=1,53
C WRITE(6,101)IBUF3(I,240)
C101 FORMAT(10X,F15.10)
C100 CONTINUE
DD=1.E9
DO 66 I=1,240
IF(IBUF3(53,I).LT.DD)DD=IBUF3(53,I)
66 CONTINUE
DO 67 I=1,240
IBUF3(53,I)=IBUF3(53,I)-DD
67 CONTINUE
C WRITE(6,69)
C69 FORMAT(/,9X,"Q(J)",8X,"T(53,J)",9X,"T(52,J)",7X,
C "TGAS(J)",10X,"H(J)",/)
DO 73 J=1,240
WRITE(6,71)SUM1(J),IBUF3(53,J),IBUF3(52,J),SUM4(J),SUM2(J)
71 FORMAT(E15.6,4F15.6)
73 CONTINUE
GO TO 76
74 PRINT *,"GAS TEMP INTERVAL INSUFF ON HIGH SIDE"
GO TO 76
75 PRINT *,"CONVERGENCE FAILED"
PRINT *,"INCREASE THE MAX NO OF ITERATIONS"
GO TO 76
80 PRINT *,"FIRST VALUE OF GAS TEMP NEGATIVE"
76 STOP
END

```

```

C THE FOLLOWING PROGRAM USES CORRECTED INSTANTANEOUS
C UPSTREAM AND DOWNSTREAM PRESSURES TO COMPUTE THE
C INSTANTANEOUS EXHAUST GASS MASS FLOW RATE.

```

```

PROGRAM PCORR(FINAL1,TAPE5=FINAL1,TEMP1,TAPE6=TEMP1,INPUT,
1OUTPUT)
DIMENSION SUM1(241),SUM2(241),SUM4(241),MEXH(241)
REAL MEXH,MTOT

```

```

DATA CC/-1.E10/,DD/1.E10/,EE/-1.E10/,FF/1 10.
1,GG/-1.E10/,HH/1.E10/
GC=32.174
GAMMA=1.3
RGAS=1544./28.59
B=0.55
CV=0.72
PI=3.141599
D=1.125/12.
MTOT=0.
PRINT *,"PRESS2 CORRECTION TERM:LOWER BY ? PSI"
READ *,PCORR2
PRINT *,"SHIFT PRESS2 DOWN(PHASE-LAG):HOW MANY PTS?"
READ *,IP
DO 25 I=1,240
10 READ(5,10)SUM1(I),SUM2(I),SUM4(I)
   FORMAT(2(1X,F14.6),16X,F14.6)
   SUM2(I)=SUM2(I)-PCORR2
   IF(IP.GE.I)GO TO 20
   SUM2(I-IP)=SUM2(I)
   GO TO 25
20 SUM2(240-IP+I)=SUM2(I)
25 CONTINUE
   DO 70 I=1,240
30 KL=1
   IF(SUM1(I).GE.SUM2(I))GO TO 40
   A=SUM1(I)
   SUM1(I)=SUM2(I)
   SUM2(I)=A
   KL=-1
40 F1=SQRT(2.*GC*GAMMA*((SUM1(I)*144.)**2)/((GAMMA-1)
1*RGAS*(459.67+SUM4(I))))
   F2=SQRT(((SUM2(I)/SUM1(I))**(2./GAMMA))-((SUM2(I)
1/SUM1(I))**((GAMMA+1)/GAMMA)))/(1.-((B**4)*(SUM2(I)
2/SUM1(I))**(2./GAMMA))))
   MEXH(I)=((CV*PI*(D**2)*(B**2))/4.)*F1*F2*KL*3600.
   IF(KL.EQ.1)GO TO 50
   BB=SUM1(I)
   SUM1(I)=SUM2(I)
   SUM2(I)=BB
50 IF(SUM1(I).GT.CC)CC=SUM1(I)
   IF(SUM1(I).LT.DD)DD=SUM1(I)
   IF(SUM2(I).GT.EE)EE=SUM2(I)
   IF(SUM2(I).LT.FF)FF=SUM2(I)
   IF(MEXH(I).GT.GG)GG=MEXH(I)
   IF(MEXH(I).LT.HH)HH=MEXH(I)
60 WRITE(6,60)SUM1(I),SUM2(I),MEXH(I)
   FORMAT(2(1X,F14.6),1X,E15.7)
   MTOT=MTOT+MEXH(I)
70 CONTINUE
   MTOT=MTOT/240.

```

```

PRINT *, "MTOT=", MTOT, "LBS/HR"
PRINT *, "PRESS1 MAX=", CC
PRINT *, "PRESS1 MIN=", DD
PRINT *, "PRESS2 MAX=", EE
PRINT *, "PRESS2 MIN=", FF
PRINT *, "MEXH MAX=", GG
PRINT *, "MEXH MIN=", HH
STOP
END

```

```

C THE FOLLOWING PROGRAM USES THE FINITE-DIFFERENCE METHOD
C TO OBTAIN THE TEMPERATURE DISTRIBUTION IN A FLAT PLATE
C WITH ONE SURFACE TEMPERATURE A KNOWN PERIODIC FUNCTION
C OF TIME.

```

```

PROGRAM FDIFF(TEMP, TAPE6=TEMP, INPUT, OUTPUT)
DIMENSION T(53,241), Q(240), A(53,241)
REAL K
TINIT=2.
PRINT *, "MAX ITERATIONS="
READ *, KMAX
KK=0
PI=3.141597
TA=2.
THETA=0.1
DO 10 J=1,241
F=(J-1)/2400.
T(53,J)=TA*COS(2.*PI*F/THETA)
10 CONTINUE
ALPHA=0.0055
K=0.00023
DELTIM=0.1/240
PRINT *, "DELTIM=", DELTIM
DELX=.156/52
COEFF=ALPHA*DELTIM/(DELX**2)
DO 20 I=1,52
T(I,1)=TINIT
20 CONTINUE
21 T(1,1)=TINIT
JK=0
KK=KK+1
DO 40 J=1,239
T(1,J+1)=TINIT
DO 30 I=2,52
T(I,J+1)=COEFF*(T(I+1,J)+T(I-1,J))+T(I,J)*(1-2*COEFF)
IF(KK.EQ.1)GO TO 29
IF(ABS((T(I,J+1)-A(I,J+1))/T(I,J+1)).GT..01)JK=1
29 A(I,J+1)=T(I,J+1)

```

```

30 CONTINUE
40 CONTINUE
   IF(KK.EQ.1)GO TO 71
   IF(KK.EQ.KMAX)GO TO 90
   IF(JK.EQ.1)GO TO 71
   QTOT=0.0
   DO 50 J=1,240
   Q(J)=(T(53,J)-T(52,J))*K/DELX+(T(53,J+1)-T(53,J))
1*K/(DELX*2.*COEFF)
   QTOT=QTOT+Q(J)
50 CONTINUE
   QTOT=QTOT/240.
C WRITE(6,51)QTOT
C51 FORMAT(//,9X,"QTOT=",5X,E15.6)
C WRITE(6,60)
C60 FORMAT(///,9X,"Q(J)",8X,"T(53,J)",9X,"T(52,J)")
   AA=0.
   BB=99999999.
   CC=0.
   DD=99999999.
   DO 70 J=1,240
   IF(Q(J).GT.AA)AA=Q(J)
   IF(Q(J).LT.BB)BB=Q(J)
   IF(T(53,J).GT.CC)CC=T(53,J)
   IF(T(53,J).LT.DD)DD=T(53,J)
   WRITE(6,65)Q(J),T(53,J),T(52,J)
65 FORMAT(E15.6,2F15.6)
70 CONTINUE
   PRINT *,"QMAX=",AA,"QMIN=",BB
   PRINT *,"T(53,J)MAX=",CC,"T(53,J)MIN=",DD
   GO TO 80
C71 PRINT *,"KK=",KK
71 DO 75 I=1,53
   T(I,1)=T(I,240)
75 CONTINUE
   GO TO 21
80 PRINT *,"CONVERGENCE SUCCESSFUL"
   PRINT *,"NO OF CYCLES FOR CONVERGENCE=",KK
   GO TO 100
90 PRINT *,"CONVERGENCE FAILED"
   PRINT *,"INCREASE THE MAX NO OF ITERATIONS"
100 STOP
   END

```

```

C THE FOLLOWING PROGRAM USES A FOURIER-SERIES EXPANSION
C METHOD TO OBTAIN THE TEMPERATURE DISTRIBUTION IN A
C FLAT PLATE WITH ONE SURFACE TEMPERATURE A KNOWN PERIODIC
C FUNCTION OF TIME.

```

```

PROGRAM SERIES(INPUT,CHECK,TAPE6=CHECK,OUTPUT)
DIMENSION Q(50),QDOT(241),TS(241)
REAL L,K
PI=3.141597
L=.156
TM=2.0
THETA=0.1
K=0.00023
A=0.0055
B=SQRT((PI*(L**2))/(A*THETA))
PRINT *,"MAX NO OF TERMS FOR SUMMATION"
READ *,LP
C
WRITE(6,25)
C25
FORMAT(8X,"QDOT(M)",10X,"SURFACE TEMP",//)
DO 300 M=1,241
F=(M-1)/2400.
G=2.*PI*F/THETA
TS(M)=TM*COS(2.*PI*F/THETA)
Q(1)=B*(SIN(G)-COS(G))/L
QD=Q(1)
DO 200 I=1,LP
X=I
JJ=X/2
IF(I.EQ.(2*JJ))D=0.
IF(I.NE.(2*JJ))D=1.
Q(I+1)=((-1)**(2*I))*B*EXP(-B*(I+D))*(SIN(G-B*(I+D))
1-COS(G-B*(I+D)))/L
QD=QD+Q(I+1)
IF(ABS((Q(I+1)-Q(I))/Q(I+1)).LT..001)GO TO 201
200
CONTINUE
PRINT *,"CONVERGENCE FAILED"
GO TO 101
201
PRINT *,"NO OF TERMS SUMMED=",X
QDOT(M)=-K*TM*QD
WRITE(6,75)QDOT(M),TS(M)
75
FORMAT(2X,E15.6,2X,F15.6)
300
CONTINUE
WRITE(6,50)
50
FORMAT(//,5X,"Q(J)",//)
DO 100 I=1,11
WRITE(6,150)Q(I)
150
FORMAT(2X,E15.6)
100
CONTINUE
101
STOP
END

C
C
C
THIS PROGRAM SIMULATES THE WALL TEMPERATURE RISE IN THE
TEST SECTION DUE TO FLOW OF GAS AT A CONSTANT TEMPERATURE
AT VARIOUS ENGINE SPEEDS WITH THE USE OF AN INITIAL

```

C TEMPERATURE DISTRIBUTION IN THE WALL CALCULATED FROM THE  
 C EXPERIMENTAL DATA AND A STEPWISE FUNCTION FOR THE HEAT  
 C TRANSFER COEFFICIENT.

```

PROGRAM PULSE(INPUT,OUTPUT,TAPE8,TAPE9)
DIMENSION T(53,241),H(241),TGAS(241),BIOTNO(241),TSWING(241)
1,THETA(241)
REAL K
PRINT *,"WATER WALL TEMPERATURE="
READ *,TINIT
PRINT *,"RPM="
READ *,NN
PRINT *,"VALUE OF GAS TEMPERATURE"
READ *,TG
PRINT *,"STEP INPUT VALUE OF H"
READ *,HG
PRINT *,"TEMPERATURE RISE TILL WHAT CRANK ANGLE"
READ *,ICA
DO 10 J=1,241
H(J)=HG/(144.*3600.)
TGAS(J)=TG
10 CONTINUE
DO 12 I=1,53
READ(8,11)T(I,1)
11 FORMAT(10X,F15.10)
12 CONTINUE
ALPHA=0.0055
K=0.00023
DELTIM=1./(2.*NN)
DELX=0.156/52
COEFF=ALPHA*DELTIM/(DELX**2)
THETA(1)=0.
T(1,1)=TINIT
TSWING(1)=0.
DO 14 J=1,239
T(1,J+1)=TINIT
BIOTNO(J)=H(J)*DELX/K
DO 13 I=2,52
T(I,J+1)=COEFF*(T(I+1,J)+T(I-1,J))+T(I,J)*(1.-2.*COEFF)
13 CONTINUE
T(53,J+1)=COEFF*(2.*T(52,J)+2.*BIOTNO(J)*TGAS(J)+T(53,J)
C*((1./COEFF)-2.*BIOTNO(J)-2.))
TSWING(J+1)=T(53,J+1)-T(53,1)
THETA(J+1)=3*J
14 CONTINUE
KJ=ICA/3+1
DO 16 J=1,KJ
WRITE(9,15)THETA(J),TSWING(J)
15 FORMAT(5X,F5.1,10X,F10.5)
16 CONTINUE

```

```

WRITE(9,17) TINIT
17  FORMAT(//,5X,"TINIT=",F10.4)
WRITE(9,18) T(53,1)
18  FORMAT(/,5X,"T(53,1)=",F10.4)
STOP
END

```

```

C   THE FOLLOWING IS A TYPICAL PLOTTING ROUTINE USED TO
C   PLOT THE INSTANTANEOUS HEAT FLUX.HEAT TRANSFER COEFF.,
C   SURFACE WALL TEMPERATURE SWING AND THE EXHAUST GAS
C   TEMPERATURE AS A FUNCTION OF THE CRANK ANGLE.

```

```

PROGRAM PLCT5 (INPUT,OUTPUT,TAPE1,TAPE2,TAPE3,TAPE4,TAPE50=
1OUTPUT)
  DIMENSION X(241),Y1(241),Y2(241),Y3(241),Y4(241)
C,A1(241),A2(241),A3(241),A4(241)
  PRINT *,"TYPE 1 FOR Q,2 FOR TWALL,3 FOR TGAS,4 FOR H"
  READ *,JJ
  PRINT *,"INPUT YMIN, YMAX,YTICK,ND"
  READ *,YMIN,YMAX,YTICK,ND
  CALL PLOTS(0.,0.,50)
  CALL BOX(0.,720.,90.,-1,YMIN ,YMAX ,YTICK,ND)
  CALL XLABEL("CRANK ANGLE!Z",0)
  IF (JJ.EQ.1)GO TO 13
  IF (JJ.EQ.2)GO TO 16
  IF (JJ.EQ.3)GO TO 19
  DO 12 I=1,240
  READ(1,11)Y1(I)
11  FORMAT(60X,F15.6)
  READ(2,25)Y2(I)
25  FORMAT(60X,F15.6)
  READ(3,26)Y3(I)
26  FORMAT(60X,F15.6)
  READ(4,27)Y4(I)
27  FORMAT(60X,F15.6)
12  CONTINUE
  CALL YLABEL("H (BTU/SQ.FT/HR/DEG.F)!Z",0)
  GO TO 50
  DO 15 I=1,240
  READ(1,14)Y1(I)
14  FORMAT(E15.6)
  READ(2,28)Y2(I)
28  FORMAT(E15.6)
  READ(3,29)Y3(I)
29  FORMAT(E15.6)
  READ(4,30)Y4(I)
30  FORMAT(E15.6)
15  CONTINUE

```

```
CALL YLABEL("Q/A (BTU/SQ. IN/SEC)!Z",0)
GO TO 50
16 X(1)=0
DO 70 I=1,240
X(I+1)=I*3
70 CONTINUE
DO 18 I=1,240
READ(1,31)Y1(I)
31 FORMAT(15X,F15.6)
READ(2,32)Y2(I)
32 FORMAT(15X,F15.6)
READ(3,33)Y3(I)
33 FORMAT(15X,F15.6)
READ(4,34)Y4(I)
34 FORMAT(15X,F15.6)
18 CONTINUE
Y1(241)=Y1(240)
Y2(241)=Y2(240)
Y3(241)=Y3(240)
Y4(241)=Y4(240)
CALL YLABEL("WALL TEMP SWING(DEG)!Z",0)
GO TO 22
19 X(1)=0
DO 80 I=1,240
X(I+1)=I*3
80 CONTINUE
DO 21 I=1,240
READ(1,20)Y1(I)
20 FORMAT(45X,F15.6)
READ(2,35)Y2(I)
35 FORMAT(45X,F15.6)
READ(3,36)Y3(I)
36 FORMAT(45X,F15.6)
READ(4,37)Y4(I)
37 FORMAT(45X,F15.6)
21 CONTINUE
Y1(241)=Y1(240)
Y2(241)=Y2(240)
Y3(241)=Y3(240)
Y4(241)=Y4(240)
CALL YLABEL("GAS TEMP (DEG.F)!Z",0)
GO TO 22
50 DO 60 I=1,240
A1(I)=Y1(I)
A2(I)=Y2(I)
A3(I)=Y3(I)
A4(I)=Y4(I)
60 CONTINUE
X(1)=0
DO 40 I=2,240
X(I)=(I-1)*3-1.5
```

```
Y1(I)=(A1(I-1)+A1(I))/2.  
Y2(I)=(A2(I-1)+A2(I))/2.  
Y3(I)=(A3(I-1)+A3(I))/2.  
Y4(I)=(A4(I-1)+A4(I))/2.  
40 CONTINUE  
X(241)=717  
Y1(241)=A1(240)  
Y2(241)=A2(240)  
Y3(241)=A3(240)  
Y4(241)=A4(240)  
22 CALL LEGEND(0.0,0.0,0.0,0.0)  
CALL L PLOT(X,Y1,241,1,0)  
CALL L PLOT(X,Y2,241,1,0)  
CALL L PLOT(X,Y3,241,1,0)  
CALL L PLOT(X,Y4,241,1,0)  
CALL PLOT(0.,0.,999)  
PRINT *, "TYPE, TAPE50 TO PLOT"  
STOP  
END
```